CODE AND RECEIVER DESIGN FOR THE NON-COHERENT FAST FADING CHANNEL

by

Arvind Krishnamoorthy

A dissertation submitted in partial fulfillment
of the requirements for the degree of
Doctor of Philosophy
(Electrical Engineering: Systems)
in The University of Michigan
2006

Doctoral Committee:

Associate Professor Achilleas Anastasopoulos, Chair
Professor Wayne E. Stark
Professor Kim A. Winick
Assistant Professor Anna Amirdjanova

श्री गुरुभ्यो नमः

To My Parents

ACKNOWLEDGEMENTS

First and foremost, I would like to thank my Thesis Advisor, Prof. Achilleas Anastasopoulos for his guidance and his patience throughout the course of my studies at the University of Michigan. He is an excellent teacher whose enthusiasm in teaching infects his students with the determination to perform at their best. I deem myself extremely fortunate to have been his student and interacted closely with him for many years. His keen eye for details have saved me from many a pitfall.

I would also like to thank Profs. Wayne Stark, Kim Winick and Anna Amirdjanova for their patience and for agreeing to serve on my Doctoral Committee. It would be fair to say that I learnt most of what I know about digital communications from Prof. Anastasopoulos and Prof. Stark. As the Financial Aid Chair, Prof. Winick was kind enough to recognize some potential in me and offer me a fellowship and financial aid throughout my course of study at the University of Michigan.

I would also like to place on record my gratitude towards my parents who have always supported me in my academic pursuits and encouraged me to do my best. I would also like to thank my brother for his unceasing support, encouragement and the many pep talks he has given me whenever I was frustrated. Also this thesis would not have been possible without my wife, Lalitha, who has been an incredible source of strength and support.

TABLE OF CONTENTS

LIST OF FIGURES

Figure

LIST OF TABLES

Table

CHAPTER 1

Introduction

Wireless devices have become ubiquitous these days with everyone using cellular and other personal communication systems like second nature. Faced with the demand for high bandwidth data and multimedia services along with the requirement of high reliability, wireless communication system design has received a fresh injection of research interest with the focus on supporting higher data rates. Since the bandwidth available for usage remains a scarce commodity, alternative approaches (*i.e.* more efficient usage of bandwidth) have been taken to improve data rates and satisfy these demands.

The techniques used to provide multiple uncorrelated versions of the transmitted signal to the receiver to facilitate the realiable information transmission over a fading channel are called *diversity techniques*. Some of the commonly used diversity techniques are:

- *Time Diversity*: The information signal is repeated in different time intervals separated by at least the *coherence interval* (see [45]) of the channel thus producing uncorrelated repetitions of the information signal. This is a form of repetition coding which is trivial. Another method of doing this is to use non-trivial channel coding with time interleaving.

- *Frequency Diversity*: Transmitting the signal on different carriers separated in frequency by at least the *coherence bandwidth* (see [45]) of the channel produces frequency diversity *i.e.* the transmitted signals undergo uncorrelated versions of the channel in different frequency bands.

- *Space Diversity*: Multiple antennas can be used to improve the received signal strength and produce what is termed space diversity. Signals originating from different antennas (spatially separated by multiples of the wavelength of transmission) are independent, thus experiencing fades at different times and frequencies, so that the combined signal has a lower probability of being attenuated beyond recovery.

A simple explanation of the idea behind using diversity techniques is the following - suppose p is the probability that a signal is attenuated beyond recovery, and suppose there are L branches of diversity. Then the probability that all L signals are faded beyond recovery is $p^L \ll p$. Wherever feasible, all possible diversity techniques should be used for best performance.

One popular method for obtaining diversity has been to use multiple transmit antennae and multiple receive antennae in the wireless systems, resulting in what is known as Multiple Input-Multiple Output (MIMO) systems. Additionally, the use of multiple antennas at the transmitter and the receiver has been shown to increase capacity over that of single antenna systems also known as Single Input-Single Output (SISO) systems. Thus MIMO systems (when used properly) are capable of improving both capacity (higher data rates) and diversity (more reliability) for a given application.

Although MIMO systems were known to improve diversity for a long time, it

wasn't until 1995 that the capacity improving feature of MIMO systems were discovered in [49] and [19]. These works showed that the capacity of a MIMO system utilizing M transmit and N receive antennae in fading channels with channel state information (CSI) available at the receiver, but not available at the transmitter, grows as $\min\{M, N\}\log(SNR)$ at high signal-to-noise ratios (SNRs) [49]. This led to an implementation called the Layered Space-Time Architecture in [18] and gave birth to the topic of space-time codes. The term *space-time code* refers to the use of channel codes on multiple-antenna systems where channel coding takes place along the *time* dimension (so that time diversity is achieved) and across antennas, *i.e.*, *space* dimension (so that space diversity is achieved). The above results are valid under the assumption that the receiver has perfect channel state information (*coherent reception*) *i.e.*, the receiver (somehow) knows the exact realization of the fading process while the transmitter has no knowledge of the CSI.

In practice, coherent reception means that the coherence interval of the channel is large enough that a small portion of it can be used to send pilot symbols that will aid the receiver in the explicit estimation of the channel parameters. When this is not true, *i.e.*, when the coherence interval is small, the receiver cannot estimate the channel path gains before they change to new, independent values. So in this case, the receiver has to proceed *without explicitly estimating* the channel parameters. This is called *non-coherent reception*. For the case of non-coherent reception over a quasi-static MIMO block fading channel with coherence interval of T symbols, [34, 56] proved that the capacity grows as $M^*(1 - M^*/T)\log(SNR)$ with $M^* = \min\{M, N, T/2\}$ at high SNR.

This work deals with the problem of designing codes and receivers for the case when both the transmitter and the receiver have no knowledge of the channel real-

ization. The rest of this chapter contains a description of the channel and system model and the notation used herein, followed by a discussion of the fundamental results from the literature under the two paradigms mentioned above. Finally a brief discussion of our contributions in the form of an outline of this dissertation is presented.

1.1 System Description

1.1.1 Channel Model

Consider a wireless communication system in which the transmitter has M antennas and the receiver has N antennas. At the transmitter, one complex signal is transmitted from each of the M antennas simultaneously in one channel use. These transmissions are collected in to the row vector[1] $\mathbf{x}_t^\top = [x_{t,1}, \ldots, x_{t,M}]$. The transmission from each antenna undergoes Rayleigh fading independently of the others and the receiver antenna j receives a noisy superposition of these Rayleigh faded signals. The received signal at time t is modelled as follows:

$$y_{t,j} = \sum_{i=1}^{M} x_{t,i} h_{i,j} + n_{t,j} \quad , \quad j = 1, \ldots, N, \quad t = 1, \ldots, T. \tag{1.1}$$

Equivalently, collecting all the received values $y_{t,j}, j = 1, 2, \ldots, N$, into a row vector $\mathbf{y}_t^\top$, we can write (1.1) as

$$\mathbf{y}_t^\top = \mathbf{x}_t^\top \mathbf{H} + \mathbf{n}_t^\top \quad , t = 1, \ldots, T \tag{1.2}$$

In (1.1), the coefficients $h_{i,j}$ represent the path gain from transmit antenna i to receive antenna j. The path gains are modelled as independent samples of a complex Gaussian random process with mean 0 and variance 0.5 per real dimension. This is equivalent to saying that the absolute value of the path gain $|h_{i,j}|$ is Rayleigh

[1] Throughout this work, we use $\mathbf{X}$, $\mathbf{x}$, $\mathbf{x}^\top$, $\mathbf{x}^*$, and $Tr(\mathbf{X})$ to denote matrices, column vectors, vector transpose, conjugate transpose, and trace, respectively.

distributed and the phase is uniformly distributed over $[0, 2\pi)$. It is assumed that these path gains are constant for one block of length T symbol periods and then change independently to another realization. This is the block independent fading assumption.

The noise process $n_{t,j}$ is a realization from a zero mean white complex gaussian process with variance 0.5 per real dimension. The noise process is assumed independent from the fading process and independent across time (t) and space (j).

The analysis is made convenient if a matrix channel equation is considered. The matrix channel equation is formed by putting the observations of each antenna at time t into a row vector $\mathbf{y}_t^\top$ and stacking the T successive vectors as the rows of a $T \times N$ matrix $\mathbf{Y}$. The resulting equation in matrix form is

$$\mathbf{Y} = \mathbf{XH} + \mathbf{N} \tag{1.3}$$

where $\mathbf{X} \in \mathcal{C}^{T\times M}$, $\mathbf{H} \in \mathcal{C}^{M\times N}$, and $\mathbf{Y}, \mathbf{N} \in \mathcal{C}^{T\times N}$. The constellation is normalized to obey the following power constraint:

$$\mathbb{E}\left[Tr\{\mathbf{X}\mathbf{X}^*\}\right] = T\gamma_s \tag{1.4}$$

so that the average received signal to noise ratio at each receive antenna is γ_s irrespective of the number of transmit antennas M. At this point, the relationship between the bit SNR (γ_b) and the symbol SNR (γ_s) is not considered to preserve clarity. The bit SNR is calculated appropriately when coded systems are considered.

Through out this thesis, the channel is assumed to be unknown at the transmitter. Also, unless otherwise mentioned, the path gains are considered unknown at the receiver *i.e.* non-coherent reception. In the section that immediately follows, some fundamental results for MIMO systems, relevant to systems employing

coherent/non-coherent reception are discussed so as to prepare the reader with sufficient background to understand our contributions.

1.1.2 System Model

The specific communication system model we consider in this thesis for moderate - to - fast fading channels, *i.e.*, for $T \approx 5 - 50$, is explained via the block diagram in Fig. 1.1. For very fast fading channels, it is emphasized that a different approach is taken that is explained in Chapter 4.

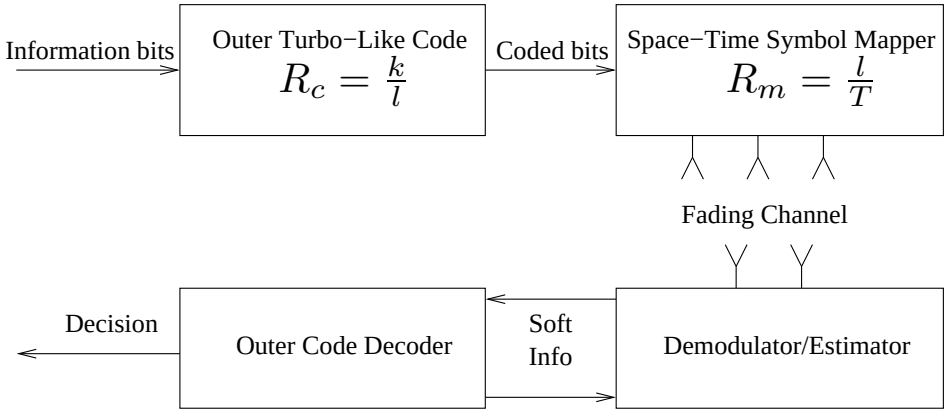

Figure 1.1: Block diagram of the wireless communication system.

The transmitter consists of an outer binary turbo-like code of rate $R_c = \frac{k}{l}$ and an inner space-time code that maps l coded bits into a space-time symbol spanning T complex dimensions (or channel uses) *i.e.*, $R_m = \frac{l}{T}$, producing an overall rate $R = \frac{k}{T}$ (bits per complex dimension). As an example, we use Low Density Parity Check (LDPC) codes [22] for the purpose of simulations. The outer LDPC code produces long codewords whereas the channel remains constant for a short duration ($T \approx 5 - 50$), so one binary codeword is encoded into multiple coherence blocks[2].

[2]We thus obtain some time diversity.

The receiver is an iterative receiver that consists of a demodulator/estimator block and an LDPC decoder. Specific demodulator designs will be presented in Chapter 2; we however mention that in the proposed receiver design, *no* explicit estimation is performed at the demodulator. These two modules exchange soft information regarding the reliability of the bits and after a preset number of iterations the decoder outputs decisions on the bits.

In the sequel we present some background results concerning both coherent and non-coherent multiple antenna communication systems that will serve the reader well in understanding the discussion that follows in the rest of the dissertation.

1.2 Background on Multiple-Antenna Communication

1.2.1 Coherent Reception

Considering the scenario that the receiver has the channel state information, *i.e.* coherent reception, we summarize the capacity results in [49] and the performance analysis in [48]. The input-output relation (M transmit and N receive antennas) assumed for the following discussion is the same as in (1.1) Since it is assumed that the receiver has CSI, there is no merit in considering blocks of transmission. Rather, we consider the vector equation representing the transmission in t^{th} channel use as in (1.2), where $\mathbf{x}_t \in \mathcal{C}^M$, $\mathbf{H} \in \mathcal{C}^{M\times N}$, $\mathbf{y}_t, \mathbf{n}_t \in \mathcal{C}^N$. The assumptions about the components of $\mathbf{H}$ and $\mathbf{n}_t$ are identical to those in Section. 1.1.1. The power constraint on the transmitted signal $\mathbf{x}_t$ is changed to[3]

$$\mathbb{E}[\|\mathbf{x}_t\|^2] \leq \gamma_s \tag{1.5}$$

such that the received SNR per receiver antenna (irrespective of the number of transmit antennas) is γ_s.

[3]This reflects the transmission in a single channel use.

Capacity Results

For a given channel known at the receiver (*i.e.*, given $\mathbf{H}$), the mutual information between the output and the input signal is maximized when the input signal ($\mathbf{x}_t$) is a circularly symmetric complex Gaussian with a covariance matrix $\mathbf{Q}$ satisfying the constraint in (1.5). In this case the output signal is complex Gaussian as well, and the mutual information is given by:

$$\mathtt{I}(\mathbf{y}_t; \mathbf{x}_t) = \log\det(\mathbf{I}_N + \mathbf{H}\mathbf{Q}\mathbf{H}^*) \tag{1.6}$$

Since the transmitter is unaware of the channel realization, the signal $\mathbf{x}_t$ that achieves capacity is complex Gaussian distributed with covariance matrix, $\mathbf{Q} = \frac{\gamma_s}{M}\mathbf{I}$, which means, equal power from each transmitter antenna. Thus, the capacity given the particular channel realization at the receiver, is:

$$C = \log\det(\mathbf{I}_N + \frac{\gamma_s}{M}\mathbf{H}\mathbf{H}^*) \tag{1.7}$$

This capacity is actually a random variable because it is dependent on the particular realization of the random matrix $\mathbf{H}$. The average capacity (averaged over the channel statistics) is given by:

$$C_{\text{average}} = \mathbb{E}_{\mathbf{H}}[\log\det(\mathbf{I}_N + \frac{\gamma_s}{M}\mathbf{H}\mathbf{H}^*)] \tag{1.8}$$

The evaluation of the average capacity is not easy for cases other than $M = 1$ and/or $N = 1$ but can be obtained in almost closed form (see [49] for the details). From the average capacity, the following observations are made:

- Fixing $M = 1$, and varying N causes capacity to increase logarithmically with N. For large N, the capacity asymptotically approaches $\log(1 + N\gamma_s)$ in the sense that the difference approaches zero.

- Fixing $N = 1$, and taking M large, causes capacity to approach $\log(1 + \gamma_s)$.
- For $M = N$, there is a linear growth of capacity with M.

The above results hold for the case when the channel is ergodic. When the channel is non-ergodic, since the Shannon capacity is zero, a meaningful approach to evaluating the theoretical performance of this channel is to consider the capacity of the channel that can be supported with some *outage probability*. The outage probability is defined as the probability that the capacity of the channel is less than a specified 'bit-rate'. This probability obviously depends on the channel statistics. Such an approach was adopted by [18] and [19] and they demonstrated that the capacity (in bits/s/Hz), at say 1% outage probability, grows linearly with the $\min\{M, N\}$ for a given total transmitted power.

These results provoked a lot of work in this area and motivated the design of a Layered Space-Time Architecture by [18] to exploit the vast capacities achievable when using multiple-antennas.

Performance Analysis

While capacity analysis provides a theoretical maximum achievable bit-rate, for practical system design, one is concerned with error probability performance analysis. The authors of [48] considered the probability that a Maximum Likelihood (ML) receiver decides erroneously in favor of the matrix symbol $\mathbf{X}' = [x'_{t,i}]$ instead of $\mathbf{X} = [x_{t,i}]$ ($t = 1, \ldots, T$ and $i = 1, 2, \ldots, M$) assuming that the latter was the actual signal transmitted and perfect CSI is available at the receiver to obtain the following upper-bound (1.9) for the average pairwise error probability

$$\Pr(\mathbf{X} \to \mathbf{X}') \leq \left(\frac{1}{\prod_{i=1}^{M} \left(1 + \frac{\gamma_s \lambda_i}{4}\right)} \right)^N \tag{1.9}$$

where λ_i is the i^{th} eigenvalue (arranged in descending order) of the matrix $\mathbf{A}$ defined as $\mathbf{A} = \boldsymbol{\Delta}\boldsymbol{\Delta}^*$ in terms of the matrix $\boldsymbol{\Delta} = (\mathbf{X} - \mathbf{X}')^\top$. By construction $\text{rank}(\mathbf{A}) = \text{rank}(\boldsymbol{\Delta})$. If r is the rank of $\boldsymbol{\Delta}$ then exactly r eigenvalues are nonzero and exactly $M - r$ eigenvalues are zero. For high SNR, ($\gamma_s \gg 1$) the following approximation can be used:

$$\Pr(\mathbf{X} \to \mathbf{X}') \leq \left[\left(\prod_{i=1}^{r} \lambda_i \right)^{\frac{1}{r}} \frac{\gamma_s}{4} \right]^{-rN} \tag{1.10}$$

From the exponent of the signal-noise ratio, the conclusion is that there are rN branches of diversity (*i.e.*, a diversity advantage of rN) and from the multiplicative factor there is a coding advantage of $(\prod_{i=1}^{r} \lambda_i)^{\frac{1}{r}}$. The maximum diversity advantage achievable is MN and is achieved when $r = M$ *i.e.*, $\boldsymbol{\Delta}$ is a full rank matrix. (This is under the assumption that $M \leq T$, otherwise the maximum diversity advantage would be TN.) This leads to the following design criteria:

- *The Rank Criterion*: In order to achieve maximum diversity advantage MN, the matrix $\boldsymbol{\Delta}$ has to be full rank for all pairs of signals $\mathbf{X}$ and $\mathbf{X}'$ in the signal constellation/codebook. If r is the minimum rank of $\boldsymbol{\Delta}$ over all pairs of signals $\mathbf{X}$ and $\mathbf{X}'$ in the signal constellation/codebook, then the actual diversity advantage is given by rN.

- *The Determinant Criterion*: If r is the minimum rank of $\boldsymbol{\Delta}$ over all pairs of signals $\mathbf{X}$ and $\mathbf{X}'$ in the signal constellation/codebook, then the determinant criterion advises that the minimum of the r^{th} root of the sum of all determinants of $r \times r$ principal cofactors of $\mathbf{A}$ over every pair of signals $\mathbf{X}$ and $\mathbf{X}'$ in the codebook should be maximized. This has the overall effect of maximizing the coding advantage involved in (1.10).

These design criteria when applied to the design of $M = 2$, full rank space-time codes, produce the simple delay-diversity codes (see [48]) which are but a small subset of full rank space-time codes. More general conditions for designing codes that possess full diversity and good coding advantages with PSK modulation formats were derived in [25].

1.2.2 Non-coherent Reception

In this paradigm, the assumption that the receiver knows the path gains is removed. As in (1.3), the channel is represented as a $M \times N$ matrix and hence there are MN complex path gains to be estimated by the receiver if it has to do coherent detection. When the fading is *fast i.e.*, T is small, (typical values being $T \approx 2-50$), the receiver cannot estimate the path gains with sufficient accuracy before the channel changes again. The approach in this case is to detect the signals without explicitly estimating the channel.

Capacity Results

The fundamental information theoretic results derived in [28, 34, 56] are summarized below:

- The capacity for $M > M^*$ is equal to the capacity when $M = M^*$, where $M^* = \min\{M, N, \lfloor T/2 \rfloor\}$, *i.e.*, there is no increase in capacity when the number of transmitter antennas M is increased beyond M^*. This is a significant result that is unique for the non-coherent communication scenario. The capacity growth was also found to be linear in where $M^*(1 - M^*/T)$, while in the coherent communication paradigm, the capacity had a linear growth in $\min\{M, N\}$ irrespective of the length of the coherence interval.

- The structure of the input signal that achieves capacity is $\mathbf{X} = \mathbf{\Phi V}$, where $\mathbf{\Phi}$ is an *isotropically distributed* $T \times M$ unitary matrix and $\mathbf{V}$ is a real non-negative diagonal $M \times M$ matrix and $\mathbf{\Phi}$ and $\mathbf{V}$ are independent. An isotropically distributed unitary matrix is one whose probability density is unchanged when it is left multiplied by any deterministic unitary matrix and for which $\mathbf{\Phi}^* \mathbf{\Phi} = \mathbf{I}$.

- For $M = N = 1$, the capacity per dimension approaches the known channel capacity asymptotically in T.

- For $T \gg M$ or for $T > M$ and $\gamma_s \gg 1$, setting $\mathbf{V} = \sqrt{\frac{T\gamma_s}{M}}\mathbf{I}$, achieves capacity, *i.e.* $\mathbf{X} = \sqrt{\frac{T\gamma_s}{M}}\mathbf{\Phi}$ is capacity achieving. Such signal constellations are given the name *unitary space-time constellations*.

The last observation above motivated the following (summary of) performance analysis results [28] and the systematic design of unitary space-time constellations [29].

Unitary Space-Time Modulation and Demodulation

Consider a discrete constellation of unitary space-time signals are given by

$$\mathbf{X}_l = \sqrt{\frac{T\gamma_s}{M}}\mathbf{\Phi}_l,\ l = 1, 2, \ldots, S.$$

where $\mathbf{\Phi}_l$, $l = 1, 2, \ldots, S$ are $T \times M$ complex unitary matrices.

The pairwise error probability (in decoding $\mathbf{X}_2$ when $\mathbf{X}_1$ was the actual transmission) has the Chernoff upper bound

$$P_e \leq \frac{1}{2} \prod_{m=1}^{M} \left[\frac{1}{1 + \frac{T^2\gamma_s^2}{M^2} \frac{(1-d_m^2)}{4\left(1+\frac{T\gamma_s}{M}\right)}} \right]^N \tag{1.11}$$

This upper bound depends on the singular values $0 \leq d_M \leq d_{M-1} \leq \ldots \leq d_1 \leq 1$, of the $M \times M$ matrix $\mathbf{\Phi}_2^* \mathbf{\Phi}_1$. The set of singular values represent the extent of correlation between the subspaces generated by the columns of $\mathbf{\Phi}_1$and $\mathbf{\Phi}_2$. The pairwise error

probability decreases with any d_i. From a further approximation of (1.11), the single parameter that controls the performance of signal constellation[4] was found to be

$$\delta = \max_{l \neq l'} \sum_{m=1}^{M} d_m^2 = \max_{l \neq l'} M \|\mathbf{\Phi}_l^* \mathbf{\Phi}_{l'}\|^2. \tag{1.12}$$

A good constellation has a small δ over all distinct pairs of signals Φ_l and $\Phi_{l'}$. A small δ indicates a small correlation between constellation points - similar to maximum Euclidean distance that guides the design of constellations for communication over the AWGN channel. Therefore to generate good constellations, the following criterion is used

$$\min_{\text{constellations}} \delta = \min_{\text{constellations}} \max_{l \neq l'} M \|\mathbf{\Phi}_l^* \mathbf{\Phi}_{l'}\|^2 \tag{1.13}$$

A systematic and iterative procedure of generating unitary space-time constellations [29] is as follows.

$$\mathbf{\Phi}_l = \mathbf{\Theta}^{l-1} \mathbf{\Phi}_1 \qquad l = 2, 3, \ldots, S. \tag{1.14}$$

where $\mathbf{\Phi}_1 = \frac{1}{\sqrt{T}}$ times a $T \times M$ matrix whose columns are M distinct columns of a $T \times T$ Discrete Fourier Transform (DFT) matrix and $\mathbf{\Theta} = \text{diag}(e^{\imath \frac{2\pi}{S} u_1}, e^{\imath \frac{2\pi}{S} u_2}, \ldots, e^{\imath \frac{2\pi}{S} u_T})$. In practice, finding a good $\mathbf{\Theta}$ *i.e.* finding the corresponding set $\{u_1, u_2, \ldots, u_T\}$ so as to to get the smallest δ, is done using a random search, as there is no systematic way of doing the minimization yet. A couple of observations regarding this approach are:

- The particular construction technique imposes a circulant nature on the set of the correlations achieved by any constellation. This is very convenient, as it reduces the number of correlations to check from $S(S-1)/2$ to $S-1$.
- The amplitude of each component of the $T \times M$ matrix is equal to $\frac{1}{\sqrt{T}}$.

[4] at high SNR

1.3 Dissertation Outline

This dissertation is organized as follows: Section 1.1 above contained the channel model and the overall system architecture which is used in the remaining chapters. In Chapter 2, we consider various receiver algorithms for the case of non-coherent reception and propose a novel family of low complexity, near optimal (with respect to ML performance) soft iterative demodulator for pilot assisted transmission schemes. In Chapter 3, we characterize the capacity achieving signal distribution for the non-coherent fading channel. Motivated by our information theoretic foray into capacity-achieving distributions for these channels, a sophisticated transmission/detection scheme is proposed in Chapter 4, that promises gains up to 1.8 dB for very fast channels with minimal added complexity. In Chapter 5, the idea of joint design of modulation and coding for the non-coherent fading channel is presented and pair-wise probability of error analysis for codes that span multiple coherence intervals is considered. Finally conclusions and directions for future work are summarized in Chapter 6.

A brief outline of our contributions in each of the above chapters follows.

1.3.1 Receiver Algorithms and System Design for Fast Fading Channels

Based on the information theoretic result that isotropically distributed unitary signals achieve the capacity of the block independent fading channel under some conditions, systematic methods for the construction of isotropically distributed unitary constellations were proposed in [29] and [35]. Recently, these signaling techniques were investigated in conjunction with powerful outer codes in [2]. We note that these systematically generated unitary constellations result from high SNR pairwise error probability bounds and have no algebraic structure and hence large receiver com-

plexity. With this observation, we researched the existence of better constellations, at least in terms of complexity reduction.

Our contribution in this topic involves the identification of the well known pilot symbol assisted modulation (PSAM) scheme as the modulation of choice for this channel. We also propose and prove the merit of a family of near-optimal low-complexity (compared to ML) joint estimation/detection receiver for a wide range of modulations exemplified by the PSAM scheme. We concluded that the PSAM scheme along with the proposed low complexity receiver outperforms the designs in [2] in terms of both bit-error-rate (BER) and complexity. This is a surprising result, since one can usually improve one or the other, but not both performance measures. The proposed low-complexity algorithm is also compared with popular receiver algorithms namely the Expectation Maximization-EM algorithm [9] and a soft version of the Sphere Decoder [47].

Given the choice of PSAM scheme, the simplest receiver performs pilot-assisted non-iterative channel estimation followed by coherent decoding. This reception scheme, which has been investigated extensively in [20, 42] is hereby referred to as the Pilot-Only (PO) detection scheme. **Another result in this work is the proof of the equivalence between the PO scheme and an identical scheme with perfect CSI at the receiver for MIMO systems. This equivalence implies that analysis and code design for both problems is the same and solving one provides the solution for the other system albeit at a different signal-to-noise ratio.** In other words, a system employing coding and pilot-assisted estimation followed by decoding is equivalent to a degraded version of a system with perfect CSI at the receiver.

1.3.2 Capacity Achieving Signal Distribution

In [34], the unitary space-time constellations with a single amplitude were shown to achieve capacity only at high SNR or when $T \gg M$. At low SNR, there are, possibly, constellations that do better than unitary constellations. For instance, [6] considered signal constellations with multiple energy levels and show that their performance in terms of frame error probability is better than that of the unitary space-time constellations.

To gain a better understanding of the theoretical limits of this channel, we investigated the channel capacity of this channel with the emphasis on identifying the input signal distribution that achieves this capacity. **In Chapter 3, we prove that the amplitude of the isotropically distributed input signal that achieves the capacity of the block Rayleigh faded channel, has bounded support. Additionally, we show through an information theoretic analysis followed by numerical evaluations that, starting from a single amplitude scheme, introduction of a zero amplitude mass point increases the mutual information. In other words, transmitting nothing (keeping the antennas silent) for some portion of the time is a better strategy than transmitting all the time.** In certain cases the portion of time for which the antennas should be kept silent can be quite significant. Although the analytical tools are developed for the SISO case, it is conjectured that the same is true for the MIMO case. Very recently (concurrent to this work), [43] showed that for the block fading channel, the capacity achieving signal distribution comprises of unitary signals but with discrete amplitude levels. A number of related results for the IID (independent and identically distributed) fading channel *i.e.* $T = 1$, and also the closely associated non-coherent AWGN channel have appeared in literature [14, 39–41].

1.3.3 System Design for the Very Fast Fading Channel

For very fast fading channels where one is forced to operate at low SNR and low rates, one can choose either to ignore any correlation between successive symbols and operate as if the channel experiences independent fading ($T = 1$) at each time instance or use the correlation between successive symbols and increase the achievable rate. The first approach is a legitimate one if very low complexity implementations are desired. However, as we show in Chapter 4, the potential loss for ignoring even the small correlation which is present for very fast fading channels is significant. Furthermore, from Chapter 3 and [14,39–41,43], there is ample evidence that a peaky transmission in time (*i.e.*, being silent for a significant portion of the transmission) has potential performance benefits for various channels including the channel under consideration. For instance, assuming that a fast fading channel can be adequately modelled by a block-independent fading channel, we show that there is roughly 1.8 dB to be gained by such peaky transmission for transmission rates of interest. Motivated by this potential gain, **we introduce a simple technique to obtain some of the gain promised by information theory while adding minimal complexity to the overall system.**

1.3.4 Joint Modulation and Code Design

Although the observations made following (1.14) are inherent strengths of the systematic constellation design technique, they might be restrictive when considered in conjunction with conventional codes[5]. Specifically the idea behind a joint modulation and code design approach is to allocate resources so that there will be maximum gain. A similar approach taken for the Additive White Gaussian Noise

[5] *e.g.* convolutional codes.

(AWGN) channel, led to the construction of asymmetric PAM, PSK and QAM constellations that showed some performance gain over the symmetric version.

Taking a cue from this, **we consider the joint modulation and code design problem in Chapter 5, with the hope that when they are optimized together, the performance might be better than that when code design and modulation design are considered separately. To this end, the exact pairwise error probability for coded systems spanning multiple coherence interval blocks is analyzed in Section 5.3.**

CHAPTER 2

Receiver Algorithms and System Design for Fast Fading Channels

In this chapter, we consider various receiver algorithms for the case of non-coherent reception and propose a novel family of low complexity, near optimal (with respect to ML performance) soft iterative demodulator for pilot assisted transmission schemes. In particular for pilot assisted modulations we consider designing receivers with increasing degree of sophistication. The first one utilizes pilots at the transmitter and a simple non-iterative channel estimation algorithm at the receiver. We show that these systems are exactly equivalent, in terms of performance analysis and design, to appropriately "degraded" systems having perfect CSI at the receiver. The second scheme utilizes pilots and a well justified and simple suboptimal iterative detection/estimation algorithm. It is shown that when turbo-like codes are considered in conjunction with this transmission scheme and receiver algorithms, the optimized unitary constellations investigated in the literature are inferior to simple pilot-assisted constellations. The performance of the proposed scheme is compared with some well known receiver schemes such as a soft Expectation Maximization (EM) algorithm and a soft iterative Sphere Decoder.

Early designs for the non-coherent fading channel were based on the work of [34]

who proved that for the case of high SNR or $T \gg M$, signals that are isotropically distributed and unitary (*i.e.*, $\mathbf{X}^*\mathbf{X} = (T\gamma_s/M)\mathbf{I}_M$ achieve the capacity of a block Rayleigh fading channel. Systematic procedures for generating these unitary constellations [29, 35] involved pairwise error probability bounds for high SNR and the asymptotic union bounds on the error probability. We refer to constellations generated by methods in [29] as systematically generated unitary constellations (SGUCs) while the unitary constellations from [35] that were generated using the asymptotic union bound (AUB) are referred to as AUB constellation. Before moving further, we note that there are two basic disadvantages associated with these constellations: (i) lack of structure, which means that an iterative demodulator has to sum over all the possible signals in the constellations to produce bit reliabilities; (ii) the constellations have been optimized with criteria that are valid at high SNR. However, when coded systems are considered, other factors such as the number of "nearest" neighbors are critical.

One might question the validity of using these constellations for the fast fading scenario or for low rates and low SNR (as opposed to the constellations designed in [5] for instance). These issues are deferred to the succeeding chapter and we continue to use these single amplitude unitary constellations (SGUCs and AUBs) for the sake of comparisons.

2.1 Pilot Symbol Assisted Modulation

The proposed constellations $\mathcal{X} \subset \mathbb{C}^{T\times M}$ consist of 2^l signals and the notation $\mathbf{X}(b_1, \ldots, b_l)$ is used to show the explicit mapping[1] of the $l = TR_m$ bits to the transmitted signal $\mathbf{X}$.

[1]Recall the system model introduced in Section 1.1.2. The modulator rate is $R_m = \frac{l}{T}$ bits per complex dimension and so $l = TR_m$ bits map a symbol to a block.

Assumption A: We impose some additional structure on $\mathbf{X}$ by assuming that

$$\mathbf{X}^\top = \left(\mathbf{X}_{pilot}^\top, \mathbf{X}_{data}^\top\right) \tag{2.1}$$

The specific structure of $\mathbf{X}_{pilot} \in \mathbb{C}^{M\times M}$ and $\mathbf{X}_{data} \in \mathbb{C}^{T-M\times M}$ will be described in later sections as the need arises. We emphasize that although a pilot transmission followed by data transmission is proposed, and a simple non-iterative estimation/detection receiver (PO detector) is a natural choice, we will also propose a novel low-complexity near-optimal non-coherent demodulator in the sequel.

2.2 Receiver Algorithms

In this section, we present the details of the receiver that is comprised of the demodulator and the LDPC decoder (see Fig. 1.1). The LDPC decoder uses the standard sum-product algorithm based on the bit reliabilities received from the demodulator. This message passing algorithm is well discussed in literature and for the sake of brevity will be omitted here.

The demodulator has to provide the decoder with extrinsic information regarding the $l = TR_m$ bits. For each bit b_i, $i \in \{1, \ldots, l\}$, the demodulator generates a message (in the logarithmic domain) of the form

$$\Lambda_i(b) = \log \sum_{\mathbf{b}:b_i=b} p(\mathbf{Y}|\mathbf{X})p(\mathbf{b}) - \log p_i(b) \qquad b \in \{0,1\}, \tag{2.2}$$

where $p(\mathbf{b}) = \prod_{i=1}^{l} p_i(b_i)$ are the a-priori probabilities generated by the LDPC decoder (initially set to 0.5 each), and the dependence of $\mathbf{X}$ on $\mathbf{b}$ is implicit.

The following subsections deal with the description of the various demodulators that interface with the LDPC decoder.

2.2.1 MAP detection for the Non-Coherent Fading Channel

For the case when CSI is not known at the receiver, (2.2) can be simplified to the following under the assumption that $\mathbf{X}^*\mathbf{X} = \mathbf{I}_M$, $\forall\ \mathbf{X} \in \mathcal{X}$

$$\Lambda_i(b) = \log \sum_{\mathbf{b}:b_i=b} \exp\left(\frac{T\,Tr(\mathbf{Y}^*\mathbf{X}\mathbf{X}^*\mathbf{Y})}{N_0(MN_0+T)}\right) p(\mathbf{b}) - \log p_i(b) \tag{2.3}$$

Note that the expression in (2.3) involves summation over $2^{TR_m}/2$ terms, thus implying $O(TR_m 2^{TR_m})$ complexity for the evaluation of all soft decisions. This complexity can be quite prohibitive even for small blocklengths.

2.2.2 Pilot-Only (PO) Detector

With the modulation structure presented in Assumption A, as mentioned earlier, the simplest detector is one that performs explicit estimation followed by "coherent" detection. Such a detector is referred to as the PO detector in this thesis. In this subsection, we analyze the statistics of the message that the PO detector provides to the LDPC decoder. In the sequel we show that there is an equivalence between PO detection and the ideal coherent detection under perfect CSI at the receiver.

For notational ease in the following analysis, we set the number of receive antennas to $N = 1$. In this case, M of the T channel uses in $\mathbf{X}$ are utilized to transmit pilot symbols to aid the receiver in performing channel estimation. Specifically, the structure of the pilot and data part of $\mathbf{X}$ is set as follows (this is a specialization of the structure in Assumption A)

$$\mathbf{X}_{pilot}^\top = \sqrt{\gamma_p}\ \mathbf{I}_M, \qquad \mathbf{X}_{data}^\top = (\mathbf{x}_{M+1}, \ldots, \mathbf{x}_T), \tag{2.4}$$

where γ_p represents the energy spent on the pilot symbol transmission. This implies the following structure for the received signal

$$\mathbf{y}^\top = \left(\mathbf{y}_{pilot}^\top, \mathbf{y}_{data}^\top\right) = \left((y_1, \ldots, y_M), (y_{M+1}, \ldots, y_T)\right). \tag{2.5}$$

Note that $\mathbf{x}_i \in \mathbb{C}^{M\times 1}$ is the vector of transmitted signals in the i^{th} time instant. To perform the following analysis, we make the additional assumption that

Assumption B: The total power radiated from all antennas at any time instant during data transmission is constant, *i.e.*, $\|\mathbf{x}_i\|^2 = \gamma_d, i \in \{M+1,\ldots,T\}$.

Energy considerations force the following relation between T, M, γ_p, γ_d and γ_s

$$M\gamma_p + (T-M)\gamma_d = T\gamma_s. \tag{2.6}$$

The PO detector provides the likelihood information corresponding to vector $\mathbf{x}_i$, based only on the observation y_i and $\mathbf{y}_{pilot}$. Denoting $\tilde{\mathbf{y}}_i = (\mathbf{y}_{pilot}^\top, y_i)^\top$, the log-likelihood function for the received signal conditioned on transmission of vector $\mathbf{x}_i$ ($i \in \{M+1,\ldots,T\}$) can be written as

$$\begin{aligned} q_{i,po} &= \log p(\mathbf{y}_{pilot}, y_i | \mathbf{X}_{pilot}, \mathbf{x}_i) = \log p(\tilde{\mathbf{y}}_i | \tilde{\mathbf{X}}_i) \\ &= -\log(\pi^{M+1}\det(\mathbf{K}_i)) - \tilde{\mathbf{y}}_i^* \mathbf{K}_i^{-1} \tilde{\mathbf{y}}_i, \end{aligned} \tag{2.7}$$

where, $\mathbf{K}_i = \mathbf{I}_{M+1} + \tilde{\mathbf{X}}_i \tilde{\mathbf{X}}_i^*$ and $\tilde{\mathbf{X}}_i = \left(\sqrt{\gamma_p}\,\mathbf{I}_M, \mathbf{x}_i\right)^\top$. After some simplification involving matrix inversion and determinant identities[2], the above expression can be reduced to

$$q_{i,po} = C + \frac{2\sqrt{\gamma_p}\,\Re(\, y_i^* \mathbf{x}_i^\top \mathbf{y}_{pilot})}{1+\gamma_p+\gamma_d} - \frac{\gamma_p\,|\mathbf{x}_i^\top \mathbf{y}_{pilot}|^2}{(1+\gamma_p)(1+\gamma_p+\gamma_d)} \tag{2.8}$$

where the constant C is independent of $\mathbf{x}_i$.

2.2.3 Equivalence Between Pilot-Only and Perfect CSI Detectors

To analyze the perfect CSI detector, we remove the "no CSI at the receiver" assumption and Assumption A and assign the following structure to the transmitted

[2] $(\mathbf{A}+\mathbf{BCD})^{-1} = \mathbf{A}^{-1} - \mathbf{A}^{-1}\mathbf{B}(\mathbf{C}^{-1}+\mathbf{DA}^{-1}\mathbf{B})^{-1}\mathbf{DA}^{-1}$
$\det(\mathbf{I}+\mathbf{AB}) = \det(\mathbf{I}+\mathbf{BA})$

and received signal (again under the $N = 1$ receive antenna assumption)

$$\mathbf{X} = (\mathbf{x}_1, \mathbf{x}_2, \ldots, \mathbf{x}_T)^\top \tag{2.9}$$

$$\mathbf{y} = (y_1, y_2, \ldots, y_T)^\top, \tag{2.10}$$

i.e., the pilot part of the signal in (2.1) is also used to transmit information. Now Assumption B is substituted by

Assumption B': The total power radiated from all antennas at any time instant is constant, *i.e.*, $\|\mathbf{x}_i\|^2 = \gamma_s, i \in \{1, \ldots, T\}$.

At the i^{th} time instant, the conditional distribution of the received signal for a given transmitted vector $\mathbf{x}_i$ and a given channel realization $\mathbf{h}$, is complex Gaussian with mean $\mathbf{x}_i^\top \mathbf{h}$ and variance 1. Thus the log likelihood function can be written as

$$\begin{aligned} q_{i,c} &= \log p(y_i|\mathbf{x}_i, \mathbf{h}) = -\log(\pi) - |y_i - \mathbf{x}_i^\top \mathbf{h}|^2 \\ &= C' + 2\Re(y_i^* \mathbf{x}_i^\top \mathbf{h}) - |\mathbf{x}_i^\top \mathbf{h}|^2. \end{aligned} \tag{2.11}$$

We now proceed with the proof of the equivalence between the PO and the perfect CSI systems. First observe that in both (2.8) and (2.11), the constants C and C' do not depend on $\mathbf{x}_i$, and thus they do not influence the overall calculation of the bit reliabilities. Under the coherent case, defining $z_{i,c} \stackrel{\text{def}}{=} \mathbf{x}_i^\top \mathbf{h}$, (2.11) can be rewritten as

$$q_{i,c} = C' + 2\Re\left(y_i^* z_{i,c}\right) - |z_{i,c}|^2. \tag{2.12}$$

Similarly, for the PO detector, setting

$$y_i' \stackrel{\text{def}}{=} \sqrt{\frac{1+\gamma_p}{1+\gamma_p+\gamma_d}}\, y_i \tag{2.13}$$

$$z_{i,po} \stackrel{\text{def}}{=} \sqrt{\frac{\gamma_p}{(1+\gamma_p)(1+\gamma_p+\gamma_d)}}\, \mathbf{x}_i^\top \mathbf{y}_{pilot} \tag{2.14}$$

(2.8) can be rewritten as

$$q_{i,po} = C + 2\Re\left(y_i'^* z_{i,po}\right) - |z_{i,po}|^2. \tag{2.15}$$

Given that $\mathbf{x}_i$ was transmitted, the random variables y_i and $z_{i,c}$ that determine the statistics of the message $q_{i,c}$ in (2.12) are jointly complex Gaussian with mean $\mathbf{0}$ and covariance matrix $\mathbf{K}_{i,c}$ given by

$$\mathbf{K}_{i,c} = \begin{pmatrix} 1+\gamma_s & \gamma_s \\ \gamma_s & \gamma_s \end{pmatrix}. \tag{2.16}$$

Similarly for the PO detector, under the assumption that $\mathbf{x}_i$ was transmitted, the random variables y_i' and $z_{i,po}$ that determine the statistics of the message $q_{i,po}$ are jointly complex Gaussian with mean $\mathbf{0}$ and covariance matrix $\mathbf{K}_{i,po}$ given by

$$\mathbf{K}_{i,po} = \begin{pmatrix} 1+\gamma_s' & \gamma_s' \\ \gamma_s' & \gamma_s' \end{pmatrix}, \tag{2.17}$$

with

$$\gamma_s' = \frac{\gamma_p \gamma_d}{1+\gamma_p+\gamma_d} \tag{2.18}$$

Comparing equations (2.12), (2.16) with (2.15), (2.17), respectively, we conclude that the messages $q_{i,c}$ and $q_{i,po}$ have exactly the same statistics but at different SNRs. In particular, a PO system (with non-iterative estimation) with parameters γ_d and γ_p is equivalent to a perfect CSI system with parameter γ_s' given by (2.18). For more than 1 receiver antenna, (*i.e.*, when $N > 1$), the same equivalence holds since it is clear that the messages $q_{i,c}$ and $q_{i,po}$ will be the sums of N *independent* terms of the form (2.11) and (2.15), respectively.

This type of equivalence between the perfect CSI detection and the PO detection schemes was initially shown through the computation of the actual message density for $M = N = 1$ and assuming antipodal signaling in [21]. While the equivalence is shown here through an examination of the statistics of the message exchanged in an iterative decoding, a similar equivalence between PO detection and perfect CSI

detection was shown in [7]. Also interesting to note is that the relationship (2.18) comes up in the capacity lower bound evaluated in [26] showing the fundamental nature of this result. An important implication of this equivalence is that analysis for a given code can be performed once for the perfect CSI case; then for any PO system with parameters γ_p and γ_d (or equivalently γ_p and γ_s) the performance can be obtained from the corresponding perfect CSI system with γ_s' given in (2.18). Using (2.18) and (2.6), for a given γ_s it is easy to optimize γ_p, the pilot energy, so as to get the largest γ_s'. An equally important implication of this equivalence is that code design for both these cases is unified: a code that is optimal for the perfect CSI channel will also be optimal when no CSI is available at the receiver and PO demodulation/detection is employed to generate the appropriate bit reliabilities that will be fed to the decoder. For instance, degree optimization of an LDPC code need to be performed only once assuming perfect CSI. If this code is optimal in the perfect CSI scenario, it will also be optimal in the non-coherent scenario under PO detection, with the only adjustment being the pilot energy allocation.

2.2.4 Soft Expectation Maximization Demodulator

The EM algorithm introduced first in [9] is widely used in many digital communications applications as a low complexity receiver with good performance. The details of the EM demodulator are described below. The channel model for a SISO system employing antipodal signalling is the same as (1.3) except it is specialized to the case of SISO systems. The only fact we wish to reiterate is that γ_p (the pilot energy) and γ_d (the average data symbol energy) are related as $\gamma_p + (T-1)\gamma_d = T\gamma_s$ where γ_s represents the average energy per transmitted symbol. While the final specialization of the results below applies to BPSK transmission, it is clearly easy to extend

this method to other modulation alphabets and we provide the starting points from which the relevant equations can be obtained for higher order modulations.

The EM algorithm is an iterative procedure itself and involves the computation of a new channel estimate h_k at the beginning of the k^{th}, $k = 0, 1, 2, \ldots$ iteration. The Expectation step or (E-step) calculation is carried out as follows

$$\begin{aligned} Q(h, h_k) &= \mathbb{E}_{\mathbf{x}|\mathbf{y},h_k} \{\log(f(\mathbf{y}, \mathbf{x}, h\} && (2.19)\\ &= \mathbb{E}_{\mathbf{x}|\mathbf{y},h_k} \left\{ -\frac{\|\mathbf{y} - \mathbf{x}h\|^2}{N_0} - |h|^2 \right\} && (2.20)\\ &= -|h|^2 - \sum_{\mathbf{x}} \sum_{i=1}^{N} |y_i - x_i h|^2 P(\mathbf{x}|\mathbf{y}, h_k) && (2.21)\\ &= -|h|^2 - \sum_{i=1}^{N} \sum_{x_i} |y_i - x_i h|^2 P(x_i|\mathbf{y}, h_k) && (2.22)\\ &= -|h|^2 - \|\mathbf{y}\|^2 - \sum_{i=1}^{N} \sum_{x_i} \left(|x_i|^2 |h|^2 - 2\Re\{y_i^* x_i h\} \right) P(x_i|\mathbf{y}, h_k) && (2.23) \end{aligned}$$

where to get to (2.20), constants have been dropped.

The M-step involves maximizing $Q(h, h_k)$ with respect to h and setting the maximizing h as the channel estimate in the next iteration *i.e.* $h_{k+1} = \arg\max_h Q(h, h_k)$. Differentiating $Q(h, h_k)$ with respect to h and setting it to 0, we find

$$h_{k+1} = \frac{\sum_{i=1}^{N} \sum_{x_i} \Re\{y_i^* x_i\} P(x_i|\mathbf{y}, h_k)}{1 + \sum_{i=1}^{N} |x_i|^2 \sum_{x_i} P(x_i|\mathbf{y}, h_k)} \tag{2.24}$$

Under the assumption that all signals in the modulation alphabet have equal energy γ_d, we can simplify (2.24) as

$$h_{k+1} = \frac{\sum_{i=1}^{N} y_i \left(\sum_{x_i} x_i^* P(x_i|\mathbf{y}, h_k) \right)}{T\gamma_s + 1} \tag{2.25}$$

In either case (equal or non-equal energy signalling), $P(x_i|\mathbf{y}, h_k)$ is calculated using Bayes rule as

$$P(x_i|\mathbf{y}, h_k) = \frac{P(y_i|x_i, h_k) P(x_i)}{\sum_{x_j} P(y_i|x_j, c_k) P(x_j)} \tag{2.26}$$

For the special case of BPSK transmission, we can further simplify (2.23) and (2.25) by converting to the log-likelihood domain, *i.e.* setting

$$\lambda_{i,soft}^{(k)} = \log \frac{P(x_i = \sqrt{\gamma_d}|\mathbf{y}, h_k)}{P(x_i = -\sqrt{\gamma_d}|\mathbf{y}, h_k)} \tag{2.27}$$

$$\lambda_{i,apriori} = \log \frac{P(x_i = \sqrt{\gamma_d})}{P(x_i = -\sqrt{\gamma_d})} \tag{2.28}$$

and using (2.26), it is possible to rewrite (2.25) and (2.27) and can be re-written as

$$h_{k+1} = \frac{\sqrt{\gamma_p} y_1}{T\gamma_s + 1} + \frac{\sum_{i=2}^{N} \sqrt{\gamma_d} \tanh(\frac{\lambda_{i,soft}^{(k)}}{2}) y_i}{T\gamma_s + 1} \tag{2.29}$$

$$\lambda_{i,soft}^{(k)} = 4\sqrt{\gamma_d}\, \Re\{y_i h_k^*\} + \lambda_{i,apriori} \qquad i = 2, \ldots, T \tag{2.30}$$

The EM algorithm is started by setting h_0 as the channel estimate obtained from the pilot symbol, namely $h_0 = \frac{\sqrt{\gamma_p}\, y_1}{T\gamma_s + 1}$ and then iterating between (2.30) and (2.29). $\lambda_{i,apriori}$ is set to 0 (corresponding to equally likely input) for the first time the EM algorithm is used. Subsequently the LDPC decoder provides fresh values for $\lambda_{i,apriori}$. From the spirit of the algorithm it is seen that each EM iteration serves to improve the estimate of the channel from both the pilot and the data transmissions and subsequently coherent detection with the updated channel estimate is carried. Hence the EM-detector is expected to perform better than the PO detector which is a non-iterative estimation/coherent detection algorithm.

For more bandwidth efficient modulations such as QPSK, QAM and PAM, the simplifications from (2.24) to (2.29) and (2.30) do not apply and slightly more complex equations result. In the sequel, the performance of the EM algorithm is compared to the other algorithms discussed in this section for the case of BPSK and Pulse Amplitude Modulation (PAM) signalling schemes on a SISO system.

2.2.5 Soft Sphere Decoder

The sphere decoder is a well known algorithm that was originally designed to search for the MAP estimate in an efficient manner. However recently with the proliferation of soft iterative detection modules, a soft sphere detector is well motivated and the details of the soft sphere detector are presented below.

The channel model and set up is identical to (1.3) and is omitted here. Note that for the sphere decoder to have reduced complexity, the transmitted signals have to belong to a subset of a lattice [16].

Converting the observation vector to the real equivalent form, we have

$$\underbrace{\begin{pmatrix} \Re\{\mathbf{y}\} & \Im\{\mathbf{y}_i\} \end{pmatrix}}_{\mathbf{Y}} = \underbrace{\begin{pmatrix} \Re\{h\} & -\Im\{h\} \\ \Im\{h\} & \Re\{h\} \end{pmatrix}}_{\mathbf{H}} \underbrace{\begin{pmatrix} \Re\{\mathbf{y}\} & \Im\{\mathbf{y}\} \end{pmatrix}}_{\mathbf{X}} + \underbrace{\begin{pmatrix} \Re\{\mathbf{n}\} & \Im\{\mathbf{n}\} \end{pmatrix}}_{\mathbf{N}} \tag{2.31}$$

Due to the special nature of $\mathbf{x}$, $\mathbf{Y}$ given $\mathbf{x}$ is normally distributed with mean $\mathbf{0}$ and covariance matrix $\frac{1}{2}(\mathbf{x}\mathbf{x}^* + \mathbf{I}_T)$. The MAP detection rule for detection of the transmitted sequence is as follows.

$$\hat{\mathbf{x}}_{MAP} = \arg\max p(\mathbf{Y}|\mathbf{X})p(\mathbf{X}) \tag{2.32}$$

$$= \arg\max \log(p(\mathbf{Y}|\mathbf{X})p(\mathbf{X})) \tag{2.33}$$

$$= \arg\max \frac{\mathbf{x}^\top \mathbf{Y}\mathbf{Y}^\top \mathbf{x}}{T\gamma_s + 1} + \sum_{k=1}^{T} \log(P(x_k)) \tag{2.34}$$

$$= \arg\min \frac{\rho \mathbf{x}^\top \mathbf{x} - \mathbf{x}^\top \mathbf{Y}\mathbf{Y}^\top \mathbf{x}}{T\gamma_s + 1} - \sum_{k=1}^{T} \log(P(x_k)) \tag{2.35}$$

$$= \arg\min \frac{1}{T\gamma_s + 1} \mathbf{x}^\top \underbrace{\left(\rho \mathbf{I}_N - \mathbf{Y}\mathbf{Y}^\top\right)}_{\mathcal{H}} \mathbf{x} - \sum_{k=1}^{T} \log(P(x_k)) \tag{2.36}$$

where $\rho = Tr\left(\mathbf{Y}^\top \mathbf{Y}\right)^3$. Defining

$$\mu(\mathbf{R},\mathbf{x})^{MAP} \stackrel{\text{def}}{=} \frac{\mathbf{x}^\top \mathcal{H} \mathbf{x}}{T\gamma_s + 1} - \sum_{k=1}^{T} \log(P(x_k)) \tag{2.37}$$

and performing the Cholesky decomposition of $\mathcal{H}$ as $\mathcal{H} = \mathbf{R}^\top \mathbf{R}$, where $\mathbf{R}$ is a real upper-triangular matrix, we can rewrite the MAP detection rule as

$$\hat{\mathbf{x}}_{MAP} = \arg\min \mu(\mathbf{R},\mathbf{x})^{MAP} = \arg\min \frac{\mathbf{x}^\top \mathbf{R}^\top \mathbf{R} \mathbf{x}}{T\gamma_s + 1} - \sum_{k=1}^{N} \log(P(x_k)) \tag{2.38}$$

The extrinsic information ($L_e(k)$) computation is as follows

$$L_e(k) = L_s(k) - L_a(k) \tag{2.39}$$

$$L_s(k) = \log\left(\frac{\sum_{\tilde{\mathbf{x}}|\tilde{x}_k=+1} e^{\frac{\tilde{\mathbf{x}}^\top \mathbf{Y}\mathbf{Y}^\top \tilde{\mathbf{x}}}{T\gamma_s+1} + \log(P(\tilde{\mathbf{x}}))}}{\sum_{\tilde{\mathbf{x}}|\tilde{x}_k=-1} e^{\frac{\tilde{\mathbf{x}}^\top \mathbf{Y}\mathbf{Y}^\top \tilde{\mathbf{x}}}{T\gamma_s+1} + \log(P(\tilde{\mathbf{x}}))}}\right) \tag{2.40}$$

$$L_a(k) = \log\left(\frac{P(x_k=+1)}{P(x_k=-1)}\right) \tag{2.41}$$

Thus in the computation of $L_s(k)$, instead of performing the metric computation over all sequences in the code space, one can limit the computation to those terms that contribute significantly to the exponent. In turn this means that only those sequences that produce small metric in (2.38) need be searched over. The Fincke-Phost algorithm or the sphere decoding algorithm is used to perform this, wherein sequences that have

$$\frac{\mathbf{x}^\top \mathbf{R}^\top \mathbf{R} \mathbf{x}}{T\gamma_s + 1} - \sum_{k=1}^{N} \log(P(x_k)) \leq r^2 \tag{2.42}$$

for a suitably chosen r are stored and used. The structure of $\mathbf{R}$ allows an efficient tree-search to be performed on the constellation. The choice of the radius r depends in turn on the statistics of the RHS of (2.38).

Following [47], it is seen that $\frac{\mathbf{x}\mathbf{R}^\top \mathbf{R}\mathbf{x}^\top}{T}$ is χ^2 distributed with $2(T-1)$ degrees of freedom. Notice that the ML metric detection rule is closely related to (2.38),

[3]Doing this causes $\mathcal{H}$ to be a positive definite matrix and hence Cholesky decomposable.

since it is obtained by omitting the second term from (2.38). It is thus possible to determine a radius r_k such that $\mu(\mathbf{R},\mathbf{x})^{ML} = \frac{1}{T\gamma_s+1}\mathbf{x}\mathbf{R}^\top\mathbf{R}\mathbf{x}^\top < r_k^2$ with probability $(1-\epsilon^k)$ (let $\epsilon = 0.1$ say). If no solution is found inside a sphere of radius r_k, then k is incremented by 1 and the search is repeated in a sphere of radius r_{k+1}, where r_{k+1} is determined by a look up table of the χ^2 distribution function. This goes on until at least one solution is found so that the soft information can be calculated.

Note that for a given radius r, the second term in (2.38), being negative serves to increase $\mu(\mathbf{R},\mathbf{x})^{ML}$. Thus if $\mu(\mathbf{R},\mathbf{x})^{MAP} < r^2$, then $\mu(\mathbf{R},\mathbf{x})^{ML} < r^2$. In other words, for a given radius r, $\epsilon^{ML} \leq \epsilon^{MAP}$.

Clearly, this technique of identifying a subset of all possible transmissions and performing the required marginalization on this set, decreases the complexity of the receiver. However, at low SNR there is a chance that the actual transmitted sequence is not in the set of sequences satisfying (2.42). This could give some loss in performance. However at high SNR, this is unlikely to happen and the sphere detector can be expected to achieve the performance of the MAP detector with cubic complexity [27] with respect to TR_m.

2.2.6 Near-Optimal Low-Complexity Iterative Receiver

Theoretical Background

Since in the PO scheme described earlier, non-iterative channel estimation/ detection followed by decoding is performed, it is expected to have poorer performance relative to a receiver employing joint iterative estimation/detection. On the other hand, the generation of optimal bit reliabilities as shown in (2.2) involves summation over 2^{TR_m-1} terms, thus implying $O(TR_m 2^{TR_m})$ complexity for the evaluation of all soft decisions. This complexity can be quite prohibitive even for small block lengths. To bridge the gap between the optimal detector and the simple PO

receiver, we observe that the high complexity of the MAP detector is due to the lack of structure of the modulations proposed in [29,35] and attempt to address this by considering PSAM schemes as in Assumption A with some additional structure given below.

Assumption A1: Consider PSAM constellations with the following structure

$$\mathbf{X}_{pilot}^{\top} = \sqrt{\gamma_p}\,\mathbf{I}_M, \qquad \mathbf{X}_{data}^{\top} = \begin{pmatrix} \mathbf{S}_2^{\top} & \dots & \mathbf{S}_t^{\top} \end{pmatrix} \tag{2.43}$$

where $T = tM$ (T is assumed to be a multiple of M), and all matrices $\mathbf{S}_i$'s have the same structure. These $\mathbf{S}_i$'s are referred to as sub-symbols in the sequel. Note that the assumption $T = tM$ is not restrictive since in reality one is faced with continuous fading with some given dynamics. In such case, the block size T is a design parameter that can be chosen as a multiple of M.

An example for the case of $M = 1$, is to transmit a constant first sub-symbol as the pilot and consider a PSK based alphabet for the remaining data sub-symbols. For systems employing multiple transmit antenna, some additional structure can be used to obtain transmit diversity. As an example, for $M = 2$, $T = 6$, we use the well known orthogonal space-time block code - Alamouti code [1] - structures for the sub-symbols so as to obtain diversity gain. The symbol $\mathbf{X}$ consists of $t = 6/2 - 1 = 2$ Alamouti sub-symbols $\mathbf{S}_i$, $i = 2, 3$, each one of which is constructed from 2 PSK (or QAM) signals a_i and b_i as follows

$$\mathbf{S}_i(a_i, b_i) = \alpha \begin{bmatrix} a_i & -b_i^* \\ b_i & a_i^* \end{bmatrix}, \tag{2.44}$$

where α is selected so that the power constraint is satisfied.

Description of Algorithm

We now describe a family of near-optimal joint estimation and detection algorithms for the approximate evaluation of the $\Lambda_i(b)$ bit metrics in (2.2). The structure assumed for the signal matrix in Assumption A1 is essential for the algorithm described below to have linear complexity in T.

To aid the precise description of the algorithm, we introduce the well known MAPSqD receivers for the coherent and the non-coherent Rayleigh block fading channel, as follows

$$\begin{aligned}
\hat{\mathbf{X}}^{(C)} &= p(\mathbf{b}|\mathbf{Y},\mathbf{H}) \\
&= \arg\max_{\mathbf{b}} \log p(\mathbf{b}) - \|\mathbf{Y}-\mathbf{X}\mathbf{H}\|^2 \\
&= \arg\max_{\mathbf{b}} \log p(\mathbf{b}) + 2\sum_{i=2}^{t} \Re\{\mathrm{Tr}\{\mathbf{Y}_i^*\mathbf{S}_i\mathbf{H}\}\} - \|\mathbf{X}\mathbf{H}\|^2 \qquad (2.45a) \\
\hat{\mathbf{X}}^{(NC)} &= p(\mathbf{b}|\mathbf{Y}) \\
&= \arg\max_{\mathbf{b}} \Lambda(\mathbf{X}) \qquad (2.45b)
\end{aligned}$$

$$\text{where,} \qquad \Lambda(\mathbf{X}) \stackrel{\text{def}}{=} \log p(\mathbf{b}) + Tr\{\mathbf{Y}^*\mathbf{X}(\mathbf{I}_M + \mathbf{X}^*\mathbf{X})^{-1}\mathbf{X}^*\mathbf{Y}\} - \log(\det(\mathbf{I}_M + \mathbf{X}^*\mathbf{X}))$$

where the structure of Assumption A1 is used in (2.45a), and $\mathbf{Y}^\top = [\mathbf{Y}_1^\top, \mathbf{Y}_2^\top, \ldots, \mathbf{Y}_t^\top]$, with $\mathbf{Y}_i \in \mathcal{C}^{M\times N}$. It is emphasized again that CSI is not available to the receiver and the reason for introducing (2.45a) will be apparent in the description of the algorithm.

The spirit of the algorithm (rather the family of algorithms) is captured in the following statement.

Fact 2.1. *The optimal maximum a-posteriori probability sequence detector* [*37, 38*] *(MAPSqD) estimate* (2.45b) *for uncoded transmission of signals* $\mathbf{X} \in \mathcal{X}$ *with the*

property that $\mathbf{X}^*\mathbf{X}$ *is independent of* $\mathbf{X}$ *over a non-coherent fading channel can equivalently be found by*

1. *Turning the maximization problem in* (2.45b) *into the double maximization problem*

$$\hat{\mathbf{X}}^{(NC)} = \arg\max_{\mathbf{b}} \max_{\hat{\mathbf{H}}} \Lambda(\mathbf{X}, \hat{\mathbf{H}}) \tag{2.46}$$

where $\Lambda(\mathbf{X}, \hat{\mathbf{H}}) \stackrel{def}{=} \log p(\mathbf{b}) + \|\mathbf{Y} - \mathbf{X}\hat{\mathbf{H}}\|^2 - \|\hat{\mathbf{H}}\|^2$

2. *Partitioning the space of channels according to the system of equations*

$$\Lambda(\mathbf{X}_1, \hat{\mathbf{H}}) = \Lambda(\mathbf{X}_2, \hat{\mathbf{H}}) \qquad \mathbf{X}_1 \neq \mathbf{X}_2 \in \mathcal{X} \tag{2.47}$$

Note that the metric in (2.46) *is decomposable into a sum of terms under Assumption A1.*

3. *Taking one channel sample, say* $\tilde{\mathbf{H}}_i$*, from each set in the partition (obtained in Step 2) and compute the set*

$$\mathcal{T} \stackrel{def}{=} \{\tilde{\mathbf{X}}_i | \tilde{\mathbf{X}}_i = \arg\max_{\mathbf{X}} \Lambda(X, \tilde{\mathbf{H}}_i)\} \tag{2.48}$$

4. *Finding the sequence in* $\mathcal{T}$ *that has the maximum non-coherent metric* i.e.

$$\hat{\mathbf{X}}^{(NC)} = \arg\max_{\mathbf{X} \in \mathcal{T}} \Lambda(\mathbf{X}) \tag{2.49}$$

While the formal proof of Fact 2.1 is shown in great detail in [38], we provide some explanation of this statement without delving into the details. The first step in understanding this is that the maximization problem over the set of sequences can actually be turned into a double maximization problem involving the channel realization as well. The metric involved in this double maximization problem is closely

related to the coherent MAP sequence detector (Step 1). By a simple change in the order of the maximization, we find that for a given received vector, not all sequences in the constellation are feasible under the coherent detection rule. This leads to a partition of the channel space, such that all the channel realizations in a given partition always leads to a particular sequence in the constellation. The decomposability of the signal constellation (Assumption A1) reduces the complexity of find this partition of the channel space for a given received signal. Thus corresponding to the partition there exists a subset of sequences in the constellation that can be proved to be a sufficient set of sequences for the purpose of detection, in the sense that the transmitted sequence is definitely in this set. The next step involves essentially performing the maximization of the original non-coherent metric over the sufficient set of sequences obtained above. The fact that this algorithm has polynomial complexity in the sequence length is proved in [38].

Although Fact 2.1 has been stated for the case of uncoded sequences, for the coded case employing iterative demodulation and decoding (similar to our assumptions in Section. 1.1.2) when the demodulator is required to provide the outer decoder with bit reliabilities, it is not necessary for the set of sequences determined from the partition of the channel space to be sufficient. It is this observation that allows the above algorithm to be used for the coded case as described below.

Fact 2.2. *The soft decision metric for a symbol,* i.e. $\lambda_i = \max_{\mathbf{X} \in \mathcal{X} \mid \mathbf{S}_i} \Lambda(X)$*, can be obtained by finding* $\max_{\mathbf{X} \in \overline{\mathcal{T}} \mid \mathbf{S}_i} \Lambda(X)$*, where* $\overline{\mathcal{T}}$ *is the set* $\mathcal{T}$ *augmented by symbol flipped versions of the sequences in* $\mathcal{T}$ *in Fact 2.1.*

The main steps in the demodulator of the low complexity receiver for a PSAM transmission scheme that obeys Assumption A1, are as follows.

---

1. Take Q samples of the channel space $\{\mathbf{H}_1, \ldots, \mathbf{H}_Q\}$.

2. Assuming that $\mathbf{H}_i$ is the channel realization obtain the MAPSqD estimates $\hat{\mathbf{X}}_i^{(C)}, i \in \{1, \ldots, Q\}$, using the coherent metric in (2.45a) and extract the corresponding bit sequences $\hat{\mathbf{b}}_1^0, \ldots, \hat{\mathbf{b}}_Q^0$.

3. For each of $\hat{\mathbf{b}}_i^0$, $i = 1, \ldots, Q$, do the following

   (a) Evaluate the non-coherent metric implied by (2.45b) for $\hat{\mathbf{b}}_i^0$ (recall that $\hat{\mathbf{b}}_i^0$ is a bit vector of size l). Let λ_i^0 denote this metric.

   (b) For each $j = 1, \ldots, l$ do the following

      i. Flip the jth bit of $\hat{\mathbf{b}}_i^0$ resulting in the vector $\hat{\mathbf{b}}_i^j$

      ii. Evaluate the non-coherent metric implied by (2.45b) for $\hat{\mathbf{b}}_i^j$, denoted by λ_i^j.

4. At the end of step 3, there are exactly $P = Q \times (l + 1)$ bit vectors tested $\hat{\mathbf{b}}_i^j$, $i = 1, \ldots, Q$, $j = 0, \ldots, l$, with corresponding metrics λ_i^j, $i = 1, \ldots, Q$, $j = 0, \ldots, l$. The final bit likelihoods are evaluated as follows.

   For each $k = 1, \ldots, l$ do

$$L_k(b) = \max_{\substack{i=1,\ldots,Q \\ j=0,\ldots,l \\ \hat{b}_{i,k}^j = b}} \lambda_i^j, \tag{2.50}$$

   where $\hat{b}_{i,k}^j$ is the kth bit of $\hat{\mathbf{b}}_i^j$.

Several comments are in order regarding the above algorithm. First, looking at the operation of this algorithm, steps 1) and 2) generate a set of Q *coherent* candidate sequences based on *hypothesized* channel estimates $\{\mathbf{H}_i\}_{i=1}^Q$ and the *coherent* MAPSqD metric in (2.45a). It is these steps that can benefit from the structured

modulation schemes as given in (2.43), since for a hypothesized channel estimate $\mathbf{H}$, the maximization in (2.45a) can be performed with complexity $\frac{T}{M}2^{MR_m}$ instead of 2^{TR_m} that is required when using the generally unstructured constellations. It is thus noted that this algorithm cannot be used effectively with the unstructured SGUCs and AUBs.

The bit flipping process (steps 3a and 3b) has also been suggested in other problems (*e.g.*, in [44]). In the present context though, this procedure has a strong theoretical justification since it is closely connected to an exact polynomial-complexity algorithm for evaluating the bit-wise metrics implied by the min-sum algorithm [31, 36, 37]. In particular, it was shown in [31, 36, 37] that one can partition the space $\mathbb{C}^{M\times N}$ of the unknown parameter $\mathbf{H}$, using S hyperplanes into $O(S^{2MN})$ polytopes with the following property. If we sample one channel realization from each polytope and perform steps 2) to 4), the *exact* soft metrics implied by the min-sum algorithm can be obtained. Furthermore, the number of required hyperplanes grows only proportionally with T, which implies an overall worst case polynomial complexity with the coherence time T, regardless of the operating SNR. The details of this optimal procedure are presented in [37]; this brief description is aiming at emphasizing the strong theoretical justification of this family of algorithms.

Regarding the choice of Q we note that its value clearly controls the complexity of the algorithm since the number of candidate sequences examined is directly proportional to Q. The choice of Q is thus determined by complexity and performance considerations.

Choice of hypothesized channel samples

From Fact 2.1, the samples of the channel parameter $\mathbf{H}_i$ are to be chosen such that they each lie on unique polytopes [38] in $\mathcal{C}^{M\times N}$ and thus lead to different candidate sequences. But this would mean that the partition of the channel space be carried out. To avoid this, one can choose samples based on the particular modulation used as is illustrated in the following examples.

Example 2.3. Consider a SISO system with block length T employing pilot symbol assisted BPSK transmission scheme. Let y_i be the observation at the receiver for the i^{th} channel use. Consider the partition of the channel space ($\hat{h} \in \mathcal{C}$), the boundary of which is represented by

$$|y_i - \hat{h}\sqrt{\gamma_d}|^2 = |y_i + \hat{h}\sqrt{\gamma_d}|^2 \tag{2.51}$$

Note that the LHS and RHS of the equation above are respectively the coherent metrics corresponding to the transmission of $\sqrt{\gamma_d}$ and $-\sqrt{\gamma_d}$ respectively. A simple manipulation gives us the equation for the line that performs the partitioning of the channel space

$$\Re\{y_i\hat{h}^*\} = 0 \tag{2.52}$$

This can be done for each $i = 1, 2, \ldots T$ and the resulting lines can be plotted. For even reasonably high SNR, the partition looks like Fig. 2.1. In Fig. 2.1, the dashed lines are for different realizations of y_i. For medium to high SNR, the lines are concentrated along the perpendicular to y_i. Thus in an effort to cover many distinct polytopes without adding unnecessary complexity, 4 channel samples are placed on axes rotated with respect to y_i. However this would mean that the hypothesized channel estimates vary with each channel use even inside a block. So to further

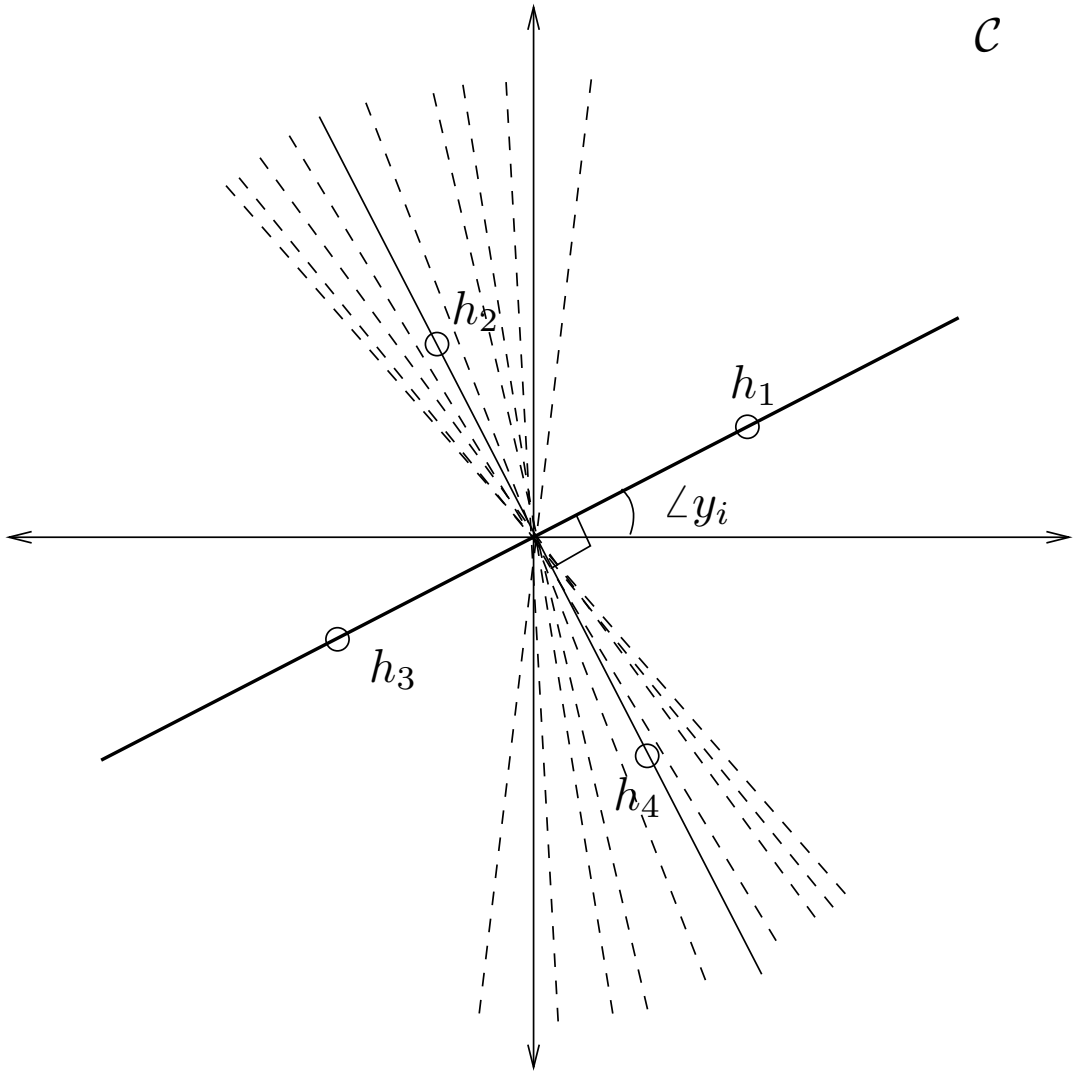

Figure 2.1: Channel space partitioning for BPSK transmission and choice of the channel samples for the proposed low complexity algorithm.

simplify the algorithm, the channel samples are aligned with respect to the minimum mean squared error (MMSE) channel estimate $\tilde{h}$. This can be compactly written as $\hat{h}_i = \tilde{h}e^{\frac{\jmath 2\pi(i-1)}{Q}}$.

We now consider a more elaborate example of the procedure employed to choose the samples, using a non-equal energy modulation alphabet such as the 4-ary PAM.

Example 2.4. Consider a SISO system with block length T employing pilot symbol assisted 4-PAM transmission scheme. Again, let y_i be the observation at the receiver for the i^{th} channel use. Consider the partition of the channel space ($\hat{h} \in \mathbb{C}$), the boundary of which is represented by

$$|y_i - \hat{h}x_1|^2 = |y_i - \hat{h}x_2|^2 \tag{2.53}$$

where $x_i \in \{\pm\sqrt{\frac{\gamma_d}{5}}, \pm 3\sqrt{\frac{\gamma_d}{5}}\}$. When x_1 and x_2 have equal amplitude, a manipulation of (2.53) leads to

$$\Re\{y_i\hat{h}^*\} = 0 \tag{2.54}$$

However, when x_1 and x_2 do not have equal energy, the partition is not described by a line, but by a circle whose equation can easily be found as

$$\left|\hat{h} - \frac{y_i}{4}\right|^2 = \frac{|y_i|^2}{16} \tag{2.55}$$

The circles and line defined by (2.54) and (2.55) partition the space of channels into Fig. 2.2. Again with the intention of sampling as many unique polytopes as possible, the channel samples are aligned with respect to y_i. Due to noise however, one would find many such circles and lines (shown in Fig. 2.2 as dashed lines and dotted circles), all of them passing through the origin. To capture this random effect due to the noise, the samples h_2, h_3, h_5 and h_6 are placed close to the perpendicular

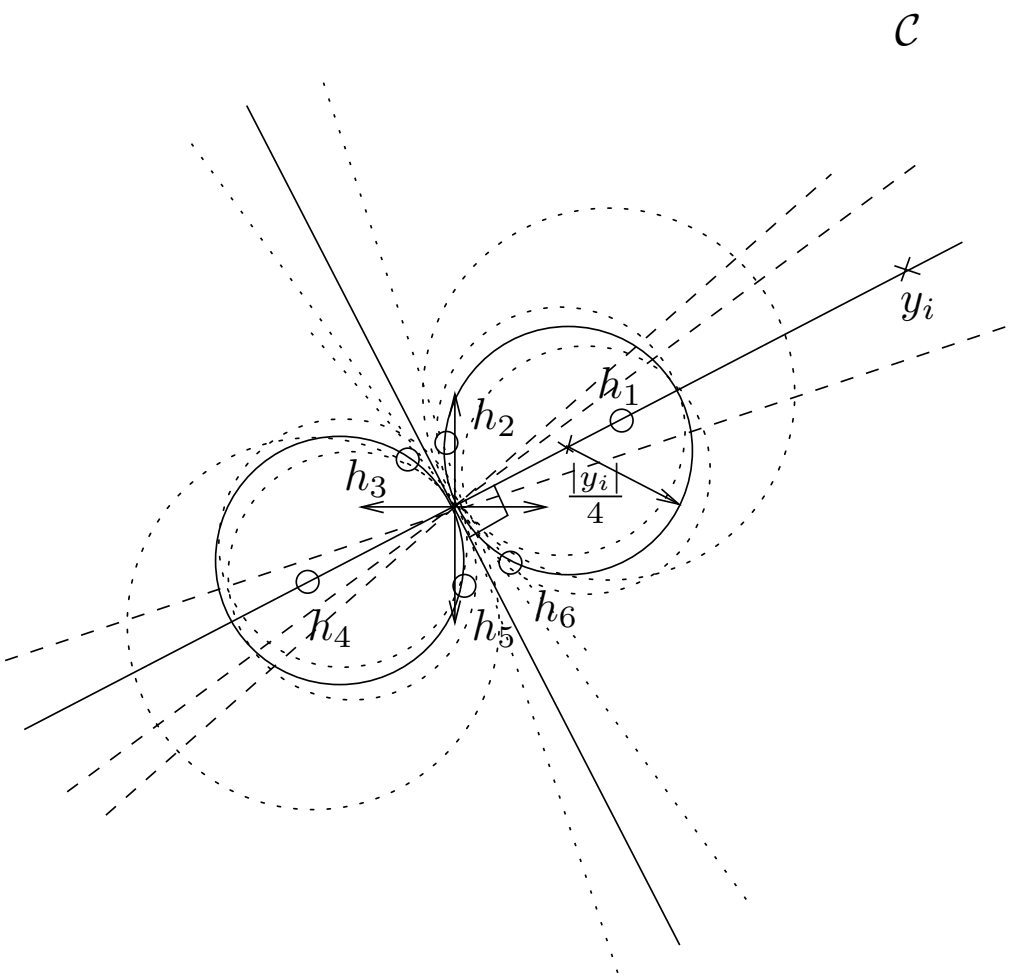

Figure 2.2: Channel space partitioning for 4-PAM transmission and choice of the channel samples for the proposed low complexity algorithm.

to y_i and closer to the origin than h_1 and h_4. Note that the contour on which the samples are placed is in the shape of an ellipse as opposed to the circle in Example 2.3. The receiver's performance has been observed to be very dependent on the placement of these channel samples and hence requires optimization. To simplify matters, the channel samples designed above, are aligned with respect to the MMSE estimate of the channel so that they remain constant for each coherence block (as done in Example 2.3).

We conclude this section by mentioning that the maximization operator in (2.50) can alternatively be substituted by the "max*" operator[4]. Finally, it should be clear from the algorithm description that its overall complexity for the evaluation of all $l = TR_m$ bit metrics at the demodulator is linear in T.

2.3 Design Examples

2.3.1 Receiver Comparison

We now compare the various receivers discussed above for the case of transmission of pilot symbol assisted BPSK, QPSK and 4-PAM alphabets over a non-coherent fading channel, employing single transmit and single receive antenna (SISO).

Pilot Assisted BPSK - SISO

We consider a channel with coherence time $T = 11$ and a SISO system employing pilot symbol assisted (PSA) BPSK modulation. With one channel use devoted to a pilot, the remaining 10 channel uses correspond to 10 data bits. The system employs an outer rate 0.5, regular LDPCC with parameters $(3, 6)$, so that the overall rate is 0.4545 bits per complex dimension. The receiver algorithms considered are the PO, EM, soft sphere detector, the ML demodulator and the proposed fast algorithm. The

[4] $\max^*(x, y) = \max(x, y) + \ln(1 + \exp(-|x - y|) = \ln(\exp(x) + \exp(y))$

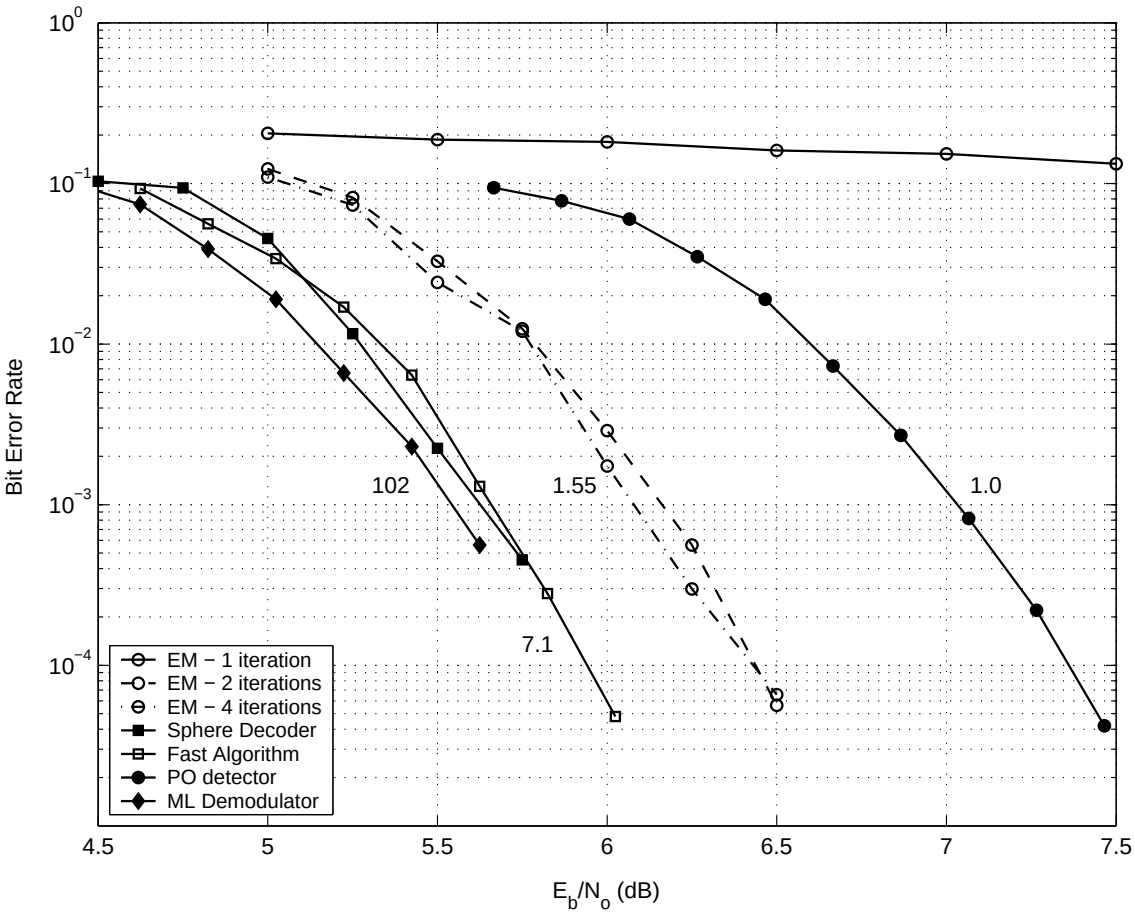

Figure 2.3: Receiver comparison for pilot assisted BPSK transmission in a SISO system using a length 4000 $(3, 6)$ regular LDPC code. The coherence time is $T = 11$.

number by the side of each performance curve in Fig. 2.3 is the normalized software complexity[5] of simulating that system. The PO receiver utilized optimal pilot energy which was found through simulations (agreed with the predicted value from theory). From Fig. 2.3, we see that as expected the EM-algorithm provides almost 1 dB advantage over the PO receiver with only a marginal increase in complexity (1.55 vs. 1). The proposed fast algorithm employing the four channel samples as in Example 2.3 provides almost 1.5 dB advantage over the PO detector and about 0.5 dB over the EM-algorithm, but it does so at a complexity of 7.1 with respect to the PO detector. However it is just 0.2 dB away from the ML-demodulator and the Sphere Decoder, which have complexities 102 and 12.9 (at 6 dB) respectively. Note that the sphere decoder's complexity [47] depends closely on the operating SNR. At low SNR, the sphere decoder is expected to collect more signals in a given radius than at high SNR. Since the complexity is dependent on the number of sequences that are captured in this set, the complexity is a function of SNR. This is illustrated through a plot of the complexity comparisons between various receivers in Fig. 2.4. For instance, at an SNR of 4.5 dB the sphere decoder's complexity is 71. Overall, we conclude that the proposed fast algorithm compares favorably in terms of performance and complexity with respect to some popular choices of receivers for PSAM transmission scheme.

[5]The software complexity numbers were obtained by running a simulation of the system under consideration and measuring the average CPU time taken to perform demodulation and detection. These numbers have been normalized with respect to the complexity of a system having perfect CSI (channel state information) or equivalently a system employing the PO receiver (since perfect CSI receiver and PO receiver have identical complexity). The software complexity figures include the code subgraph part and hence indicate the complexity in performing demodulation and decoding. For a fair comparison all measurements were done for the same packet length and for the same number of decoding iterations and on the same CPU and OS platform.

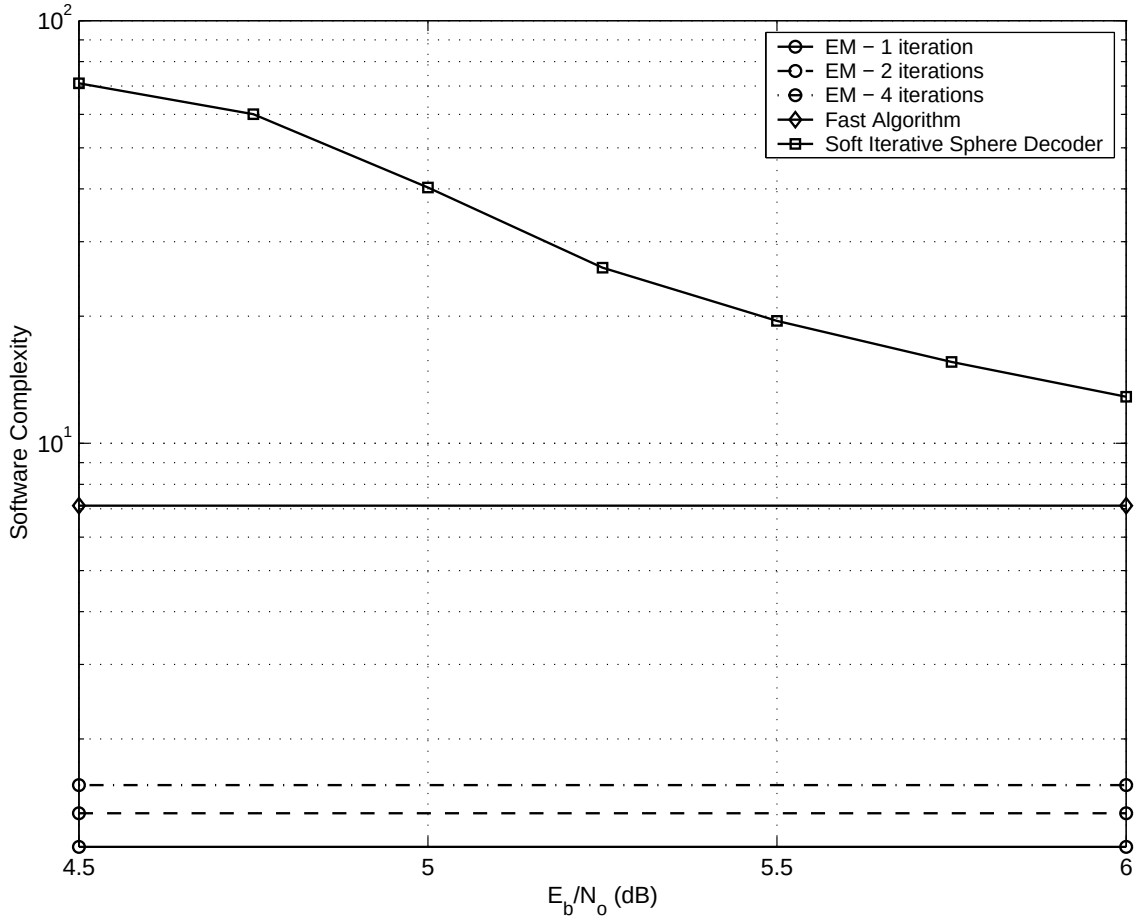

Figure 2.4: Receiver complexity comparison for pilot assisted BPSK transmission in a SISO system using a length 4000 $(3, 6)$ regular LDPC code. The coherence time is $T = 11$.

Pilot Assisted QPSK - SISO

We now compare the proposed algorithm with the PO, EM and the ML receivers, when using higher modulation alphabets for the sub-symbols such as the QPSK modulation. We considered a SISO system on a Rayleigh fading channel with coherence time $T = 5$. The overall rate was 0.8 bits per complex dimension due to the use of an outer regular $(3, 6)$ LDPCC with length 4000. The performance of the various receivers are shown in Fig. 2.5. From the figure it is apparent that the EM algorithm

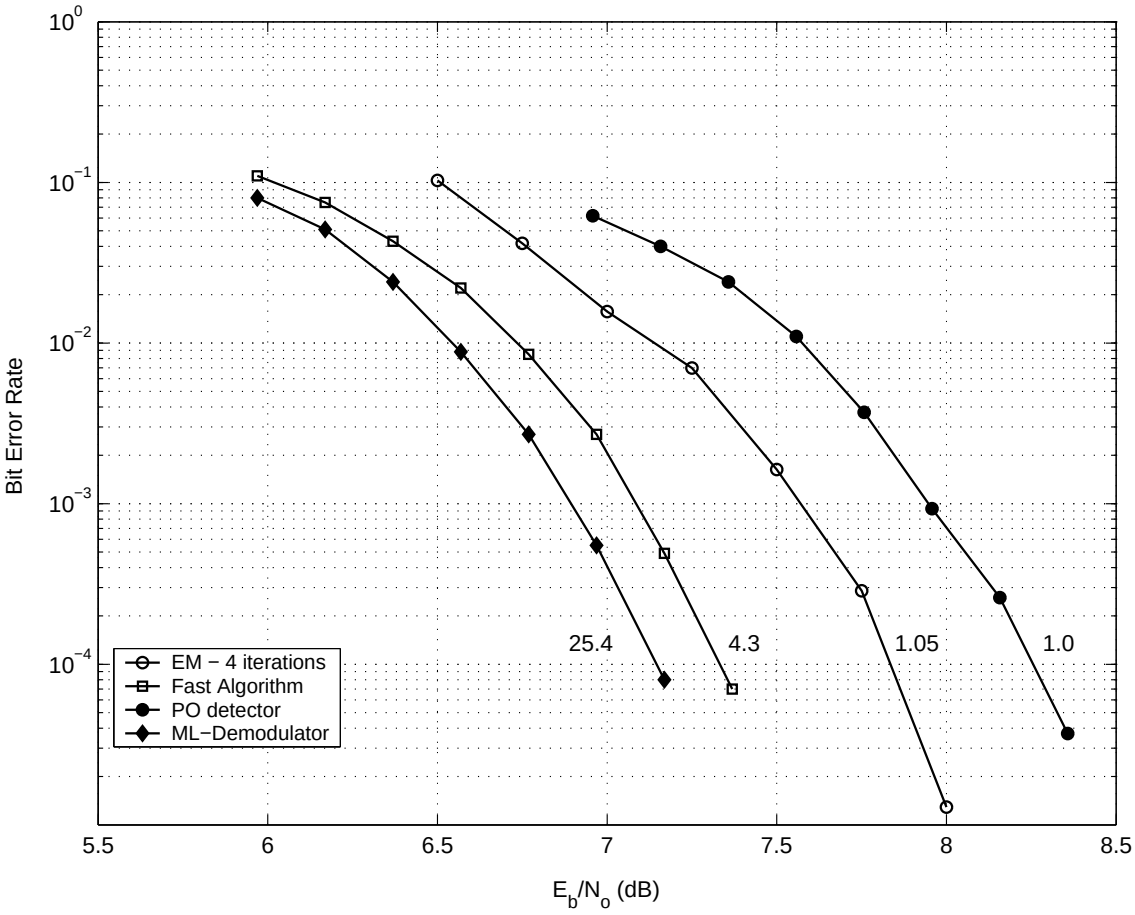

Figure 2.5: Receiver comparison for pilot assisted QPSK transmission in a SISO system using a length 4000 $(3, 6)$ regular LDPC code. The coherence time is $T = 5$.

gains about 0.5 dB from the PO receiver while the proposed fast algorithm gains an-

other 0.6 dB over the EM algorithm. The fast algorithm used $Q = 6$ channel samples that were determined as $h_i = \tilde{h}e^{\frac{j2\pi(i-1)}{Q}}, i = 1, \ldots, 6$ where $\tilde{h}$ is the MMSE estimate of the channel that is easily determined from the pilot transmission. In comparison, the ML demodulator which has much higher complexity is just 0.2 dB better than the proposed algorithm. Whether or not this extra complexity is warranted for the sake of the 0.2 dB gain is a question that is answered best by the application that it is intended for. Nevertheless the merit of the proposed algorithm in terms of achieving good performance with low complexity is well illustrated through this example.

Pilot Assisted 4-PAM - SISO

Although the algorithm is described for equal energy signals, we show its applicability for systems employing non-equal energy modulations such as PAM. Specifically we consider a SISO system employing a length 4000 regular $(3, 6)$ LDPCC and using 4-ary PAM modulation over a Rayleigh fading channel with coherence time $T = 5$. Since each data sub-symbol carries 2 bits, the overall rate is 0.8 bits per complex dimension. The various receivers compared are the proposed fast algorithm, the PO detector, the EM-algorithm and the standard ML demodulator. All the algorithms under comparison have to be modified to take into account the unequal energy between the signals. The performance of these receivers are shown in Fig. 2.6. The EM algorithm gains about 0.6 dB over the PO detector, while the proposed fast algorithm gains another 0.6 dB over the EM algorithm. Note that the fast algorithm is actually 0.2 dB better than the ML demodulator. This was a surprising result since in terms of the demodulator, the ML demodulator performance is actually better than the proposed algorithm, but seemingly the statistics of bit reliability is better suited for the outer code for the proposed algorithm. The channel samples for this

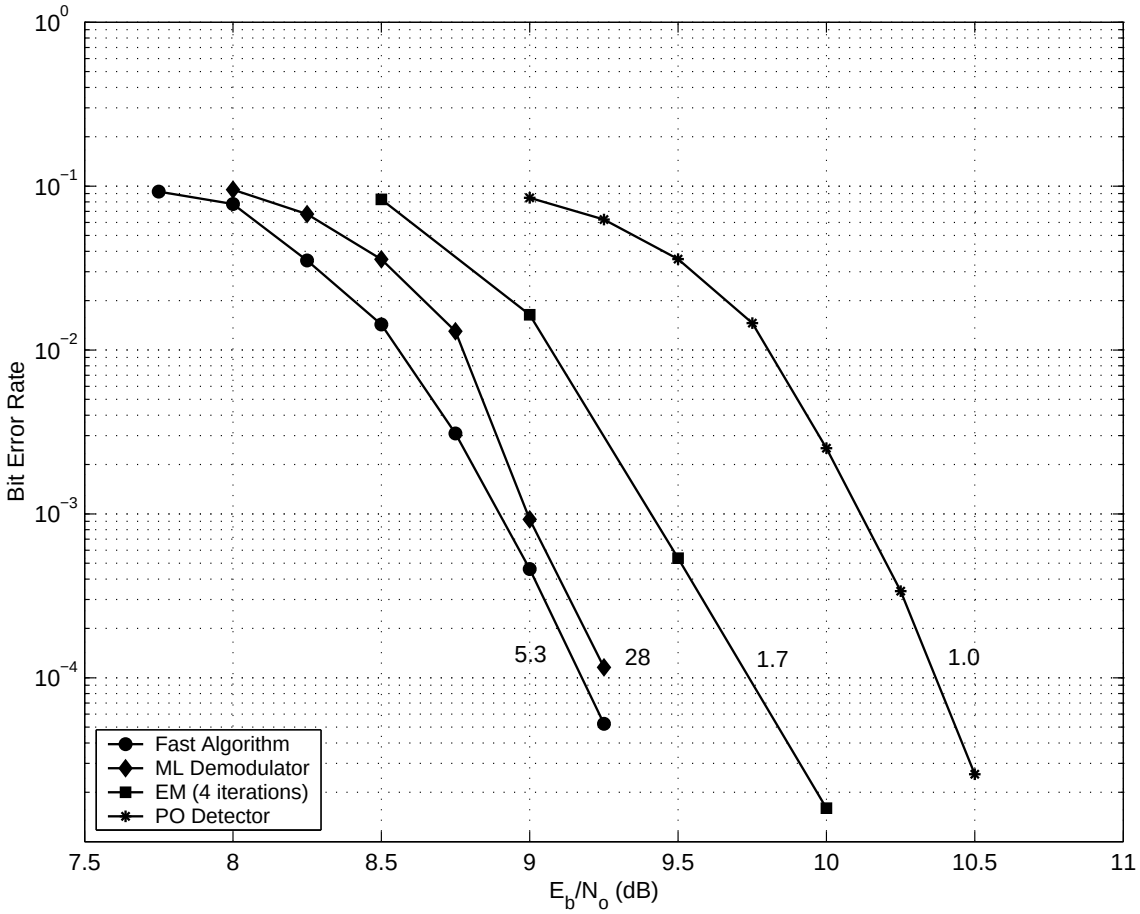

Figure 2.6: Receiver comparison for pilot assisted 4-PAM transmission in a SISO system using a length 4000 $(3, 6)$ regular LDPC code. The coherence time is $T = 5$.

case required optimization (via simulation) and the channel samples were chosen such the h_1 and h_4 had unit amplitude, while h_2, h_3, h_5 and h_6 had amplitude 0.1 (normalized with respect to the MMSE estimate of the channel - $\tilde{h}$). Also h_2, h_3, h_5 and h_6 were placed symmetrically about the perpendicular to $\tilde{h}$ and h_2 was placed at an angle of 62 degrees with respect to $\tilde{h}$.

The complexities of the various algorithms are indicated beside the corresponding performance curve. Again we see that the proposed algorithm achieves a good tradeoff between performance and complexity.

2.3.2 LDPCC Design

LDPC code design for all the examples shown below was done using the EXIT chart [50] technique following the development in [53]. Fig. 2.7 shows the combined transfer characteristics of the variable node decoder and the detector for various values of d_v, where the detector is the low complexity demodulator described in section 2.2.6. The underlying system is a 2×1 channel with channel coherence time $T = 6$ and QPSK with Alamouti modulation with overall rate 1 bit/ch.use. The E_b/N_o for all these plots were fixed at 8.7 dB. It is noted that for $d_v = 1$, the combined detector and variable node decoder transfer function represents just the detector's transfer function.

As an example, the transfer characteristics of a code are plotted in Fig. 2.8. Also plotted in the same figure is the average evolution of the mutual information quantities during the actual simulation of the code at these signal to noise ratios. There is some deviation between the tracking values and the predicted transfer function, which we believe is due to the significant assumption about the Gaussian nature of the messages. However our observation has been that these EXIT charts accurately

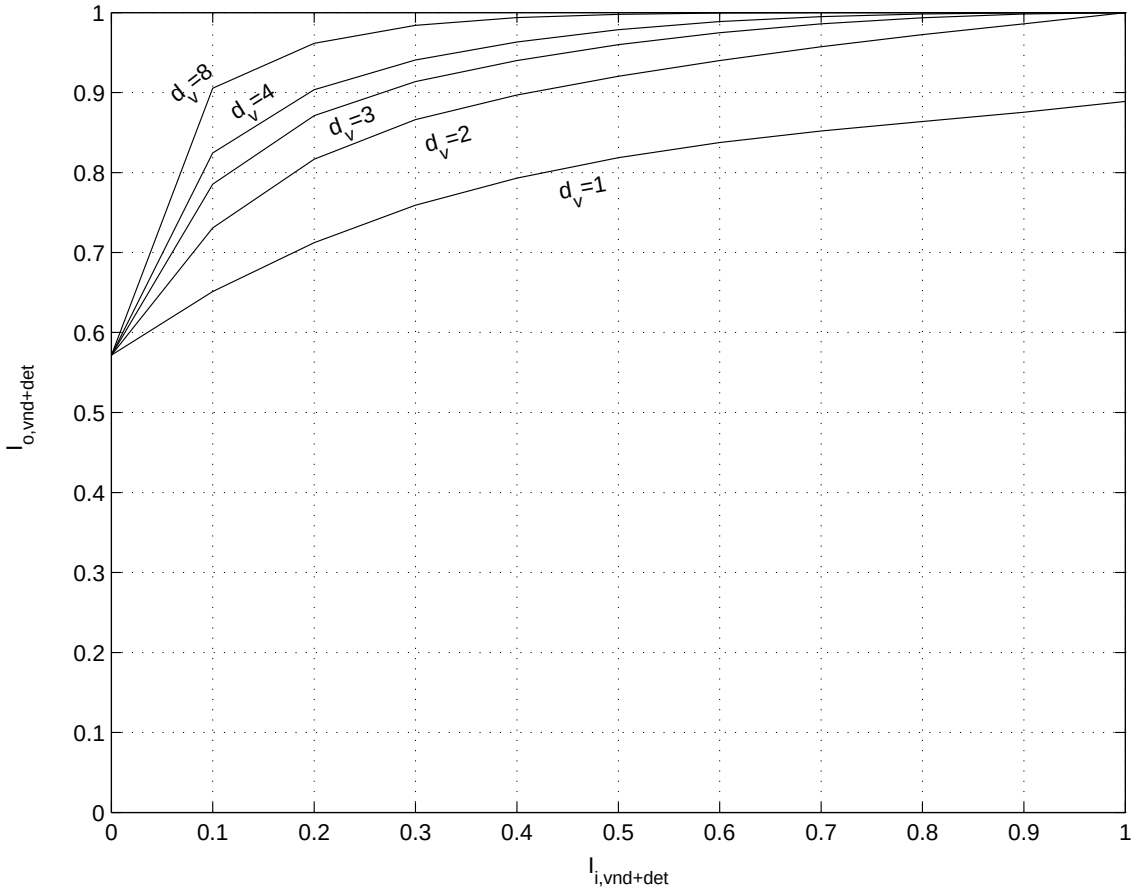

Figure 2.7: Transfer Characteristic of variable node decoder and detector for various values of d_v

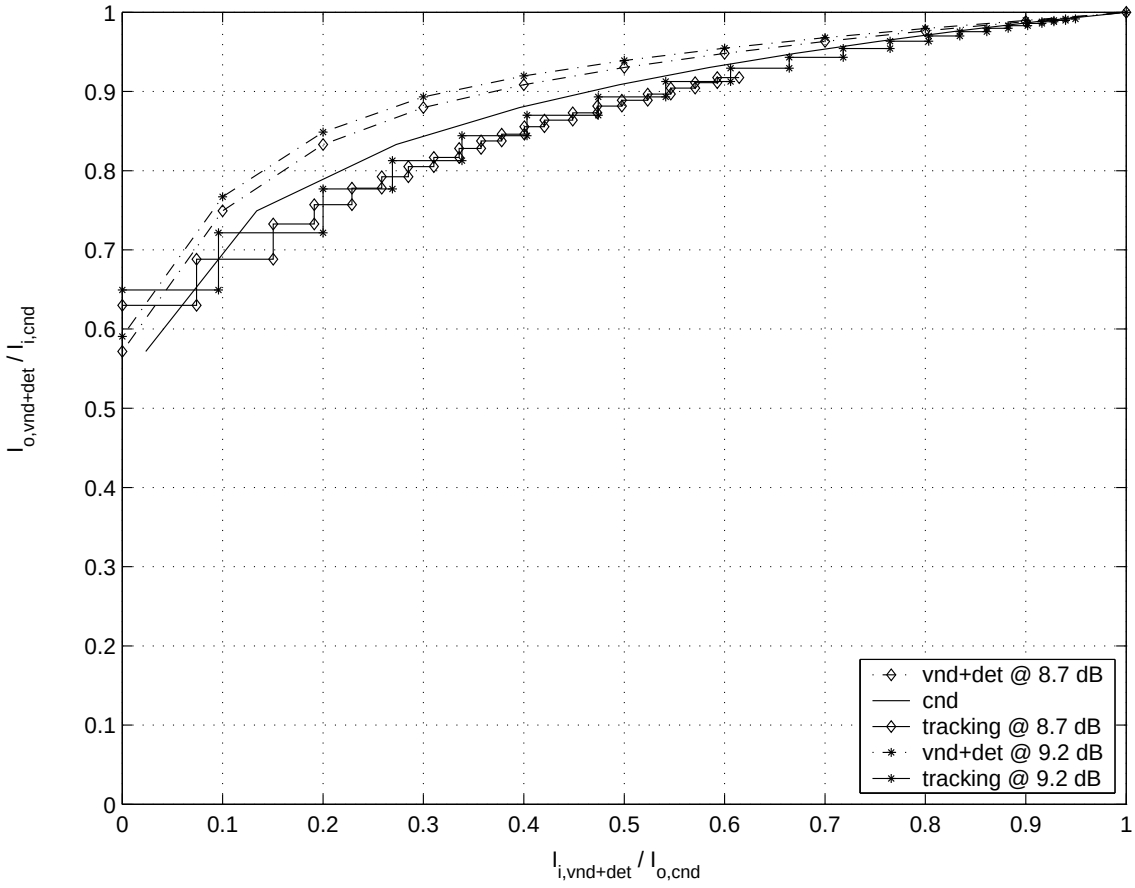

Figure 2.8: (a). EXIT Chart and actual code tracking for a length 10000 rate 0.75 LDPCC with $\lambda(x) = 0.838088x + 0.038695x^2 + 0.069892x^3 + 0.001538x^7 + 0.051787x^8$ and $\rho(x) = 0.435934x^7 + 0.264787x^8 + 0.299279x^9$. Tracking was done for 20 iterations and the graph shown is averaged over 200000 bits.

describe the overall iterative decoder's behavior as regards to whether or not the decoding process converges.

It is seen that at 8.7 dB, the gap between the 2 exit curves is not sufficient to allow the convergence of the iterative decoding process, but that at 9.2 dB, the iterative process almost converges to $(1, 1)$ implying nearly error free decoding. The gap between the EXIT curves is called the *EXIT tunnel*.

Our goal is to optimize the variable and check node degrees so as to have convergence in the iterative decoding process at the minimum γ_b possible (close to capacity). From Fig. 2.8, it is seen that to have convergence of the iterative process it is necessary to have a wider EXIT tunnel. Thus code design is done with a view to have the widest EXIT tunnel at desired signal to noise ratio.

The constrained capacity of this system was evaluated and it was found that $E_b/N_o = 8.45$ dB is required to support rate 1 bit/ch.use. Hence, LDPC code optimization design was initiated conservatively at $E_b/N_o = 8.7$ dB. The performance of the best code thus found is shown in Section 2.3.3 and beyond.

2.3.3 Example: Rate-1 system

In this example we consider a $T = 6$ channel and operate with 2 transmit and 1 receive antenna ($M = 2$,$N = 1$).

Perfect CSI and PO receivers

In order to investigate the performance limits of our receiver algorithms, we considered a PO scheme with the first two complex dimensions used as a pilot and the remaining 4 complex dimensions in the block used to transmit data. For diversity gain, the Alamouti block code structure is used for the data sub-symbols. This is the same construction outlined in the previous section. The same scheme is considered

for the perfect CSI system where the pilot is replaced by another data sub-symbol. The constituent signals in the sub-symbols come from a QPSK constellation. For the PO system to have an over all rate of 1 bit per complex dimension, an outer code of rate 0.75 is required. For this a rate 0.75 outer LDPC code was designed (optimized using EXIT technique) for the perfect CSI scheme and its performance is plotted in Fig. 2.9. Also plotted in the same figure is the performance of a PO receiver with the same outer code designed above with $\frac{\gamma_p}{\gamma_s} = 1$ (0 dB). Using the equivalence relation in (2.18), it is easy to compute the optimal $\frac{\gamma_p}{\gamma_s} = 10^{0.1}$ (1 dB). The performance of a PO system with this optimal γ_p which is also plotted in Fig. 2.9 shows the same improvement of 0.13 dB as predicted by theory.

The large gap between the perfect CSI performance and the PO receiver performance as seen from Fig. 2.9 begs the use of more sophisticated non-coherent detectors to bridge this gap.

SGUC, AUB and PSAM construction

For an overall rate of 1 bit per complex dimension, three modulation schemes are considered - SGUC, AUB and the proposed PSAM. The first two are unstructured unitary constellations.

System design for this case begins by first identifying the combination of outer code rate and inner modulation rate so that the over all rate of 1 bit per complex dimension is achieved. It should be noted that it is straightforward to design a 2^l-ary SGUC or AUB for an arbitrary l, while using a PSK/QAM constellation with Alamouti puts a restriction on l. This is a disadvantage of using the PSAM structure.

To achieve a target rate of 1 bit per complex dimension and for the outer code rate to be in a reasonable range, three choices of l were taken, namely $l = 7, 8, 9$. This

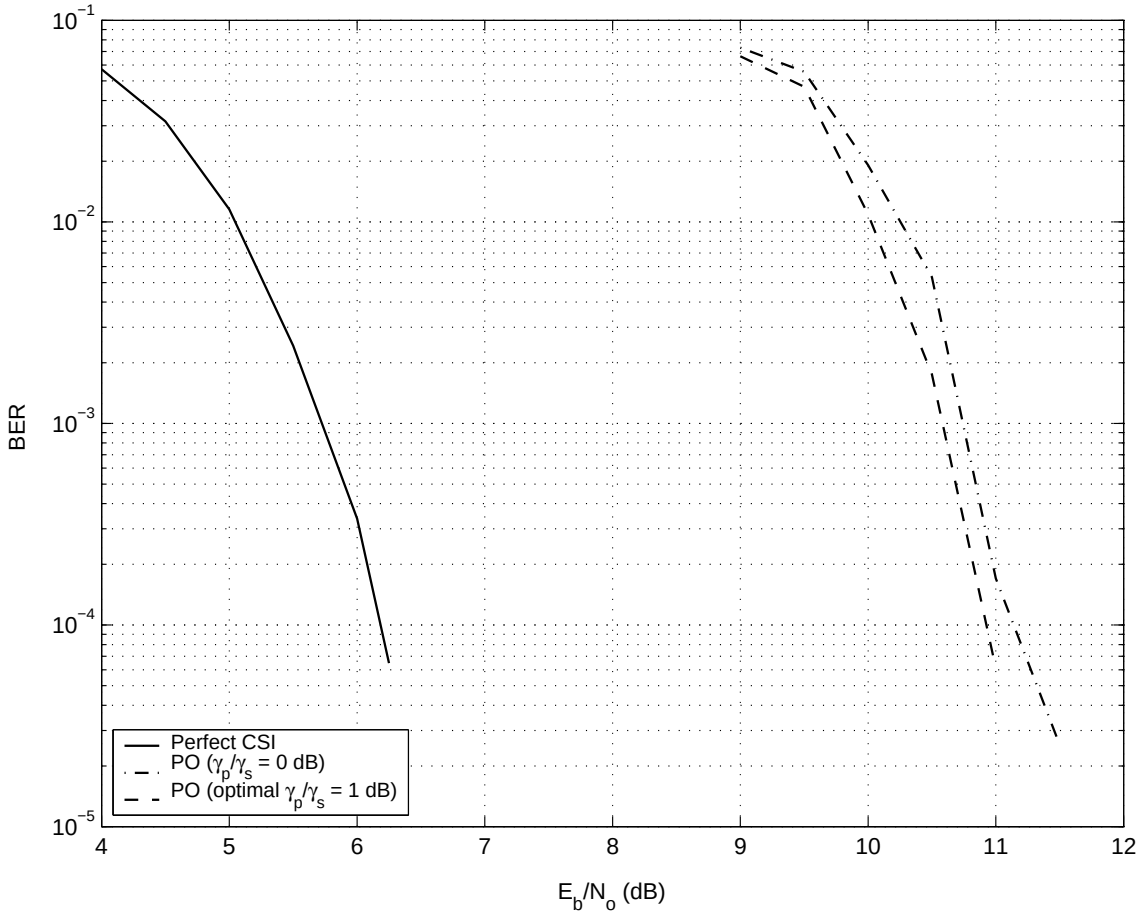

Figure 2.9: Performance of Perfect CSI and PO receivers (with and without optimized pilot power). The complexity of both schemes is the same and it is normalized to 1 for bench-marking complexity of subsequent schemes.

leads to size 128, 256 and 512 constellations[6]. The corresponding outer binary LDPC code rates are thus 6/7, 3/4 and 2/3 respectively. The low complexity receiver used $Q = 16$ channel samples chosen as $\mathbf{h} \in \{(\hat{h}_1 e^{\frac{\jmath 2\pi(i-1)}{\sqrt{Q}}}, \hat{h}_2 e^{\frac{\jmath 2\pi(j-1)}{\sqrt{Q}}})^\top | i, j \in \{1, \ldots, \sqrt{Q}\}\}$ where $\hat{\mathbf{h}} = (\hat{h}_1, \hat{h}_2)^\top$ is the MMSE estimate of the channel obtained from the pilot symbol.

The performance of the SGUC and AUB constellations are shown in Fig. 2.10. For each code rate/modulation pair two experiments were performed. The solid curves in Fig. 2.10 refer to the performance of a system employing 1 demodulation followed by 20 iterations of LDPC decoding. The dash-dash curves indicate the performance of a system employing 5 iterations of demodulation and 20 iterations of decoding (each iteration of the demodulator is followed by an iteration of the LDPC decoder). The first conclusion to draw from Fig. 2.10 is that the AUB constellations are better than the SGUC of corresponding size at each iteration by roughly 1 dB. This is expected since AUB constellations are highly optimized and understandably much harder to generate than the SGUC for arbitrary sizes. The software complexity of each system (normalized by the complexity of the perfect CSI receiver) is shown next to its performance curve. For the sake of clarity, since the software complexity for 512-ary SGUC is identical to that of a 512-ary AUB, the complexity numbers are mentioned once for each modulation size and iteration number. Observing that the receiver complexity for a size 512 constellation is roughly twice the complexity of a 256-ary constellation it is interesting to note that the system with $(R_c, 2^l) = (3/4, 256)$ has the same performance as the $(R_c, 2^l) = (2/3, 512)$ system but with half the

[6]The SGUC constellations designed using the random search technique outlined in [29], had the following parameters - 128 SGUC - (1,3) & (58,25,62,55,6,30), 256 SGUC - (1,5) & (58,232,83,44,231,183), 512 SGUC - (2,4) & (97,406,247,368,389,502) where the first pair of numbers indicate the columns of the 6×6 DFT matrix used to create the first signal, while the second string of numbers indicate the rows of the $2^l \times 2^l$ DFT matrix whose second column entries form the entries of the Θ matrix. See [29] for details.

complexity. As noted above AUB constellations are better than SGUCs and hence we use only the 256 AUB constellation for further comparisons with the 256 QPSK PSAM scheme. Also, all subsequent comparisons are made at a BER of 10^{-4}.

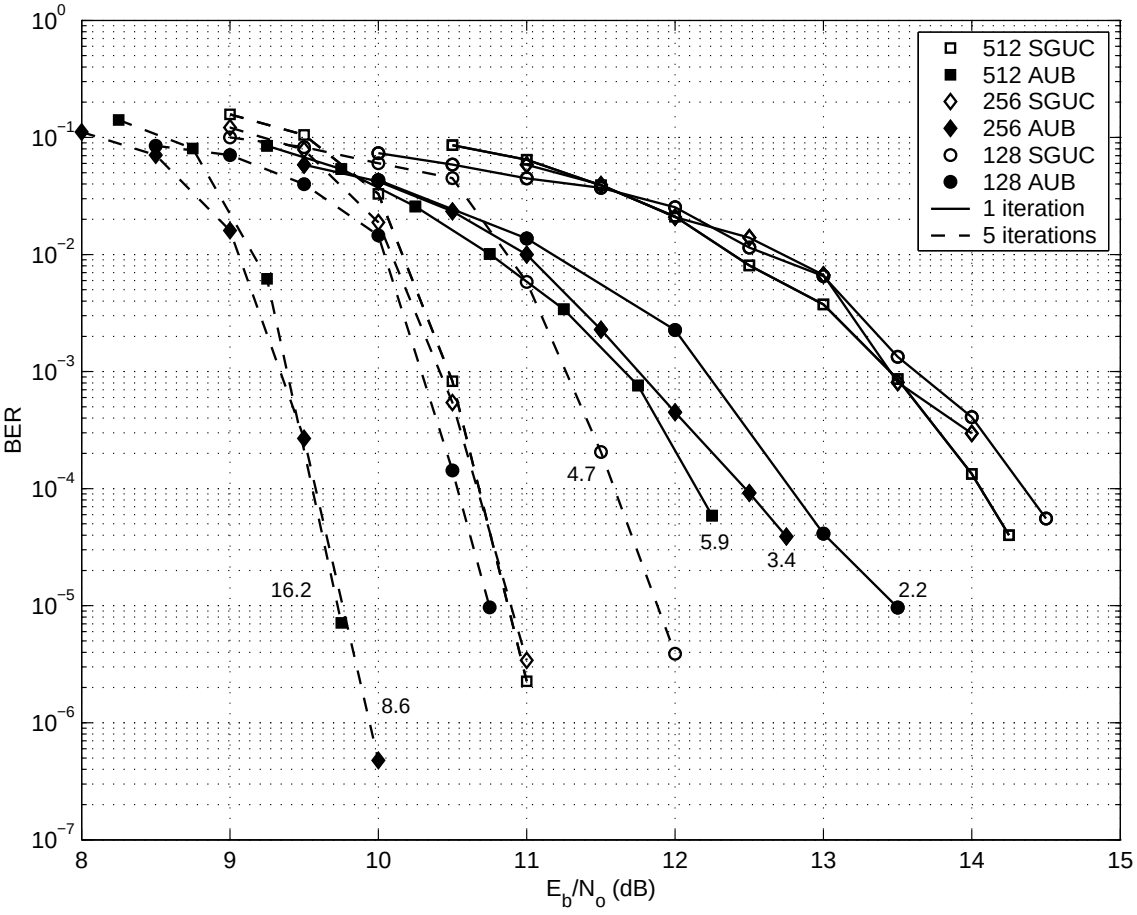

Figure 2.10: Tradeoff between performance and complexity through the choice of l. Overall rate = 1 bit/ch.use.

In Fig. 2.11, the performance of the AUB and PSAM schemes, when operating with 1,5 and 7 demodulation iterations and 20 decoding iterations are compared (the PSAM scheme used in conjuction with the proposed low complexity receiver is identical to the one used with the PO receiver in 2.3.3). It is seen that the first iteration of the low complexity demodulator is better than the corresponding curve of the AUB constellation by 0.7 dB. However for 5 and 7 iterations, the performance is

comparable to the AUB. Indeed for 7 demodulation iterations, the AUB outperforms the QPSK-PSAM by 0.2 dB. From the normalized software complexity of these systems (indicated by the side of each performance curve), it is noted that such a comparison in terms of fixed number of iterations does not take into account the lower complexity of the receiver structure used for the PSAM scheme.

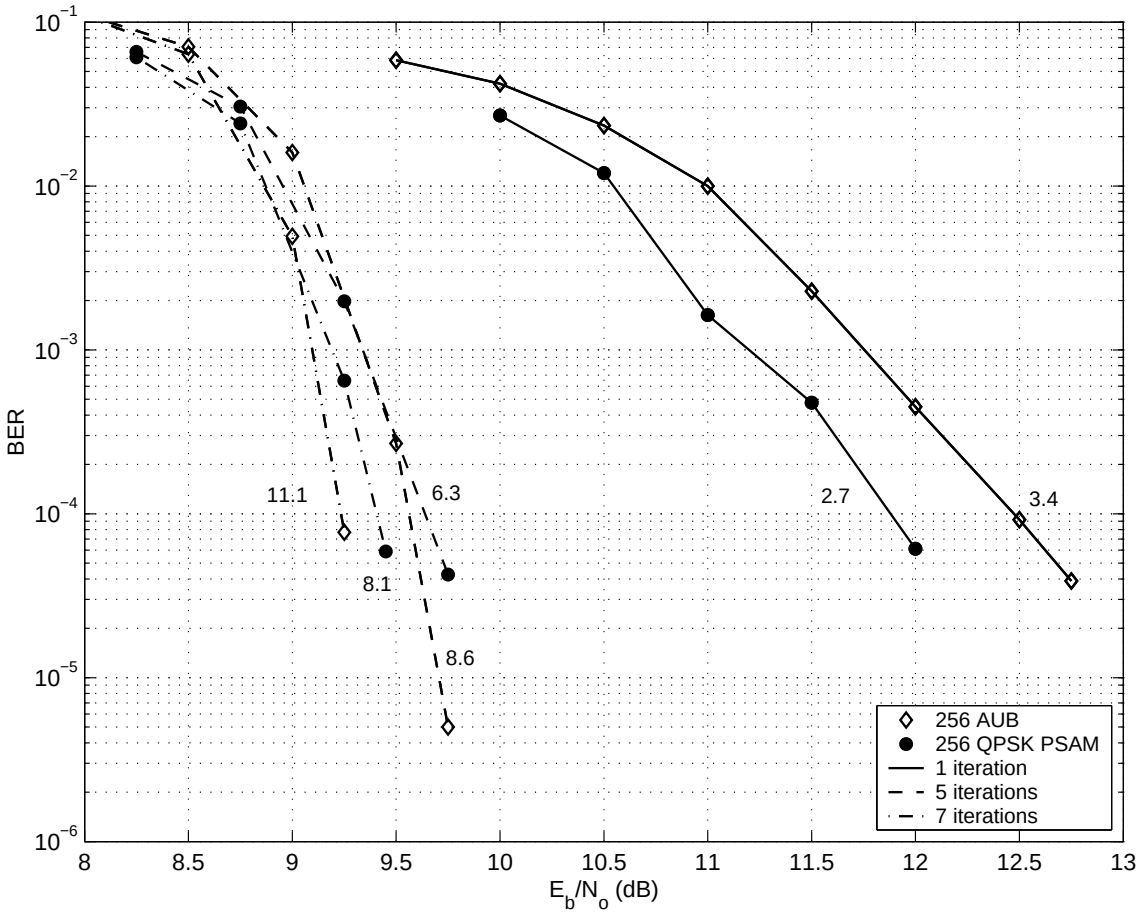

Figure 2.11: Comparison of performance of the QPSK/Alamouti PSAM vs AUB constellations, with same number of demodulation iterations. ($T = 6$ channel with $M = 2$ and $N = 1$.) Q = 16 samples were used for the low complexity algorithm.

To account for the receiver complexity, Fig. 2.12 shows the performance of these three schemes with different number of iterations so that schemes with the same complexity can be compared. In this figure, the numbers beside the curves indicate

the number of demodulation iterations performed to achieve the complexity specified by the legend. For a given complexity, it is possible to perform more demodulation iterations for the PSAM scheme than for the AUB. At a complexity of 3.9, the QPSK-PSAM with the low complexity algorithm outperforms the AUB by 2.2 dB, while the performance gap decreases to 0.5 dB and 0.1 dB at complexity 6.2 and 11 respectively.

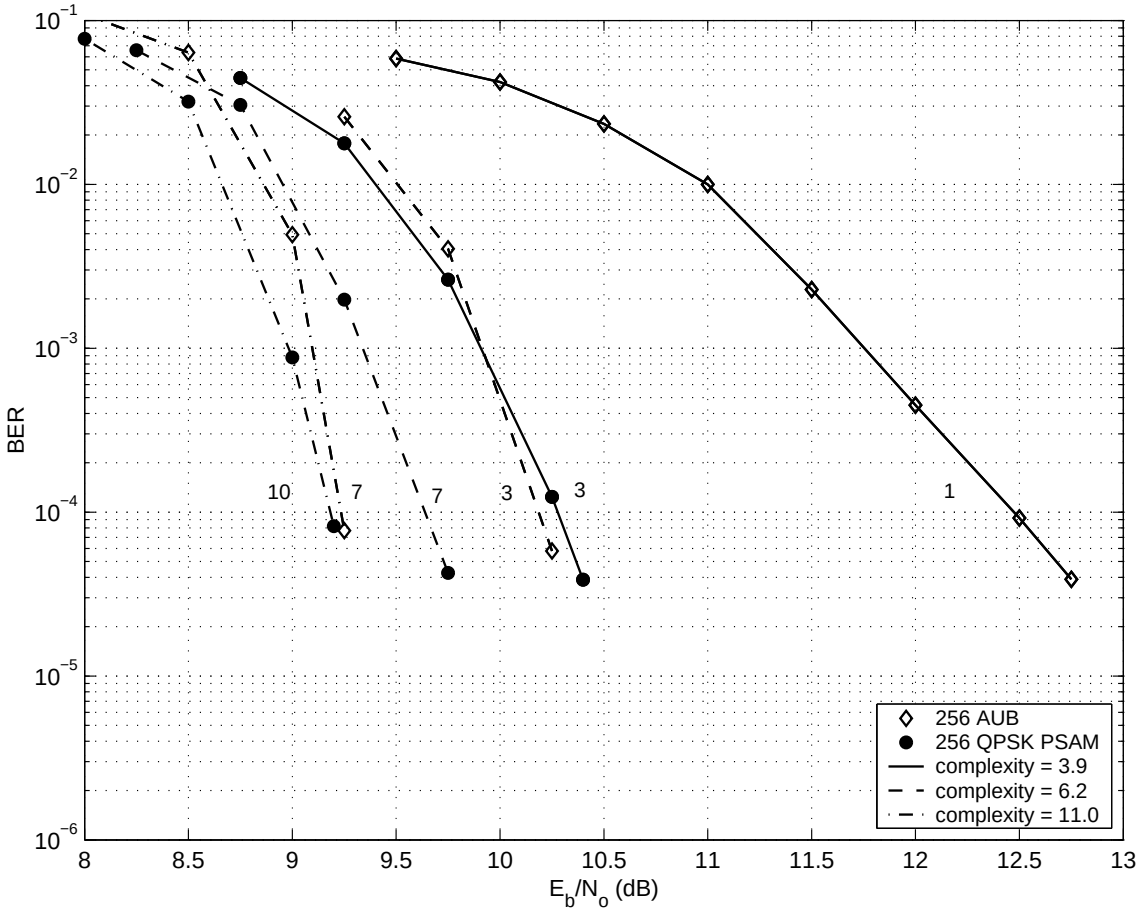

Figure 2.12: Comparison of performance of the QPSK/Alamouti PSAM vs AUB constellations, with same software complexity. ($T = 6$ channel with $M = 2$ and $N = 1$.) Q = 16 samples were used for the low complexity algorithm.

From Fig. 2.11 and Fig. 2.12, it might appear that there is only limited benefit in using the PSAM scheme with the proposed low complexity receiver over the AUB

constellation with optimal demodulation. However, this is only true due to the small values of T and/or rate R considered in this example. It is important to note that the utility of the PSAM construction will become apparent when the operating rate is increased (for a fixed block length) or when the block length is increased (for a fixed rate). This is expected since the complexity of demodulating the SGUC and AUB schemes grows exponentially in T and R, while the complexity of PSAM with the proposed receiver grows only linearly. An example illustrating the effect of increasing the rate for the same block length $T = 6$ is shown in the following section.

2.3.4 Example 2: Rate-1.5 system

For the higher rate of 1.5 bits per complex dimension using 2 transmit and 1 receive antenna over a $T = 6$ channel, a nominal code rate of 3/4 was chosen for the outer code and this necessitates the use of an inner modulation of size 4096. Random search for a 4096 SGUC led to the use of the SGUC with the parameters parameters (1,3) & (443,220,359,3605,1661,1750). At the time of these experiments we did not have large enough AUB constellations to compare the performance of our PSAM construction. A 4096 point PSAM scheme is constructed using an Alamouti scheme with constituent signals coming from an 8-PSK constellation.

The performance curves of the low complexity demodulator for 1, 5 and 10 iterations are shown in Fig. 2.13. Also shown in Fig. 2.13 is the performance of the 4096 SGUC employing 1 and 5 demodulation iterations. The LDPC code is 8400 bits long. For the choice of $Q = 36$ (channel samples were chosen as outlined in the previous example), it was seen that the software complexity of the low complexity demodulator is 10.1 while that of the optimal demodulator for a 4096 size SGUC is 37.7. Due to its severe complexity, the performance of the 4096 SGUC system is

shown only for 1 and 5 iterations in Fig. 2.13.

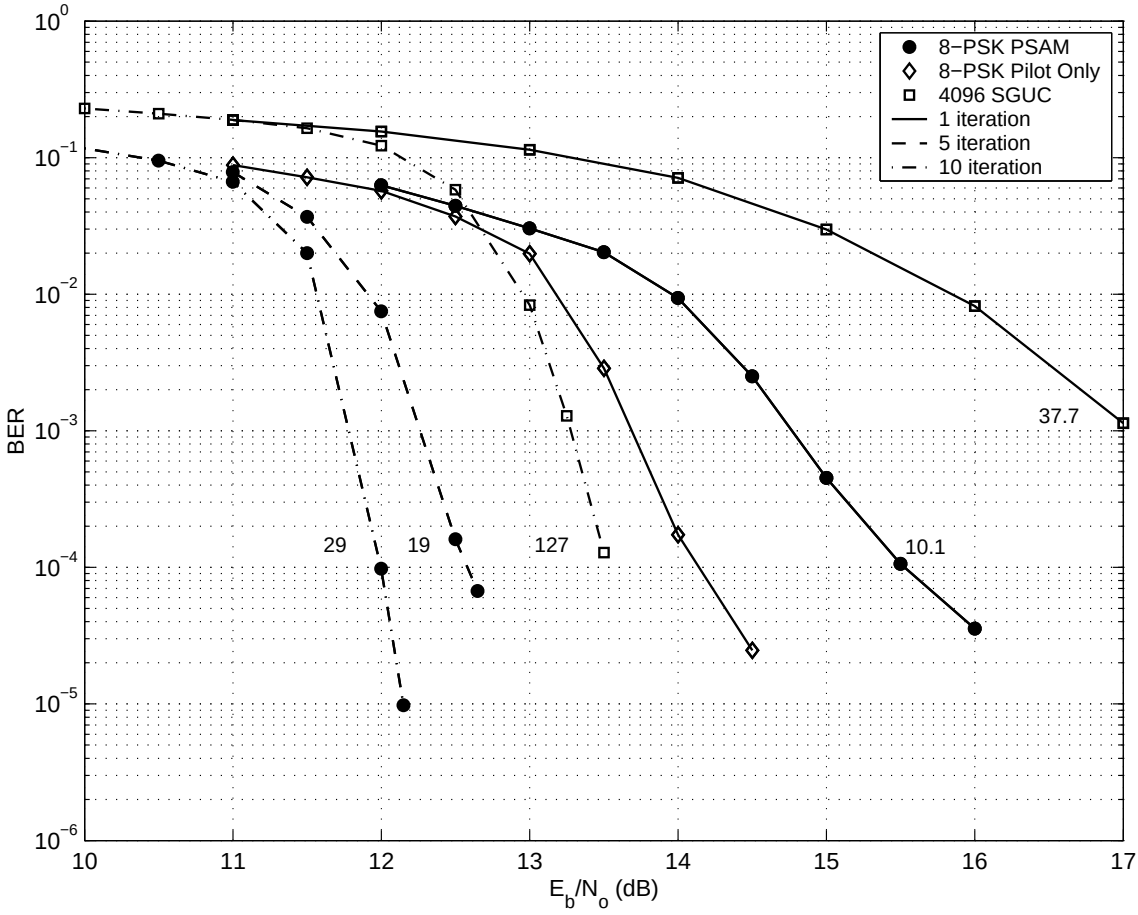

Figure 2.13: Performance of the 8-PSK/Alamouti PSAM scheme and the 4096-ary SGUC over a $T = 6$ channel with $M = 2$ and $N = 1$. Q = 36 samples were used in the low complexity algorithm.

In this high rate scenario, the PSAM scheme (with 1 iteration) outperforms the SGUC with 1 iteration while being almost a factor of 4 less complex. Performing 5 demodulation iterations has a complexity of 19 and 127 for the PSAM and SGUC respectively while the performance improvement is 1 dB. The low complexity demodulator for the PSAM scheme allows performing 10 iterations with only a complexity of 29 and this improves the performance over the 5 iteration curve by 0.6 dB.

We note here that AUB constellation of size 4096 has the same demodulation complexity as the 4096 SGUC and even if the performance is better than the SGUC,

the high complexity of the demodulator dictates that the PSAM scheme be used. Fig. 2.13 also shows the performance of a PO receiver with the PSAM scheme. It is noted that the new joint estimation/detection receiver provides an advantage of 2 dB over the PO receiver. We note that PSAM schemes can be further improved by using 8-QAM signals instead of 8-PSK signals in the data sub-symbols. These examples clearly demonstrate the utility of both the low complexity receiver proposed herein and the PSAM schemes investigated widely in the literature.

2.3.5 Example 3: Rate-1.0 system in Continuous Fading

In this example we simulate a continuous fading channel using an auto-regressive (AR) model[7] with the pole at 0.99. This closely approximates a $T = 6$ channel since there is strong correlation between channel realizations separated by 6 time instances. Although the channel model was changed, the same receivers (which assume block independent fading) were used in order to test their robustness in a continuous fading regime. We report the simulated performance of the 256-ary AUB constellation and the PSAM scheme (Q=16) from 2.3.3 on this channel in Fig. 2.14. With increasing number of iterations, it is seen that the AUB gains about 1 dB over the PSAM scheme.

We note that in a practical scenario, the structured nature of the PSAM construction allows an optimization to be done over the block length chosen without any change in the inherent modulation scheme, whereas SGUCs and AUB constellations have to be generated from scratch if a new block length is chosen.

[7] $\mathbf{h}_0 = \mathbf{w}_0, \mathbf{h}_n = 0.99\mathbf{h}_{n-1} + \sqrt{1 - 0.99^2}\mathbf{w}_n, n = 1, 2, 3, \ldots$, where $\mathbf{w}_n$ is $\mathcal{CN}(\mathbf{0}; \mathbf{I}_M)$ distributed and i.i.d over n.

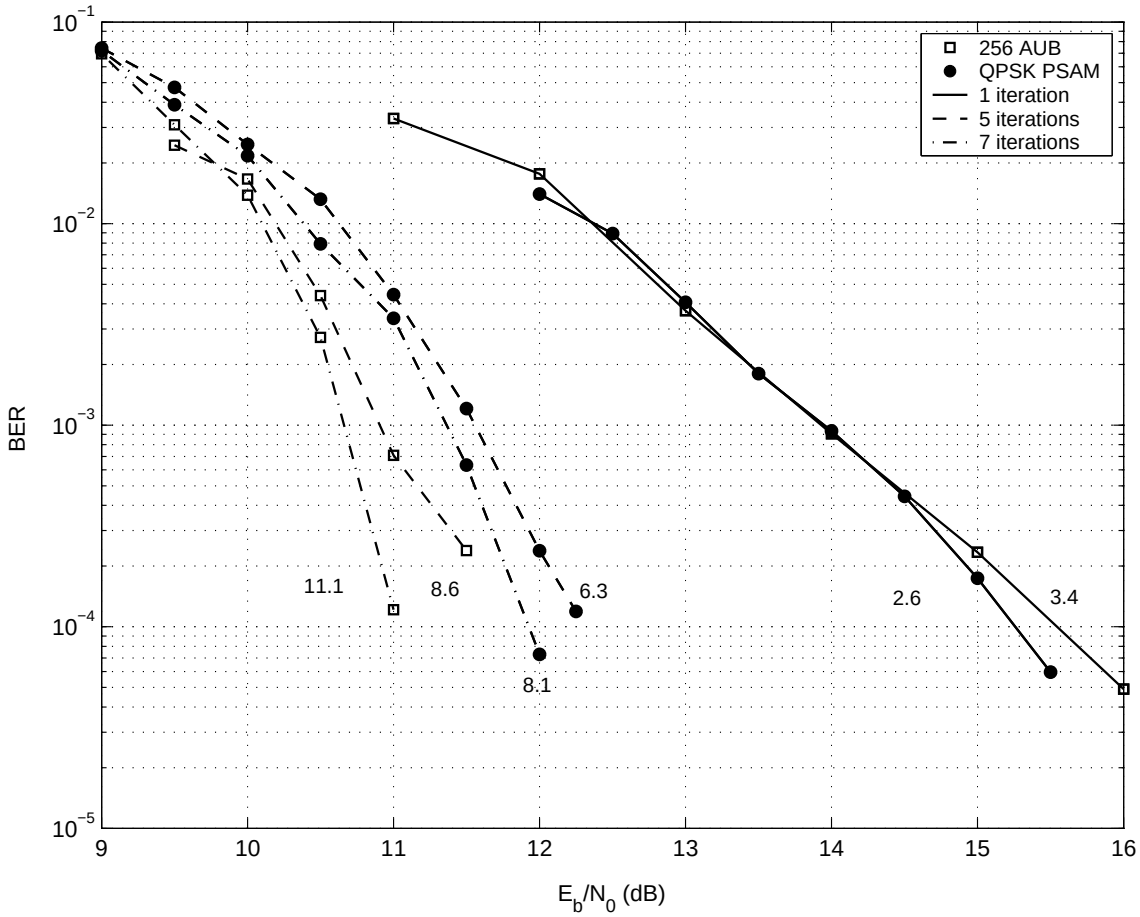

Figure 2.14: Performance of the QPSK/Alamouti PSAM scheme and the 256-ary AUB constellation over a continuous fading channel, approximated by a $T = 6$ block fading channel with $M = 2$ and $N = 1$. Q = 16 samples were used for the low complexity algorithm.

CHAPTER 3

Capacity Achieving Signal Distribution

Chapter 1 introduced the capacity of the MIMO wireless channel under the two cases of coherent and non-coherent reception. Particularly, in the non-coherent reception paradigm, [34, 56] have shown that isotropically distributed unitary signals with an independent amplitude factor achieve the Shannon capacity of this channel. These works also showed that at high SNR, the amplitude of these signals has a single probability mass point.

However many digital communications applications particularly in wireless, deep-space and satellite communications operate in a power-limited regime where both the spectral efficiency (in bits/s/Hz) and energy per bit are low. It is well known that MIMO communication techniques would be wasted in this scenario since the capacity gain afforded by MIMO systems is significant at high SNR. There is thus both an academic and a practical reason for the interest in characterizing the capacity of a Rayleigh block faded channel, especially since at low SNR (and equivalently, when operating at low rates), neither the capacity nor the signal distribution that achieves this capacity is known.

Recent literature indicates an increasing interest in this problem. Smith [?] showed that for amplitude and variance constrained scalar gaussian channels,For

a general class of fading channels, it was proved in [43] that when the input is constrained in such a way that $E[\|\mathbf{x}\|^{2+\epsilon}] \leq a$, $(\forall \epsilon > 0)$ then the amplitude of the input is a discrete random variable that takes on finite number of values. It was conjectured that the result would hold for $\epsilon = 0$ also. Subsequently in [23, 55], the importance of flash signaling for the case of peak limited Rician block faded channels as an optimal signalling scheme for the wideband regime (low spectral efficiency) was established. Very recently, the body of work in [24] indicates that with just an average power constraint for a Rayleigh block faded channel, the optimal input amplitude distribution has bounded support.

Interestingly, the problem of characterizing the capacity achieving input distribution for the closely related non-coherent AWGN channel has been solved [32, 33, 39]. The optimal input amplitude distribution has been shown to be discrete and the probability mass function has infinite number of mass points, one of which is always at zero.

In the sequel we investigate the signal structure that achieves the capacity of block-independent Rayleigh faded channel with only an average power constraint.

Consider a wireless communication system operating with one transmit and one receive antenna, *i.e.* $M = N = 1$. The input-output relationship for the k^{th} block is given by (1.3) and the assumptions about the channel and the noise carry over from Section. 1.1.1. Given $\mathbf{x}$, $\mathbf{y}$ is complex gaussian with mean $\mathbf{0}$ and covariance matrix $\mathbf{K} = \mathbf{I}_T + \mathbf{x}\mathbf{x}^*$. The conditional density (after simplification using matrix identities) is given by

$$p(\mathbf{y}|\mathbf{x}) = \frac{1}{(\pi)^T(1+\|\mathbf{x}\|^2)} \exp\left(-\|\mathbf{y}\|^2 + \frac{\mathbf{y}^*\mathbf{x}\mathbf{x}^*\mathbf{y}}{1+\|\mathbf{x}\|^2}\right) \tag{3.1}$$

We operate in a power limited communication system, so the power constraint im-

posed on the signal distribution is given by (in accordance with (1.4))

$$E[\|\mathbf{x}\|^2] \leq T\gamma_s \tag{3.2}$$

where γ_s denotes the average signal-to-noise ratio.

3.1 Signal structure that achieves capacity

The capacity is given by

$$\mathsf{C} = \sup_{p(\mathbf{x}), E(\|\mathbf{x}\|^2) \leq T\gamma_s} I(\mathbf{x};\mathbf{y}) \tag{3.3}$$

$$\text{where,} \quad I(\mathbf{x};\mathbf{y}) = \underbrace{\int\int}_{\mathbb{C}^{2T}} p(\mathbf{y}|\mathbf{x})p(\mathbf{x}) \log \frac{p(\mathbf{y}|\mathbf{x})}{p(\mathbf{y})} d\mathbf{x}d\mathbf{y} \tag{3.4}$$

From [34 . Theorem 2], we know that the capacity achieving signal has the structure $\mathbf{x} = \tilde{\mathbf{x}}\nu$, where $\tilde{\mathbf{x}}$ is an isotropically distributed unit vector (*i.e.* a vector whose density depends only on the direction and whose norm is 1) and ν is a real random variable independent of $\tilde{\mathbf{x}}$. Note that this is true even for the case $T = 1$. Thus the density of $\mathbf{x}$ is related to the density of $\tilde{\mathbf{x}}$ and the density of ν.

The following holds for all integer valued T. The density of a unit isotropically distributed random vector $\tilde{\mathbf{x}}$ is of the following form

$$p(\tilde{\mathbf{x}}) = \frac{(T-1)!}{\pi^T} \delta(\|\tilde{\mathbf{x}}\|^2 - 1) \tag{3.5}$$

Similarly the density of an isotropically distributed random vector with amplitude ν is

$$p(\mathbf{x}|\nu) = \frac{(T-1)!}{\pi^T \nu^{2T-1}} \delta(\|\mathbf{x}\|^2 - \nu^2) \tag{3.6}$$

Therefore the density of $\mathbf{x}$ is

$$\begin{aligned} p(\mathbf{x}) &= \int_\nu p(\mathbf{x}|\nu)p_\nu(\nu)d\nu \\ &= \int_\nu \frac{(T-1)!}{\pi^T \nu^{2T-1}} \delta(\|\mathbf{x}\|^2 - \nu^2)p_\nu(\nu)d\nu \end{aligned} \tag{3.7}$$

and it depends only the magnitude of $\mathbf{x}$ and not its direction, *i.e.*, it is circularly symmetric. In order to completely determine the structure of $\mathbf{x}$, we only need to determine $p_\nu(\nu)$.

Lemma 3.5. *For a circularly symmetric input* $\mathbf{x}$*, the output* $\mathbf{y}$ *is also circularly symmetric.*

Proof. From (3.1), it is seen that for a deterministic unitary matrix $\mathbf{\Phi}$, $p(\mathbf{\Phi}^*\mathbf{y}|\mathbf{x}) = p(\mathbf{y}|\mathbf{\Phi}\mathbf{x})$. Hence

$$\begin{aligned} p(\mathbf{\Phi}^*\mathbf{y}) &= \int_{\mathbb{C}^T} p(\mathbf{\Phi}^*\mathbf{y}|\mathbf{x})p(\mathbf{x})d\mathbf{x} && (3.8)\\ &= \int_{\mathbb{C}^T} p(\mathbf{y}|\mathbf{\Phi}\mathbf{x})p(\mathbf{x})d\mathbf{x} && (3.9)\\ &= \int_{\mathbb{C}^T} p(\mathbf{y}|\mathbf{\Phi}\mathbf{x})p(\mathbf{\Phi}\mathbf{x})d\mathbf{x} && (3.10)\\ &= \int_{\mathbb{C}^T} p(\mathbf{y}|\mathbf{x})p(\mathbf{x})d\mathbf{x} && (3.11)\\ &= p(\mathbf{y}) && (3.12) \end{aligned}$$

and the lemma follows. □

Lemma 3.5 implies that conditioned on $\mathbf{x}$ being circularly symmetric, $\mathbf{y}$ is also circularly symmetric, *i.e.*, it depends on the amplitude $\|\mathbf{y}\|$ only. We can therefore write $p(\mathbf{y}) = 2^T q(\sqrt{2}\|\mathbf{y}\|)$ for some function $q : \mathbb{R}^+ \to \mathbb{R}^+$, where the factor 2^T has been introduced as a normalizing factor. Using this and the conditional density in (3.1), we simplify the inner integral with respect to $\mathbf{y}$ in (3.4) as follows.

3.2 Simplification of the Inner Integral

Define $\mathbf{U}$ as the unitary matrix with the first row equal to $\frac{\mathbf{x}^*}{\|\mathbf{x}\|}$ and the remaining rows orthonormal to each other and to $\mathbf{x}$. Making a change of variables to $\mathbf{y} =$

$\frac{1}{\sqrt{2}}\mathbf{U}^*\tilde{\mathbf{y}}$, where $\tilde{\mathbf{y}} = [\tilde{y_1}e^{\jmath\theta_1}, \tilde{y_2}e^{\jmath\theta_2} \ldots, \tilde{y_T}e^{\jmath\theta_T}]^T$, the inner integral with respect to $\mathbf{y}$ in (3.4) becomes (after converting from rectangular to polar coordinates)

$$\frac{1}{(2\pi)^T(1+\|\mathbf{x}\|^2)} \underbrace{\int_0^\infty \ldots \int_0^\infty \int_{-\pi}^{\pi} \ldots \int_{-\pi}^{\pi}}_{2T} \exp\left(-\frac{\|\tilde{\mathbf{y}}\|^2}{2} + \frac{\tilde{y_1}^2\|\mathbf{x}\|^2}{2(1+\|\mathbf{x}\|^2)}\right) \left(\frac{\tilde{y_1}^2\|\mathbf{x}\|^2}{2(1+\|\mathbf{x}\|^2)} - \frac{\|\tilde{\mathbf{y}}\|^2}{2} - \log\left((2\pi)^T(1+\|\mathbf{x}\|^2)\right) - \log(q(\|\tilde{\mathbf{y}}\|))\right) \tilde{y_1}\ldots\tilde{y_T}d\tilde{y_T}\ldots d\tilde{y_1}d\theta_1\ldots d\theta_T \tag{3.13}$$

We substitute $\tilde{y}^2 = \|\tilde{\mathbf{y}}\|^2 = \sum_{i=1}^T \tilde{y_i}^2$ in place of $\tilde{y_2}$ and let $\sqrt{2}\|\mathbf{x}\| = a$, and integrate over all remaining variables[1] but $\tilde{y}$ and $\tilde{y_1}$, the above integral can expressed as (after renaming $\tilde{y}$ and $\tilde{y_1}$ as y and y_1 respectively)

$$\int_0^\infty \int_0^y \frac{yy_1}{(1+\frac{a^2}{2})(T-2)!}\left(\frac{y^2-y_1^2}{2}\right)^{T-2} \exp\left(-\frac{y^2}{2} + \frac{y_1^2a^2}{4(1+\frac{a^2}{2})}\right) \left[\frac{y_1^2a^2}{4(1+\frac{a^2}{2})} - \frac{y^2}{2} - \log(q(y)) - \log\left((2\pi)^T(1+\frac{a^2}{2})\right)\right] dy_1dy \tag{3.14}$$

It is easily verified that the term outside the square parenthesis integrates to unity and identifying it as the joint density of y and y_1 given a, *i.e.* as $p(y, y_1|a)$, (3.14) can be written compactly as

$$-\log\left((2\pi)^T(1+\frac{a^2}{2})\right) + \frac{a^2}{2(1+\frac{a^2}{2})}\int_0^\infty\int_0^y \frac{y_1^2}{2}p(y,y_1|a)dy_1dy - \int_0^\infty\int_0^y \frac{y^2}{2}p(y,y_1|a)dy_1dy - \int_0^\infty\int_0^y p(y,y_1|a)\log(q(y))dy_1dy \tag{3.15}$$

Noticing that marginalizing $p(y, y_1|a)$ with respect to y_1 yields the conditional density of y given a as $p_T(y|a)$, while a similar process with respect to y yields the

[1]Note that $\underbrace{\int\ldots\int}_{\tilde{\mathbf{y}}\in\mathbb{C}^{T-2}, \|\tilde{\mathbf{y}}\|^2 \le y^2-y_1^2} d\tilde{\mathbf{y}} = \frac{\pi^{T-2}(y^2-y_1^2)^{T-2}}{(T-2)!}$

conditional density of y_1 given a as $p_1(y_1|a)$ where[2]

$$p_n(y|a) = \frac{(1+\frac{a^2}{2})^{n-2}}{(\frac{a^2}{2})^{n-1}} y e^{-\frac{y^2}{2(1+\frac{a^2}{2})}} P\left(n-1, \frac{y^2a^2}{4(1+\frac{a^2}{2})}\right) \tag{3.16}$$

$$P(n,x) = \frac{\gamma(n,x)}{\Gamma(n)} = \frac{1}{\Gamma(n)} \int_0^x t^{n-1} e^{-t} dt = 1 - e_{n-1}(x)e^{-x} \tag{3.17}$$

$$e_n(x) = \sum_{j=0}^{n} \frac{x^j}{j!} \tag{3.18}$$

Lemma 3.6. *With the conditional density $p_n(y|a)$ defined as in* (3.16)*, we have the following two identities*

$$\int_0^\infty y^2 p_n(y|a) = a^2 + 2n \tag{3.19}$$

$$\int_0^\infty y^4 p_n(y|a) = 4n(n-1) + 8(1+\frac{a^2}{2})(n-1) + 8(1+\frac{a^2}{2})^2 \tag{3.20}$$

Proof. The proof of these identities is by straightforward integration – substituting v in place of $\frac{y^2}{2(1+\frac{a^2}{2})}$ and interchanging the order of integration, it is easily seen that (3.19) and (3.20) hold true. □

Using Lemma 3.6, (3.15) is clearly equivalent to

$$-\log\left((2\pi e)^T(1+\frac{a^2}{2})\right) - \int_0^\infty p_T(y|a)\log(q(y))dy \tag{3.21}$$

By a similar evaluation of integrals, it is seen that if we let $y = \sqrt{2}\|\mathbf{y}\|$, then

$$p(\mathbf{y}) = 2^T q(y) = \int_0^\infty \int_{\mathbb{C}^T} p(\mathbf{y}|\mathbf{x}) p(\mathbf{x}|a) p_a(a) d\mathbf{x} da \tag{3.22}$$

$$= \frac{(T-1)!}{2\pi^T y^{2T-1}} 2^T p_T(y) \tag{3.23}$$

where $p_T(y) = \int_0^\infty p_T(y|a)p_a(a)da$. Combinig (3.21) and (3.23), the mutual information (3.4) achieved by an input amplitude density $p_a(a)$ over the block independent non-coherent fading channel can be written as

$$I(p_a(a)) = \int_0^\infty \left\{ -\log\left(1+\frac{a^2}{2}\right) - \int_0^\infty p_T(y|a)\log\left(\frac{c_T p_T(y)}{2y^{2T-1}}\right) dy \right\} p_a(a)da \tag{3.24}$$

[2] using $P(0,x) = 1$.

where $c_n = (2e)^n(n-1)!$. Calling the expression inside the curly parenthesis $F_{p_a}(a)$, the capacity of the channel thus becomes

$$\mathsf{C} = \sup_{p_a(a), E(a^2) \leq 2T\gamma_s} \int_0^\infty F_{p_a}(a) p_a(a) da \tag{3.25}$$

3.3 The I.I.D. fading channel

The channel model for this case becomes the complex scalar equation $y = xh + n$ where h and n are zero mean, unit variance independent complex gaussian distributed random variables. The resultant transition density is

$$p(y|x) = \frac{1}{\pi(1+|x|^2)} \exp\left(\frac{-|y|^2}{1+|x|^2}\right) \tag{3.26}$$

The capacity is given by

$$\mathsf{C} = \sup_{p(x), E(|x|^2) \leq \gamma_s} I(x;y) \tag{3.27}$$

$$= \sup_{p(x), E(|x|^2) \leq \gamma_s} \underbrace{\int\int}_{\mathbb{C}^2} p(y|x)p(x) \log \frac{p(y|x)}{p(y)} dxdy \tag{3.28}$$

Following Lemma 3.5, we conclude that given that x has its phase uniformly distributed between 0 and 2π, the density of y depends only on its absolute value or length. Equating $p(y) = 2q(\sqrt{2}|y|)$, the inner integral in (3.25) can be simplified as follows by using $y = y_1 e^{\jmath\theta_1}$,

$$\frac{1}{\pi(1+|x|^2)} \int_0^\infty \int_{-\pi}^{\pi} y_1 e^{-\frac{y_1^2}{1+|x|^2}} \left(-\frac{y_1^2}{1+|x|^2} - \log(\pi(1+|x|^2)) - \log(2q(\sqrt{2}y_1))\right) d\theta_1 dy_1$$

$$= -\log(2\pi(1+|x|^2)) - \frac{2}{1+|x|^2} \int_0^\infty y_1 e^{-\frac{y_1^2}{1+|x|^2}} \left(\frac{y_1^2}{N_0+|x|^2} + \log(q(\sqrt{2}y_1))\right) dy_1$$

$$= -\log(2\pi e(1+|x|^2)) - \frac{2}{1+|x|^2} \int_0^\infty y_1 \exp\left(\frac{-y_1^2}{1+|x|^2}\right) \log(q(\sqrt{2}y_1)) dy_1 \tag{3.29}$$

$$= -\log(1+\frac{a^2}{2}) - \int_0^\infty \frac{y}{1+\frac{a^2}{2}} e^{-\frac{y^2}{2(1+\frac{a^2}{2})}} \log\left(\frac{c_1 p_1(y)}{2y}\right) dy \tag{3.30}$$

where (3.30) resulted from making the change of variables $|x|^2 = a^2/2$ and $y_1^2 = y^2/2$. It is easily seen that (3.30) is equivalent to the intermediate result in [15].

3.4 Characterizing the Input Density

3.4.1 Kuhn-Tucker Condition

The constrained optimization problem in (3.25) is easily turned into an unconstrained optimization problem using the theory of Lagrange multipliers. Using the Kuhn-Tucker Theorem, it can be shown that the optimal input distribution p_a^* satisfies

$$F_{p_a}(a) \leq \mathsf{C} + \lambda(a^2 - 2T\gamma_s) \quad \forall a \geq 0 \tag{3.31}$$

with equality holding when $a \in \mathcal{A}$, where $\mathcal{A}$ is the support set of p_a^*. Using the definition of $F_{p_a}(a)$, (3.31) can be written as

$$\int_0^\infty p_T(y|a) \log\left(\frac{p_T(y)}{y^{2T-1}}\right) + \log\left(1 + \frac{a^2}{2}\right) + \log(\frac{c_T}{2}) + \mathsf{C} + \lambda(a^2 - 2T\gamma_s) \geq 0 \tag{3.32}$$

3.4.2 Bounded support

For the discrete memoryless Rician fading channel, it has been shown that under an average input power constraint, the optimal input amplitude distribution has bounded support [24]. We now extend this result to the case of block-independent Rayleigh faded channels with the power constraint as in (1.4).

Theorem 3.7. *For block independent Rayleigh fading channel with the average input power constraint in* (1.4)*, the optimal input amplitude distribution has bounded support.*

Proof. The proof is through contradiction. Assume that the input amplitude a has

unbounded support. As in [24], we first lower bound $\frac{p_T(y)}{y^{2T-1}}$ as follows

$$\frac{p_T(y)}{y^{2T-1}} = \frac{1}{y^{2T-1}} \int_0^\infty p_T(y|a)p(a)da \tag{3.33}$$

$$\geq \frac{1}{y^{2T-2}} \int_M^\infty \frac{(1+a^2/2)^{T-2}}{(a^2/2)^{T-1}} e^{-\frac{y^2}{2(1+a^2/2)}} P\left(T-1, \frac{y^2a^2}{4(1+a^2/2)}\right) p(a)da \tag{3.34}$$

$$\geq \frac{1}{y^{2T-2}} e^{-\frac{y^2}{2(1+M^2/2)}} P\left(T-1, \frac{y^2a^2}{4(1+a^2/2)}\right) \int_M^\infty \left(1+\frac{2}{a^2}\right)^{T-2} \frac{2}{a^2} p(a)da \tag{3.35}$$

$$= \frac{1}{y^{2T-2}} e^{-\frac{y^2}{2(1+M^2/2)}} P\left(T-1, \frac{y^2a^2}{4(1+a^2/2)}\right) K_{p_a}(M) \tag{3.36}$$

where M can be chosen large enough that $K_{p_a}(M)$ is smaller than unity[3].

Substituting this into the left-hand side (LHS) of (3.31), we can bound the LHS of (3.31) as

$$LHS \geq \int_0^\infty p_T(y|a) \log\left(\frac{P(T-1, \frac{y^2M^2}{4(1+M^2/2)})}{y^{2T-2}}\right) dy + \log(1+\frac{a^2}{2})$$
$$- \frac{1}{2+M^2} \int_0^\infty y^2 p_T(y|a)dy + \log(\frac{c_T K_{p_a}(M)}{2}) + \lambda(a^2 - 2T\gamma_s) + \mathsf{C} \tag{3.37}$$

$$= \int_0^\infty p_T(y|a) \log\left(\frac{P(T-1, \frac{y^2M^2}{4(1+M^2/2)})}{y^{2T-2}}\right) dy + \log(1+\frac{a^2}{2})$$
$$+ (\lambda - \frac{1}{2+M^2})a^2 + \log(\frac{c_T K_{p_a}(M)}{2}) - 2T\lambda\gamma_s + \mathsf{C} - \frac{2T}{2+M^2} \tag{3.38}$$

The first term in (3.38) is negative $\forall\, a$, since $\log\left(\frac{P(T-1, \frac{y^2M^2}{4(1+M^2/2)})}{y^{2T-2}}\right) < 0 \;\forall\; y \geq 0$ and hence is upper bounded by 0. We next proceed to lower bound the first term

[3]It basically suffices that $K_{p_a}(M)$ be finite.

in (3.38) as follows by first substituting $u = y^2/2$,

$$G(a) = \int_0^\infty p_T(y|a) \log \left(\frac{y^{2T-2}}{P\left(T-1, \frac{y^2M^2}{4(1+M^2/2)}\right)} \right) dy \tag{3.39}$$

$$= \frac{(1+a^2/2)^{T-2}}{(a^2/2)^{T-1}}(T-1) \int_0^\infty e^{-\frac{2u}{2+a^2}} P\left(T-1, \frac{ua^2}{2+a^2}\right) \log(2u) du \tag{3.40}$$

$$- \frac{(1+a^2/2)^{T-2}}{(a^2/2)^{T-1}} \int_0^\infty e^{-\frac{2u}{2+a^2}} P\left(T-1, \frac{ua^2}{2+a^2}\right) \log\left(P\left(T-1, \frac{uM^2}{2+M^2}\right)\right) du \tag{3.41}$$

$$\leq \frac{(1+a^2/2)^{T-2}}{(a^2/2)^{T-1}}(T-1) \int_0^\infty e^{-\frac{2u}{2+a^2}} \log(2u) du \tag{3.42}$$

$$- \frac{(1+a^2/2)^{T-2}}{(a^2/2)^{T-1}} \int_0^\infty e^{-\frac{2u}{2+a^2}} P\left(T-1, \frac{ua^2}{2+a^2}\right) \log\left(P\left(T-1, \frac{uM^2}{2+M^2}\right)\right) du \tag{3.43}$$

$$= -\frac{(1+a^2/2)^{T-1}}{(a^2/2)^{T-1}} \left(\gamma_E - (T-1)\log 2 + \log(\frac{2}{2+a^2}) \right) \tag{3.44}$$

$$- \frac{(1+a^2/2)^{T-2}}{(a^2/2)^{T-1}} \int_0^\infty e^{-\frac{2u}{2+a^2}} P\left(T-1, \frac{ua^2}{2+a^2}\right) \log\left(P\left(T-1, \frac{uM^2}{2+M^2}\right)\right) du \tag{3.45}$$

where $\gamma_E \approx 0.577216$ is the Euler-Gamma constant. The second term in (3.45) (without the multiplicative factor) is lower bounded so that an upper bound on $G(a)$ is obtained. Note that for large enough M, $\frac{uM^2}{2+M^2} \approx u$. Since we are interested in the behavior of this term for $a \to \infty$, we again make the approximation $\frac{ua^2}{2+a^2} \approx u$. Since $P(n,x)\log(P(n,x))$ is a continuous function, it is possible to write

$$P\left(T-1, \frac{ua^2}{2+a^2}\right) \log\left(P\left(T-1, \frac{uM^2}{2+M^2}\right)\right) = P(T-1,u)\log(P(T-1,u)) - \epsilon \tag{3.46}$$

for some small $\epsilon > 0$. Observing also that $f(x) = x\log(x), x \in [0,1]$ achieves its

minimum of $-e^{-1}$ at $x = e^{-1}$, the second term in (3.45) is lower bounded as

$$\frac{(1+a^2/2)^{T-2}}{(a^2/2)^{T-1}} \int_0^\infty e^{-\frac{2u}{2+a^2}} P\left(T-1, \frac{ua^2}{2+a^2}\right) \log\left(P\left(T-1, \frac{uM^2}{2+M^2}\right)\right) du \quad (3.47)$$

$$\geq -\frac{(1+a^2/2)^{T-2}}{(a^2/2)^{T-1}}(e^{-1}+\epsilon) \int_0^\infty e^{-\frac{2u}{2+a^2}} du \quad (3.48)$$

$$= -\frac{(1+a^2/2)^{T-1}}{(a^2/2)^{T-1}}(e^{-1}+\epsilon) \quad (3.49)$$

Thus, overall

$$\left(\frac{2+a^2}{a^2}\right)^{T-1} \left(\gamma_E - e^{-1} - \epsilon - \log(2^{T-1}(1+\frac{a^2}{2}))\right) \quad (3.50)$$

$$\leq \int_0^\infty p_T(y|a) \log\left(\frac{P(T-1, \frac{y^2M^2}{4+2M^2})}{y^{2T-2}}\right) dy \leq 0 \quad (3.51)$$

and (3.38) can be written as

$$LHS \geq \left(\frac{2+a^2}{a^2}\right)^{T-1} \left(\gamma_E - e^{-1} - \epsilon - \log(2^{T-1})\right) + \left(1 - \left(\frac{2+a^2}{a^2}\right)^{T-1}\right) \log(1+\frac{a^2}{2})$$

$$+ (\lambda - \frac{1}{2+M^2})a^2 + \log(\frac{c_T K_{p_a}(M)}{2}) - 2T\lambda\gamma_s + \mathsf{C} - \frac{2T}{2+M^2} \quad (3.52)$$

Thus, when M is chosen large enough so that $\lambda > \frac{1}{2+M^2}$, the right hand side of (3.52) diverges to ∞ when $a \to \infty$. This is a contradiction since from the Kuhn-Tucker condition, the LHS of (3.31) is required to be zero infinitely often as $a \to \infty$. Thus the optimal input amplitude is required to have bounded support. □

3.4.3 Mass point at Zero

It has been conjectured [43] that with only a second moment constraint, the input amplitude random variable namely a is mostly like discrete and has finite number of mass points. As opposed to the high SNR regime, where single amplitude schemes have been shown to achieve the capacity of this channel, we prove below that when the input amplitude random variable a has mass at zero, the mutual information is non-decreasing.

Theorem 3.8. *Under an average power constraint, for a block independent non-coherent Rayleigh fading channel, starting from a single amplitude scheme, assigning probability mass to a zero amplitude signal while maintaining the same average power, does not decrease the mutual information.*

Proof. The proof proceeds similar to the work in [39]. Let us assume an input amplitude distribution specified by $\mathbf{p} = \{0, 1\}$ and $\mathbf{a} = \{0, a\}$. This corresponds to an input alphabet that has constant amplitude a. Now consider a second input amplitude distribution that is obtained from the first by assigning some probability mass to the zero amplitude, namely $\mathbf{p}(x) = \{x, 1-x\}$ and $\mathbf{a}(x) = \{0, \frac{a}{\sqrt{1-x}}\}$ $(x \geq 0)$. Note that the non-zero amplitude in $\mathbf{a}(x)$ has been increased so as to maintain the same average amplitude a. Proof of the claim lies in verifying that $I(\mathbf{a}(x), \mathbf{a}(x)) > I(\mathbf{p}, \mathbf{a})$. Referring to $I(\mathbf{a}(x), \mathbf{a}(x))$ as $I(x)$ in the following, we prove that $\frac{dI(x)}{dx}|_{x=0} > 0$.

After some simplification[4] it follows that

$$\begin{aligned}\left.\frac{dI(x)}{dx}\right|_{x=0} &= \log\left(1+\frac{a^2}{2}\right) - \frac{a^2}{2(1+\frac{a^2}{2})} \\ &\quad - \frac{a^2}{2(1+\frac{a^2}{2})^2}\int_0^\infty f(y,a)\log\left(\frac{c_T p_T(y|a)}{2y^{2T-1}}\right) \end{aligned} \tag{3.53}$$

where

$$\begin{aligned} f(y,a) = \Bigg\{ &\left(\frac{y^2}{2} - \left(1+\frac{a^2}{2}\right) - \frac{(1+\frac{a^2}{2})^2}{a^2/2}\right) p_T(y|a) \\ &+ \frac{(1+\frac{a^2}{2})^2}{a^2/2} p_T(y|0) - (T-1)p_{T+1}(y|a)\Bigg\} \end{aligned} \tag{3.54}$$

The first two terms of (3.53) is easily seen to be positive since it is of the form $\log(1+u) - \frac{u}{1+u}$ which is positive for $u > 0$. Since it can be safely assumed that

[4] $p_T(y|a=0)$ is obtained from $p(y, y_1|a=0)$ by marginalizing y_1, as $\frac{y^{2T-1}e^{-y^2/2}}{2^{T-1}(T-1)!} \forall\, y \geq 0$

$a > 0$, it only remains to be shown that the third term in (3.53) is negative. Using Lemma 3.6, it is easily verified that

$$\int_0^\infty f(y,a)dy = 0 \tag{3.55a}$$

$$\int_0^\infty y^2 f(y,a)dy = 0 \tag{3.55b}$$

Note that

$$\frac{c_T p_T(y|a)}{2y^{2T-1}} = \frac{c_T e^{-\frac{y^2}{2}}}{2(1+\frac{a^2}{2})} g_{T-1}\left(\frac{y^2a^2}{4(1+\frac{a^2}{2})}\right) \tag{3.56a}$$

where,

$$g_n(x) = x^{-n}e^x P(n,x) \tag{3.56b}$$

Using (3.55), the third term in (3.53) can be rewritten as

$$\int_0^\infty f(y,a)\log\left(\frac{c_T p_T(y|a)}{2y^{2T-1}}\right) = \int_0^\infty f(y,a)\log\left(g_{T-1}\left(\frac{y^2a^2}{4(1+\frac{a^2}{2})}\right)e^{\lambda+\mu y^2}\right) \tag{3.57}$$

for any λ and μ. Observe that $g_n(x)$ is an increasing function in x, $\forall n > 1$. Note that for any $a > 0$, there exist 2 positive numbers Y_1 and Y_2[5] such that $f(y,a) < 0$ for $y \in (Y_1, Y_2)$ and $f(y,a) > 0$ otherwise. Choosing

$$\lambda = \frac{Y_1^2}{Y_2^2 - Y_1^2} g_{T-1}\left(\frac{Y_2^2a^2}{4(1+\frac{a^2}{2})}\right) - \frac{Y_2^2}{Y_2^2 - Y_1^2} g_{T-1}\left(\frac{Y_1^2a^2}{4(1+\frac{a^2}{2})}\right) \tag{3.58}$$

$$\mu = \frac{g_{T-1}\left(\frac{Y_1^2a^2}{4(1+\frac{a^2}{2})}\right) - g_{T-1}\left(\frac{Y_2^2a^2}{4(1+\frac{a^2}{2})}\right)}{Y_2^2 - Y_1^2} \tag{3.59}$$

we can force $f(y,a)$ and $\log\left(g_{T-1}\left(\frac{y^2a^2}{4(1+\frac{a^2}{2})}\right)e^{\lambda+\mu y^2}\right)$ to have opposite signs for all y except at Y_1 and Y_2, where both are identically zero. This forces the integrand and hence the integral in the third term (3.53) to be negative. Therefore, $I(x)$ is shown to be an increasing function of x at $x = 0$ and the theorem is proved. □

[5]Without loss of generality, we can assume that $Y_1 < Y_2$

3.5 Numerical Results

The simplifications of the mutual information expression to (3.24) allow us to compute the constrained capacity of the SISO block fading channel numerically in the following cases

1. Unitary Signal Constellations with Single Amplitude: Suppose a is a discrete random variable that takes the value $\sqrt{2T\gamma_s}$ with probability 1. From (3.25) and (3.24), we directly get the mutual information achieved by this input over the channel (in nats) as

$$-\log(1+T\gamma_s) - \int_0^\infty p_T(y|a=\sqrt{2T\gamma_s}) \log\left(\frac{c_T p_T(y|a=\sqrt{2T\gamma_s})}{2y^{2T-1}}\right) dy \quad (3.60)$$

2. Unitary Signal Constellations with additional mass point at 0: Suppose a is a discrete random variable that has two mass points, one at 0 (with probability $1-\alpha$) and the other at A (with probability α). The amplitude A must satisfy $A^2\alpha = 2T\gamma_s$. The constrained capacity when using such an input signal distribution becomes

$$-\alpha \log\left(1+\frac{T\gamma_s}{\alpha}\right) - \int_0^\infty \left(\alpha p_T\left(y|a=\sqrt{\frac{2T\gamma_s}{\alpha}}\right) + (1-\alpha)p_T(y|a=0)\right) \log\left(\frac{c_T p_T(y)}{2y^{2T-1}}\right) dy \quad (3.61)$$

Numerical evaluation (using Mathematica) of (3.60) and (3.61) give the constrained capacities of unitary constellations and 2-mass point constellations respectively. Through these numerical evaluations, the minimum information bit SNR (dB) required to achieve a given rate (bits/channel use) has been calculated for block lengths $T = 1, 2, 3, 4$ and the corresponding graphs are plotted below in Fig. 3.1.

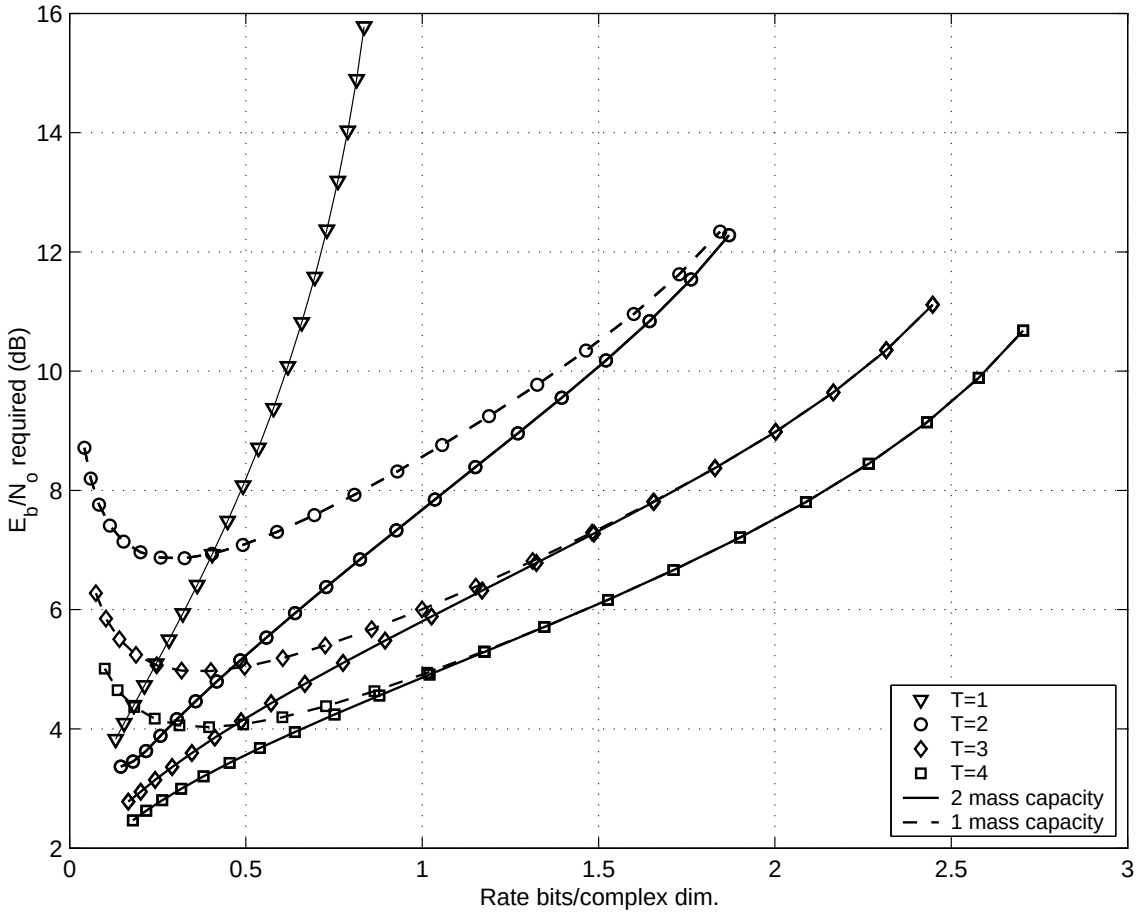

Figure 3.1: Minimum E_b/N_o dB required to achieve a certain rate for unitary and isotropically distributed signals and for unitary and isotropically distributed signals augmented by the zero symbol (2 mass constellations) with optimized probability of zero.

It is also possible to numerically optimize the probability α that gives the maximum achievable rate for a given SNR. For block lengths, $T = 1, 2, 3, 4$, Fig. 3.2 shows the probability of the zero symbol (found numerically) that maximizes the mutual information. It is seen that the probability of the zero-symbol decreases with both increasing SNR and increasing rate.

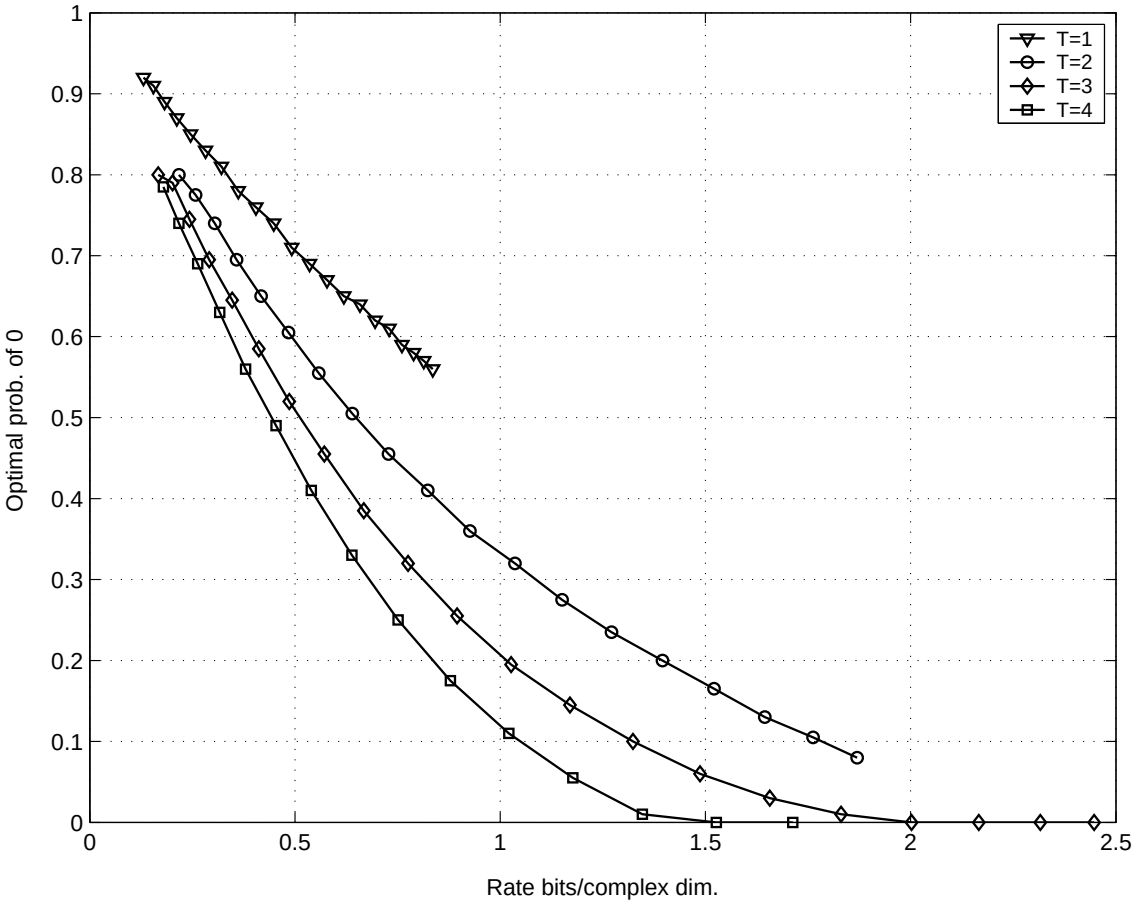

Figure 3.2: Optimal Probability of using the Zero Symbol vs. Rate for short block lengths, $T \sim 1 - 4$.

CHAPTER 4

System Design for the Very Fast Fading Channel

While it was shown in [14] and [24] that the capacity achieving signal distribution for the symbol-by-symbol independent fading[1] channel has some mass at *zero*. This result is valid for all SNR values but is more pronounced at low SNR. In Chapter 3, we proved a slightly weaker result that holds for block independent fading channels. The result which was in two parts, says that (a) the optimal input is isotropically distributed, unitary and has an independent amplitude distribution that has bounded support, and (b) starting from a single amplitude unitary scheme, introducing a zero mass point to the input distribution increases the mutual information. Subsequently numerical evaluation (Fig. 3.1) of the mutual information expression led us to conclude that for low rates (equivalently low SNR) and for very fast fading channels, the use of modulation schemes that remain silent for a significant proportion of the time is more power efficient than modulations that have signals with a single non-zero energy level[2]. We also computed the probability of zero symbol usage that maximizes the capacity and plotted the same in Fig. 3.2. Interestingly, similar observations were drawn for the closely related non-coherent (phase-noisy AWGN) block-independent channel in [39, 41].

[1] This holds for both Rician and Rayleigh fading channels

[2] for a given rate

From these figures, it is apparent that for $T = 2$ and a target rate of 0.5 bits/c.d., using a signal constellation augmented by the zero symbol with the appropriate probability of zero, it is possible to gain almost 1.8 dB over a system not utilizing the zero symbol. For the $T = 3$ and $T = 4$ channels, this gain is around 1.0 and 0.6 dB respectively for the same target rate. Furthermore, it is clear that ignoring the correlation between consecutive symbols incurs a significant loss. Indeed, at a target rate of 0.5, the difference in the required E_b/N_0 for a system with $T = 1$ and $T = 2$ is around 3 dB. These observations show a significant potential gain for coding/modulation schemes that utilize constellations including the zero mass point. Thus motivated, in the rest of this chapter, we propose a simple (and sub-optimal) system for introducing the zero symbol in the constellation, that will enable us to capture some of the potential gain.

4.1 Proposed Scheme

Consider *frames* comprising L coherence blocks. We choose to transmit zeros in $L_0 \in \{0, 1, \ldots, L-1\}$ of them and unitary signals in the rest. This way we achieve a zero mass point with probability $p_0 = L_0/L$. There are $\binom{L}{L_0}$ ways to generate such configurations. This implies that there are exactly $m_0 = \log_2 \binom{L}{L_0}$ bits that can be transmitted through the positions of the L_0 zero blocks. The rest of the information is transmitted through the unitary signal points. When L and L_0 are small, one can generate the bit reliabilities in an optimal way, as in (2.2). We note that the performance of this method and the complexity of generating the bit reliabilities according to (2.2) increases with L. In fact for large L the number of bits that are transmitted through the position of the zero blocks is exactly $\log_2 \binom{L}{p_0 L} \approx LH_2(p_0)$, where $H_2(\cdot)$ is the binary entropy function. In order to accommodate

large values of L with reasonable complexity, we present in the following a simple transmission/reception scheme. In Fig. 4.1, the basic block diagram of the proposed system is shown.

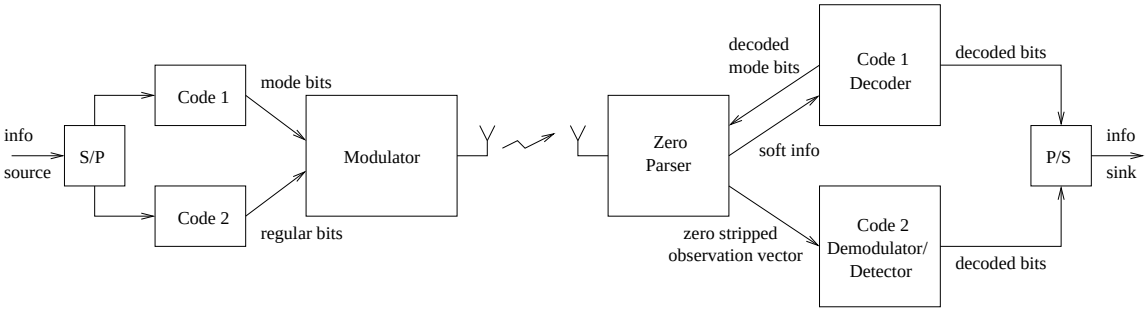

Figure 4.1: Block diagram of system utilizing zero symbol.

The information sequence is split in two segments. One segment is encoded using Code 1 as indicated in Fig. 4.1, and the resulting encoded bits determine the position of zeros by determining which one of the $\binom{L}{L_0}$ configurations is transmitted. The other segment is encoded by Code 2 and the encoded bits determine the unitary signals transmitted in the $L - L_0$ blocks. Fixing the target rate is R_{eff} and the rates R_0 and R_1 of Code 1 and Code 2 respectively, should satisfy the following equations

$$m_0 R_0 + m_1 R_1 = m_0 L T R_{\text{eff}} \tag{4.1}$$

$$\text{fraction of information bits assigned to Code 1} = \frac{R_0}{L T R_{\text{eff}}} \tag{4.2}$$

At the receiver, the observation vector is sent to a device called the *zero-parser* that essentially compares the power received in the L blocks that make up the frame and from the L_0 lowest received power values, determines the configuration of the zeros in the frame. This is the simplest and most naive method of determining the position of the zeros. Having determined the output bits of Code 1, they are decoded by the decoder of Code 1 to obtain the corresponding information bits (alternatively,

one can generate sensible soft decisions (*e.g.*, the L_0 lowest power values from the L blocks can be fed to the decoder). The $L-L_0$ blocks left that correspond to non-zero transmissions are decoded using the techniques presented in Chapter 2.2.

4.2 Analysis of Proposed Scheme

Upon receiving the observation vector, the zero-parser forms the statistic

$$z_j = \sum_{i=1}^{T} \frac{|y_{i,j}|^2}{T}, \qquad j = 1, \ldots, L \tag{4.3}$$

which is a measure of the power of the jth block. Under hypothesis H_0 (zero transmission occurred), z_j has a chi-square distribution with $2T$ degrees and variance per degree $\sigma_0^2 = 1/T$ and hence has a characteristic function $\Phi_{z_j}(s) = \frac{1}{(1-s\sigma_0^2)^T}$. Under hypothesis H_1 (non-zero transmission occurred), z_j has a characteristic function $\Phi_{z_j}(s) = \frac{1}{(1-s\sigma_0^2)^{T-1}(1-s\sigma_1^2)}$, where $\sigma_1^2 = \frac{1}{T} + \frac{\gamma_s}{1-p_0}$ with $\gamma_s = R_{\text{eff}}\gamma_b$.

The analysis of the capacity of such a scheme for general T, L and L_0 is difficult but for the case $T = 2$, $L = 2$ and $L_0 = 1$, the analysis simplifies as follows ($M = N = 1$ is assumed in the development for notational simplicity). For $L = 2$ and $L_0 = 1$, *i.e.* $p_0 = 0.5$ the channel output can be thought of as the difference between z_2 and z_1. Consider the case where the first block is used to transmit the zero point, *i.e.* the configuration chosen was a [zero block, non-zero block] (denoted [0 1] for simplicity). The characteristic function and the probability density function of the difference $z = z_2 - z_1$ is given by

$$\Phi_{z|[01]}(s) = \frac{1}{(1+s\sigma_0^2)^2(1-s\sigma_0^2)(1-s\sigma_1^2)} \tag{4.4}$$

$$f(z|[01]) = \begin{cases} \frac{\sigma_0^2+3\sigma_1^2}{4(\sigma_1^2+\sigma_0^2)^2}\exp(\frac{z}{\sigma_0^2}) - \frac{1}{2\sigma_0^2(\sigma_1^2+\sigma_0^2)}z\exp(\frac{z}{\sigma_0^2}), & z \le 0 \\ \frac{\sigma_1^4}{(\sigma_1^2-\sigma_0^2)(\sigma_1^2+\sigma_0^2)^2}\exp(-\frac{z}{\sigma_1^2}) - \frac{1}{4(\sigma_1^2-\sigma_0^2)}\exp(-\frac{z}{\sigma_0^2}), & z > 0 \end{cases} \tag{4.5}$$

Similarly, the quantity $f(z|[10])$ can be found to be $f(z|[10]) = f(-z|[01])$. For illustration, the probability density function of z given that the zero point was transmitted in the first block while a unitary space time signal was transmitted in the second block is plotted in Fig. 4.2. From simulations, the histogram of the same density was plotted and was found to be identical to the ones plotted in Fig. 4.2. From the same it is seen that with increasing signal to noise ratio, $\Pr(z > 0)$ also increases indicating that the statistic z that is formed by the zero parser is reasonable. The question to be asked at this juncture is whether this system has capacity gains over the traditional unitary signalling schemes.

To simplify notation, consider the output of this channel to be the log-likelihood ratio

$$l \stackrel{\text{def}}{=} \log \frac{f(z|[01])}{f(z|[10])} = \log \frac{f(z|[01])}{f(-z|[01])} \tag{4.6}$$

The decoder of Code 1 can now operate with the soft inputs l and thus, Code 1 can be a powerful turbo-like code. The capacity of the equivalent channel seen by the zero-parser can be easily evaluated numerically using (4.5) and is denoted by $C_0(T, \gamma_s, L, L_0)$ (in bits per complex dimension). Assuming that a long enough codeword is transmitted, any rate below this capacity will result in a probability of sequence error arbitrarily small. This means that with arbitrarily small probability the zero-parser followed by the decoder will identify the positions of the zero blocks. Once this is done, the zero blocks are stripped from the frames and decoding of the remaining coded unitary transmissions is performed. The resulting overall capacity (in bits per complex dimension) can be written as

$$C_{tot}(T, \gamma_s, L, L_0) = \frac{L - L_0}{L} C_{1pt}(T, \frac{\gamma_s}{1 - p_0}) + C_0(T, \gamma_s, L, L_0) \tag{4.7}$$

where $C_{1pt}(T, \gamma_s)$, the capacity of the single amplitude unitary constellation shown

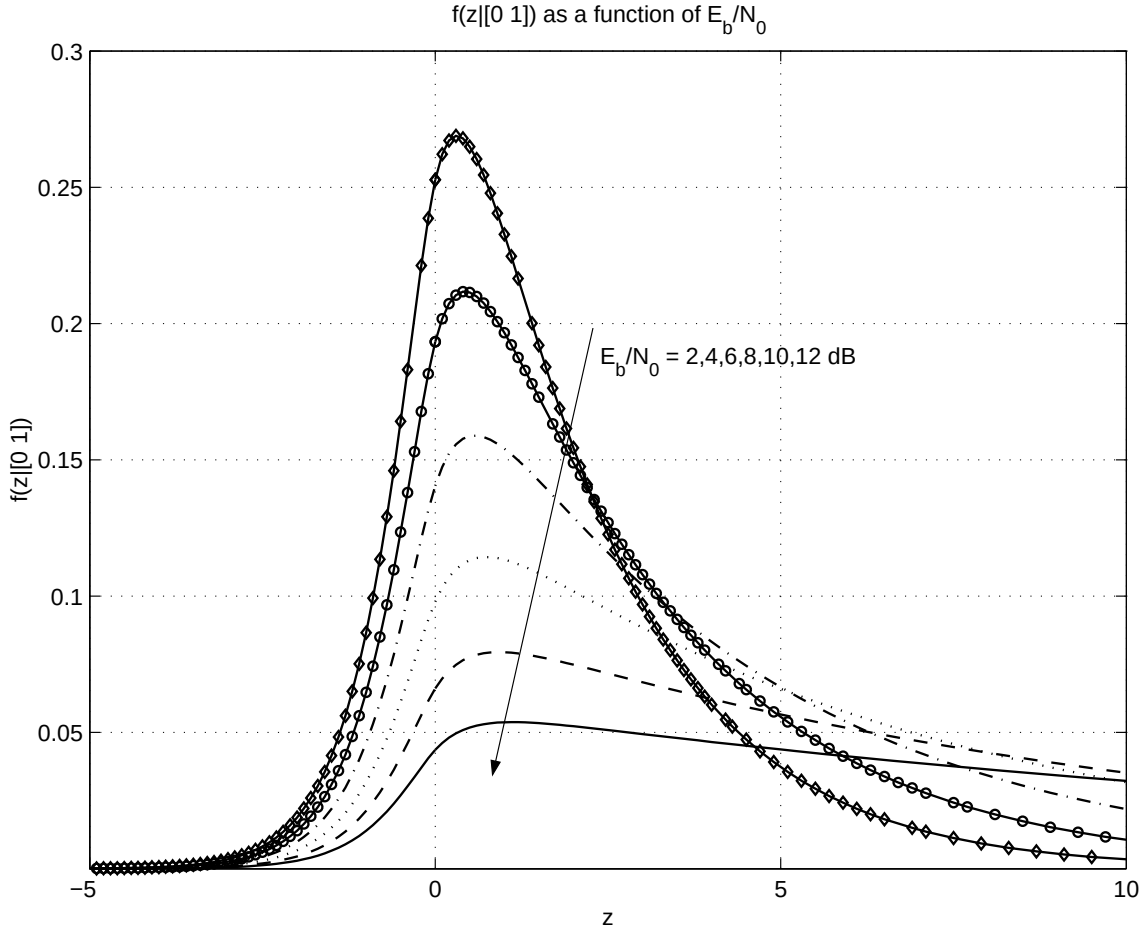

Figure 4.2: Likelihood function of z given transmission of zero in the first block and unitary signals in the second block for various values of E_b/N_0. Overall rate of 0.5 bits/complex dimension is assumed.

in Fig. 3.1 via the dashed-dot curves. For a given γ_s, T, one needs to optimize over $L \in \{2, 3, \ldots\}$ and $L_0 \in \{0, 1, \ldots, L-1\}$. If the resulting capacity is larger than $C_{tot}(T, \gamma_s, L, 0) = C_{1pt}(T, \gamma_s)$ and close to the two-mass-point capacity numerically evaluated and shown in Fig. 3.1, then this simple transmission scheme is adequate.

4.3 Numerical Results

As an example of a practical scheme, we have numerically evaluated $C_{tot}(2, \gamma_s, 2, 1)$ when using a size 4 systematically generated unitary constellation for the non-zero transmission. For comparison, we also numerically evaluated (through Monte Carlo simulations) the capacity of a standard scheme using the same size 4 systematically generated unitary constellation. These results plotted in Fig. 4.3 show that an $\gamma_b = E_b/N_0 = 8.27$ dB is required to support 0.5 bits/ch.use for the proposed system, while the standard system requires 9.25 dB to support the same rate. Thus even in a practical system, there is a 1.0 dB advantage in using the proposed scheme.

For the very fast fading channel, a 1×1 channel with a coherence interval of $T = 2$ was considered. We observed through experiments that, the block independence of the channel is not crucial to the performance of the receiver. This implies that the schemes proposed in this chapter can be extended to the case of continuous fading with almost no change in performance. It is noted however that this may not be a good solution to the problem of combating continuous fading, since there is additional reliability to be obtained about the bits transmitted in one block from the channel observations in adjacent blocks.

From Fig. 3.2, we notice that the optimal probability of zero for a 2-mass system over a channel with $T = 2$ is ≈ 0.6. Accordingly, we designed a system such that the probability of the zero symbol is 0.5. The simplest possible choice of $L = 2, L_0 =$

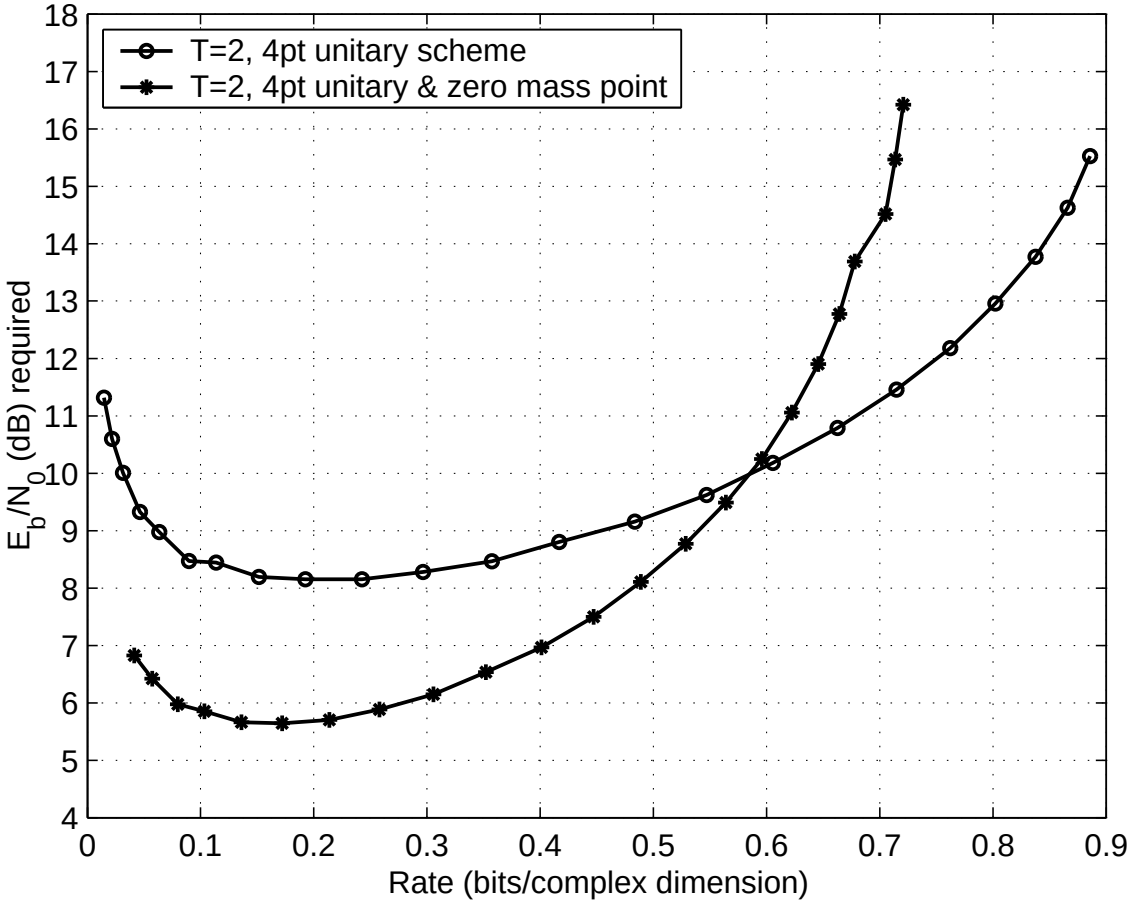

Figure 4.3: E_b/N_0 required for the above system when utilizing a unitary constellation of size 4 in conjunction with the zero symbol. Also shown is E_b/N_0 required when utilizing the size 4 unitary constellation only.

1 guarantees that the probability of the zero symbol is 0.5 while allowing us the opportunity to compare our results with analysis.

We fixed an overall rate of 0.5 bits/ch.use. The system employing a single amplitude constellation, used an optimized[3] rate 0.5 LDPCC (with 4000 information bits) along with a 4 point SGUC across 2 complex dimensions. As shown in Fig. 4.4, this system reaches 10^{-4} bit error rate at 10.35 dB.

For the sake of comparison, the number of information bits transmitted per codeword was fixed at 4000. Hence 1333 information bits were transmitted through using Code 1 with rate $R_1 = 2/3$, while 2667 bits were transmitted through Code 2 with rate[4] $R_2 = 2/3$. For the non-zero symbols, we used the same size 4 SGUC as mentioned above. This system reaches 10^{-4} bit error rate at 9.8 dB gaining 0.55 dB in performance over the single amplitude system. However the predicted performance gain at the target rate of 0.5 bits/complex dimension is 1 dB. We observe that the choice of $L = 2, L_0 = 1$ is a possible reason for not achieving the predicted gain. It is expected that increasing L and $L_0 = p_0 L$ will improve the performance. Besides, the fact that the receiver is inherently sub-optimal is another reason for the decreased performance gain.

Nevertheless using the proposed simple scheme provides a gain of 0.55 dB without any extra complexity and so has merit in practical applications.

---

[3]The code parameters are $\lambda(x) = 0.237613x + 0.246978x^2 + 0.193680x^3 + 0.067187x^7 + 0.124508x^8 + 0.078134x^{13} + 0.051901x^{14}, \rho(x) = 0.378314x^5 + 0.607545x^7 + 0.000298x^8 + 0.013843x^9$.

[4]Code 1 had parameters $\lambda_1(x) = 0.365655x + 0.296262x^2 + 0.084730x^3 + 0.246900x^7 + 0.006453x^8, \rho_1(x) = 0.073673x^5 + 0.194008x^7 + 0.150743x^8 + 0.581577x^9$, while Code 2 had parameters $\lambda_2(x) = 0.265121x + 0.485057x^2 + 0.023998x^3 + 0.031946x^7 + 0.105075x^8 + 0.045764x^{12} + x^{13} + 0.043039x^{14}, \rho_2(x) = 0.071969x^6 + 0.130419x^7 + 0.090424x^8 + 0.707188x^9$.

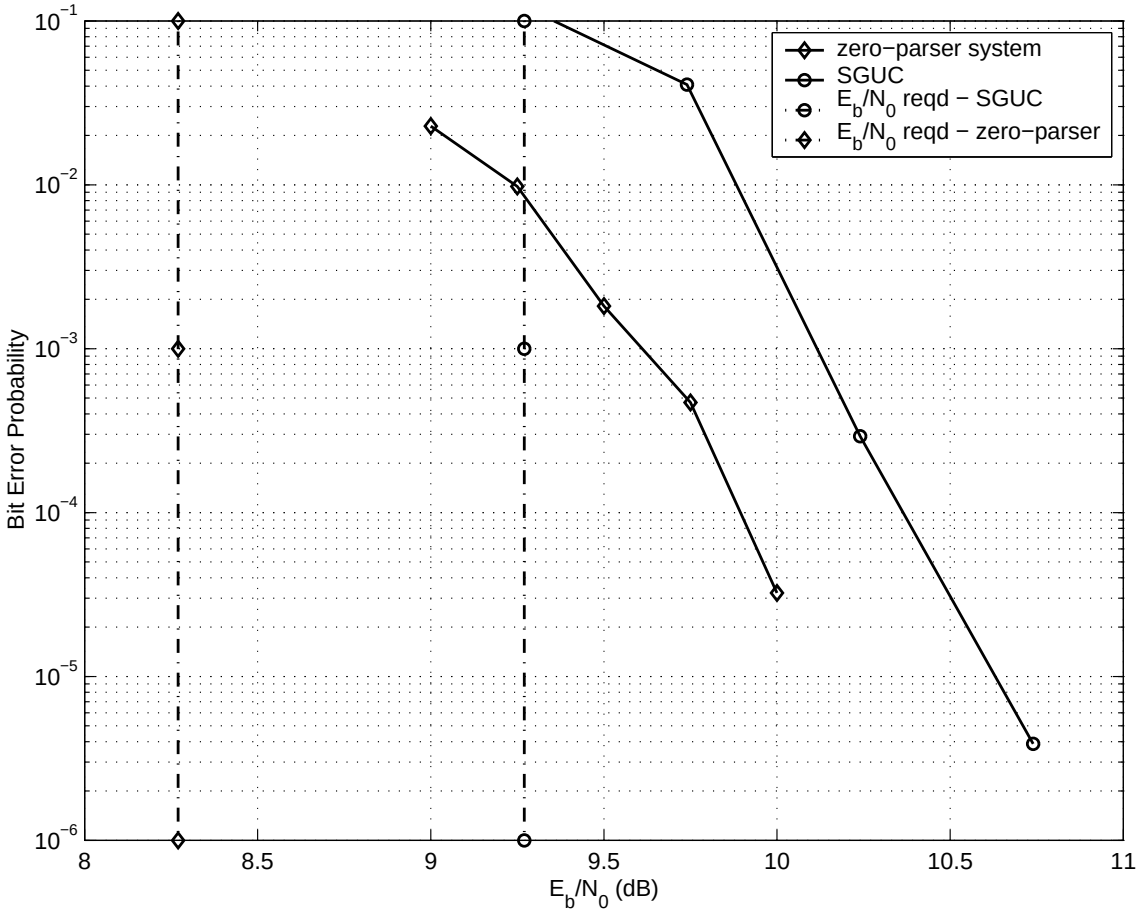

Figure 4.4: Performance in the Very Fast Fading scenario.

CHAPTER 5

Joint Code and Modulation Design

5.1 Motivation for Joint Modulation and Code Design

As A lot of work has been done in the design of good signal constellations, for example - [28], [56], [29], [6]. Also, in [2], trellis-coded unitary space-time modulation codes have been designed using the best signal constellations created in [29], while turbo coded unitary space-time modulation schemes for multiple antenna systems were designed in [3] and [46]. Though the SGUC's have many convenient strengths (as mentioned in Chapter 1), it was our opinion that these modulations might be restrictive when considered in conjunction with coding. Specifically the idea behind a joint modulation and code design approach is to allocate resources so that there will be maximum gain. However, till date, no effort has gone into the joint design of modulation and code for the non-coherent block fading channel when using multiple antennas. For the case of the AWGN channel, a joint approach to the design of modulation and code was taken in [10–13]. These works led to the design of asymmetric signal constellations for trellis coded modulation on the additive white Gaussian noise (AWGN) channel and gains were seen over the conventional systems. An approach of this sort has merit because essentially it is shifting resources to places where they are needed *i.e.*, the code can be used to protect from bad (high) correlations while

good (low) correlations can be made better and used where the code does not protect it (parallel transitions).

The concept of joint modulation and code design is introduced in Section 5.2 with a simple, easy to visualize example of asymmetric QPSK constellations in trellis coded modulations for the AWGN channel. This concept is then extended to the design of asymmetric space-time codes for the fading channel and specific examples are discussed in Section 5.4. In all our designs, we do not optimize the modulation size S from the capacity viewpoint.

5.2 An example for the AWGN case

For a trellis coded modulation (TCM) system on the AWGN channel, the maximum likelihood sequence detector selects the sequence closest — in Euclidean distance sense — to the received sequence. For soft decision decoding of convolutional codes and trellis coded modulation, the maximum likelihood sequence detector is essentially the Viterbi algorithm used to minimize the sum of euclidean distances over all possible trellis paths. As an example (from [4 . Sec. 5.6]), let us take a 2 state, rate 0.5 trellis coded modulation system using 4-PSK signals. The 4-PSK signals and their labelling are shown in Fig. 5.1(a). The overall rate is 1 bit/channel use. The output label assignments (based on the Ungerboeck partitioning [54]) for the corresponding TCM scheme are shown in Fig. 5.2. For a general TCM system, the bit-error probability has the upper bound (using the union bound):

$$\mathrm{P}_b \leq \sum_l d_h^{(l)} N_l \, \mathrm{Q}\left(\sqrt{\frac{d^2(\mathbf{e})}{2N_0}}\right). \tag{5.1}$$

where N_l is the number of error paths of length l, $d_h^{(l)}$ is the hamming weight of the input sequence that produces the error sequence $\mathbf{e}$ of length l, and d^2 is the Euclidean

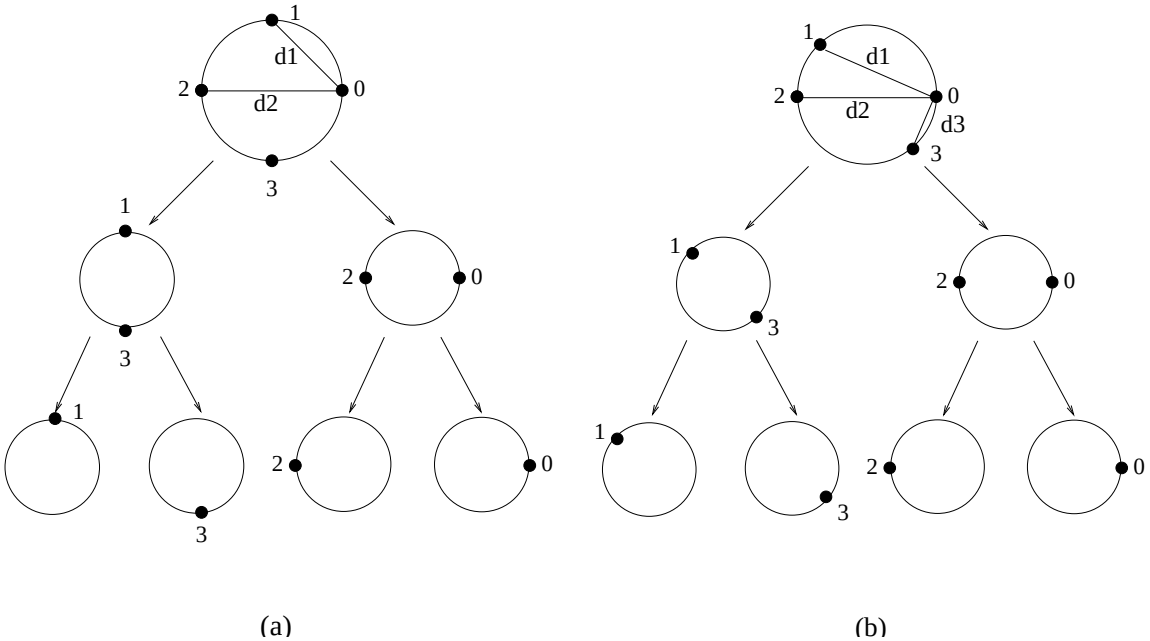

Figure 5.1: 4-PSK signal constellation and labelling. (a) Symmetric, (b) Asymmetric.

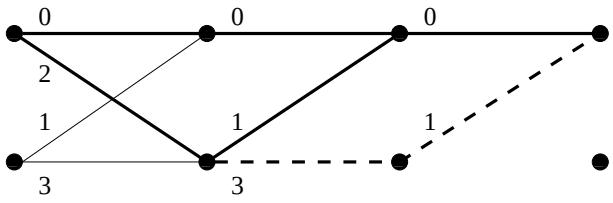

Figure 5.2: 2 state trellis with output label assignment and length 2 and length 3 error paths.

distance between the error sequence $\mathbf{e}$ and the $\mathbf{0}$ codeword. The values N_l, $d_h^{(l)}$ and d^2 are usually obtained by finding the transfer function for the particular system (see [4]).

The asymmetric 4-PSK constellation of Fig. 5.1(b) is obtained by rotating the signals 1 and 3 counter-clockwise (by the same amount) such that the phase between 0 and 3 is θ. By this rotation the distance d_1 between signals 0 and 1 is increased at the cost of the distance d_3 between signals 0 and 3. From this construction of the asymmetric constellation, it is seen that any asymmetric 4-PSK constellation is completely specified by the angle θ, where $\theta \in [0, \pi/2]$.

For the trellis shown in Fig. 5.2, the transfer function mentioned above is given by

$$T(N, I, D) = \frac{NI^2 D^{d_2^2+d_1^2}}{1 - NID^{d_3^2}} \tag{5.2}$$

$$= \sum_{l=2}^{\infty} N^{l-1} I^l D^{d_2^2+d_1^2+(l-2)d_3^2} \tag{5.3}$$

$$\left.\frac{\partial T(N, I, D)}{\partial N}\right|_{N=1, I=1} = \sum_{l=2}^{\infty} (l-1) D^{d_2^2+d_1^2+(l-2)d_3^2} \tag{5.4}$$

For the code of Fig. 5.2, the upper bound for the bit error probability (as a function of the asymmetry angle θ) is obtained from (5.4) as:

$$\mathrm{P}_b \leq \sum_{l=2}^{\infty} (l-1)\, \mathrm{Q}\left(\sqrt{\frac{d_1^2 + d_2^2 + (l-2)d_3^2}{2N_0}}\right) \tag{5.5}$$

$$= \sum_{l=2}^{\infty} (l-1) \mathrm{Q}\left(\sqrt{\frac{6 + 2\cos^2(\theta/2) + (l-2)2\sin^2(\theta/2)}{2N_0}}\right) \tag{5.6}$$

$$= \sum_{l=2}^{\infty} (l-1) \mathrm{Q}\left(\sqrt{\frac{8 + (l-3)2\sin^2(\theta/2)}{2N_0}}\right) \tag{5.7}$$

At high SNR, the performance of the system is determined by the $d_{\min}$, the minimum Euclidean distance between a simple error path and the all 0 codeword.

From Fig. 5.2, it is seen that for this output label assignment, the square of the minimum Euclidean distance is $d^2_{\min} = d_2^2 + d_1^2 = 4 + 2 + 2\cos^2(\theta/2) = 6 + 2\cos^2(\theta/2)$. For the symmetric 4-PSK system ($\theta = \pi/2$) the minimum distance is 6. However, since $6 + 2\cos^2(\theta/2) \geq 6$ for $\theta \in [0, \pi/2]$, the trellis code with the modulation in Fig. 5.1(b) is expected to perform better at high SNR. If we also take into account longer error events, then it can be shown that for $l \geq 4$, in the asymmetric case, the performance deteriorates. Thus there must be an optimal θ. The optimum value of θ can be found by minimizing the bit-error probability with respect to θ.

The upper bound is evaluated numerically from (5.7) and is shown for various θ values in Fig. 5.3. There is an optimum θ at each SNR and as it can be seen, there is a gain of 0.6 dB at high SNR (10^{-6} bit-error rate) with the use of $\theta = \pi/4$.

Further, the approximation that the system performance is controlled only by the minimum distance, motivates the following calculation of the asymptotic gain achievable due to asymmetry. The distance d_1 is maximum when signals 1 and 3 merge with 2 and 0, respectively, *i.e.*, $\theta = 0$. Though this results in a catastrophic code, it is an indication of the maximum gain achievable when asymmetric constellations are used with the trellis code in Fig. 5.2. In this case $d^2_{\text{min,asymmetric}} = 8$. Thus the maximum gain is $10\log_{10}(\frac{d^2_{\text{min,asymmetric}}}{d^2_{\text{min,symmetric}}}) = 10\log_{10}(\frac{8}{6}) = 1.25$dB. It is noted that the performance at low SNR is determined not only by the minimum distance, but also the next couple of terms in (5.7) and also the number of error paths at this distance. Since the distance d_3 is decreased in the asymmetric constellations, the next smallest distances after $d_{\min}$ are lower than the corresponding ones in the symmetric case. Therefore, at low SNR, the asymmetric TCM system is worse than the symmetric TCM system. In order to get improved performance at high SNR, the performance at low SNR is sacrificed.

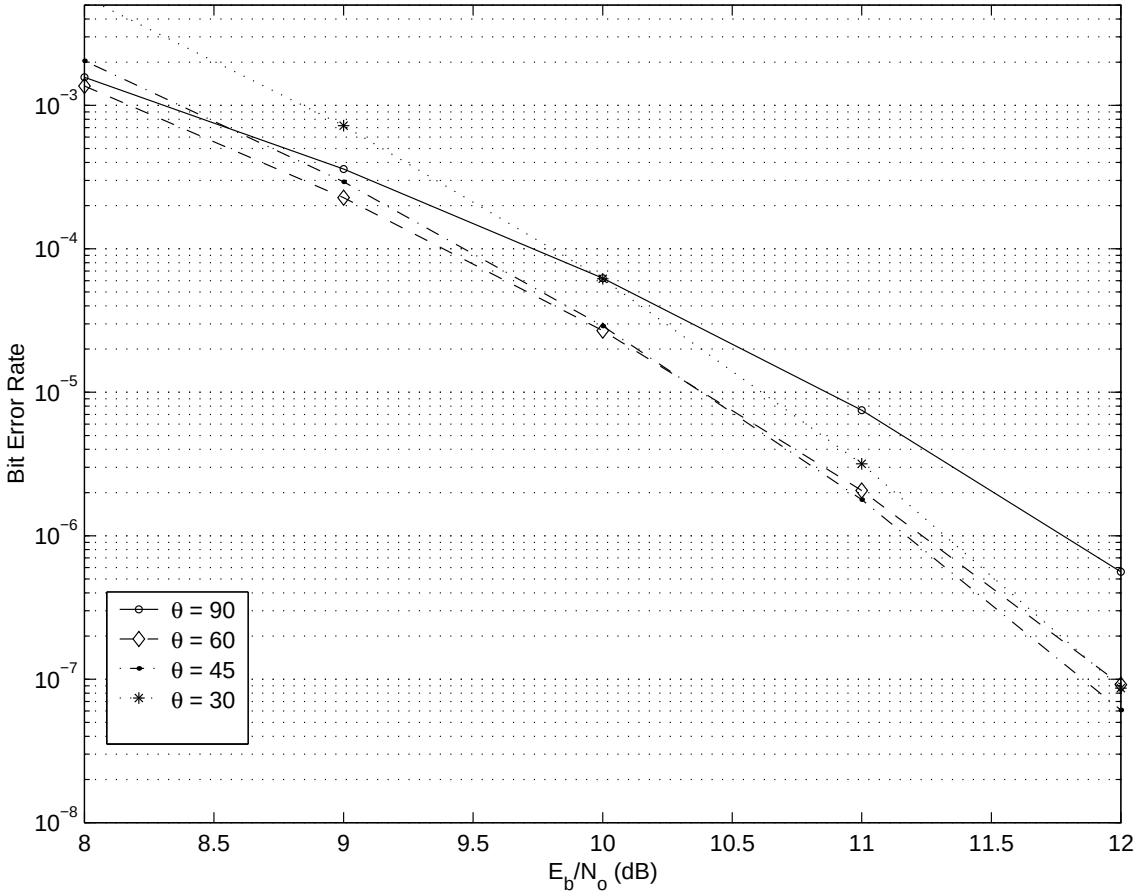

Figure 5.3: Upper bounds to the performance of the TCM system as a function of θ

This potential gain in performance at high SNR is the motivation to design modulation and code in a joint fashion for the fading channel. However there are significant differences between the fading channel and the AWGN channel including the metrics used by the Viterbi Algorithm. In order to understand the factors that control the error performance, in the following we perform the exact pairwise error probability analysis for various cases of M and N.

5.3 Exact Pairwise Error Probability Analysis

In the following, pairwise error probability analysis is done for the following different cases

- $M = N = 1$, general signal structure with power constraint (1.4).
- $M > 1, N = 1$ using unitary space-time constellations.
- $M, N > 1$ using unitary space-time constellations.
- $M = N = 1$ but different energy levels allowed.

The analysis done here is for codes that span multiple coherence blocks and is to serve as tools for the joint design of code and modulation for the space-time channel. The analysis is different from the single block analysis done in [28]. Very recently results similar in nature were published by [35].

5.3.1 Pairwise Probability of Error derivation ($M = N = 1$)

Consider the discrete time channel equation (1.3) specialized to the SISO channel. We consider the transmissions in L blocks and index the received observation vectors with k, where k denotes the block index ($1 \leq k \leq L$). The conditional density of $\mathbf{y}_k$ given $\mathbf{x}_k$ is given by (3.1).

Specializing to the case of equal energy signals *i.e.* $\|\mathbf{x}_k\|^2 = T\gamma_s$. Consider $\mathbf{Y}$ to be a $LT \times 1$ matrix obtained by stacking the received vector in each of the L blocks. Let $\mathbf{X}$ be the matrix form of the transmitted sequence over the L blocks. Since h_k changes independently from block to block and since the noise process $\mathbf{n}_k$ is white, the probability density function of $\mathbf{Y}$ given $\mathbf{X}$ can be written as

$$\begin{aligned} p(\mathbf{Y}|\mathbf{X}) &= \prod_{k=1}^{L} p(\mathbf{y}_k|\mathbf{x}_k) \\ &= \pi^{-LT}(1+T\gamma_s)^{-L} \exp\left(\sum_{k=1}^{L}\left(-\|\mathbf{y}_k\|^2 + \frac{\mathbf{y}_k^*\mathbf{x}_k\mathbf{x}_k^*\mathbf{y}_k}{(1+T\gamma_s)}\right)\right) \end{aligned} \tag{5.8}$$

The maximum likelihood codeword receiver does the following: Choose $\hat{\mathbf{X}}$ as the codeword transmitted if

$$\hat{\mathbf{X}} = \arg\max_{\mathbf{X}} \left(\sum_{k=1}^{L} \mathbf{y}_k^*\mathbf{x}_k\mathbf{x}_k^*\mathbf{y}_k\right) \tag{5.9}$$

$$= \arg\max_{\mathbf{X}} \left(\sum_{k=1}^{L} |\mathbf{y}_k^*\mathbf{x}_k|^2\right) \tag{5.10}$$

The probability of error in decoding $\mathbf{X}^2$ given that $\mathbf{X}^1$ was transmitted (pairwise probability of error; denoted as $\Pr(\mathbf{X}^1 \to \mathbf{X}^2)$ is given by

$$\Pr(\mathbf{X}^1 \to \mathbf{X}^2) = \Pr\left(\sum_{1}^{L} \mathbf{y}_k^*(\mathbf{x}_k^2\mathbf{x}_k^{2*} - \mathbf{x}_k^1\mathbf{x}_k^{1*})\mathbf{y}_k > 0|\mathbf{X}^1\right)$$

Let $W = \{k : 1 \le k \le L, \mathbf{x}_k^2\mathbf{x}_k^{2*} \ne \mathbf{x}_k^1\mathbf{x}_k^{1*}\}$ and $|W| = d_h$ denoting the Hamming distance between the two sequences. Thus the above probability of error is

$$\Pr(\mathbf{X}^1 \to \mathbf{X}^2) = \Pr\left(\sum_{k\in W} \mathbf{y}_k^*(\mathbf{x}_k^2\mathbf{x}_k^{2*} - \mathbf{x}_k^1\mathbf{x}_k^{1*})\mathbf{y}_k > 0|\mathbf{X}^1\right)$$

Let $x_k^1 = \mathbf{x}_k^{1*}\mathbf{y}_k$ and $x_k^2 = \mathbf{x}_k^{2*}\mathbf{y}_k$. Thus

$$\Pr(\mathbf{X}^1 \to \mathbf{X}^2) = \Pr\left(\sum_{k\in W} (|x_k^2|^2 - |x_k^1|^2) > 0|\mathbf{X}^1\right)$$

Obviously x_k^1 and x_k^2 are correlated complex gaussian random variables (because they are linear combinations of the same jointly complex gaussian random variables).

However, given $\mathbf{X}^1$, $\mathbf{y}_k$ are independent over k so that x_k^1 and x_k^2 ($k \in W$) are d_h independent and identical pairs of correlated random variables such that

$$
\begin{aligned}
E[x_k^1|\mathbf{X}^1] &= E[x_k^2|\mathbf{X}^1] = 0 \\
E[x_k^1 x_k^{1*}|\mathbf{X}^1] &= E[\mathbf{x}_k^{1*}\mathbf{y}_k\mathbf{y}_k^*\mathbf{x}_k^1|\mathbf{X}^1] = \mathbf{x}_k^{1*}(\mathbf{x}_k^1\mathbf{x}_k^{1*} + \mathbf{I}_T)\mathbf{x}_k^1 = T\gamma_s(T\gamma_s + 1) \\
E[x_k^2 x_k^{2*}|\mathbf{X}^1] &= E[\mathbf{x}_k^{2*}\mathbf{y}_k\mathbf{y}_k^*\mathbf{x}_k^2|\mathbf{X}^1] = \mathbf{x}_k^{2*}(T\mathbf{x}_k^1\mathbf{x}_k^{1*} + N_0\mathbf{I}_T)\mathbf{x}_k^2 = T\gamma_s(T\gamma_s|\rho_k|^2 + 1) \\
E[x_k^2 x_k^{1*}|\mathbf{X}^1] &= E[\mathbf{x}_k^{2*}\mathbf{y}_k\mathbf{y}_k^*\mathbf{x}_k^1|\mathbf{X}^1] = \mathbf{x}_k^{2*}(T\mathbf{x}_k^1\mathbf{x}_k^{1*} + N_0\mathbf{I}_T)\mathbf{x}_k^1 = T\gamma_s\rho_k(T\gamma_s + 1)
\end{aligned}
$$

where $\rho_k = \frac{\mathbf{x}_k^{2*}\mathbf{x}_k^1}{T\gamma_s}$. Thus,

$$
E\left[\begin{pmatrix} x_k^2 \\ x_k^1 \end{pmatrix}\begin{pmatrix} x_k^{2*} & x_k^{1*} \end{pmatrix}\middle|\mathbf{X}^1\right] = \begin{pmatrix} T\gamma_s(T\gamma_s|\rho_k|^2 + 1) & T\gamma_s\rho_k(T\gamma_s + 1) \\ T\gamma_s\rho_k^*(T\gamma_s + 1) & T\gamma_s(T\gamma_s + 1) \end{pmatrix}
$$

Let the random variable z be defined as

$$
z\colon = \sum_{k\in W} z_k = \sum_{k\in W} (|x_k^2|^2 - |x_k^1|^2)
$$

By finding the characteristic function of z_k and multiplying over k we can get the characteristic function $\Phi_z(s)$ of the random variable z.

The characteristic function of $(|x_k^2|^2 - |x_k^1|^2)$ is found as

$$
\begin{aligned}
\Phi_{z_k}(s) &= E[\exp(-s(|x_k^2|^2 - |x_k^1|^2)] \\
&= \left|\mathbf{I}_2 + s\begin{pmatrix} T\gamma_s(T\gamma_s|\rho_k|^2 + 1) & T\gamma_s\rho_k(T\gamma_s + 1) \\ T\gamma_s\rho_k^*(T\gamma_s + 1) & T\gamma_s(T\gamma_s + 1) \end{pmatrix}\begin{pmatrix} 1 & 0 \\ 0 & -1 \end{pmatrix}\right|^{-1} \\
&= \frac{-1}{T^2\gamma_s^2(T\gamma_s + 1)(1 - |\rho_k|^2)\left[\left(s + \frac{1}{2(T\gamma_s+1)}\right)^2 - \mu_k^2\right]} \\
&= \frac{-1}{A_k(s - q_k)(s + p_k)}
\end{aligned}
$$

where

$$A_k = T^2\gamma_s^2(T\gamma_s+1)(1-|\rho_k|^2) \tag{5.11}$$

$$\mu_k^2 = \frac{1}{4(T\gamma_s+1)^2} + \frac{1}{T^2\gamma_s^2(T\gamma_s+1)(1-|\rho_k|^2)} \tag{5.12}$$

$$q_k = \mu_k - \frac{1}{2(T\gamma_s+1)} \tag{5.13}$$

$$p_k = \mu_k + \frac{1}{2(T\gamma_s+1)} \tag{5.14}$$

and the ROC is given by $-p_k < \Re\{s\} < q_k$.

The probability density function of z can be found by inverse Laplace transforming the characteristic function of z. Since we are interested in $\Pr(z>0)$, we get for $z>0$,

$$f(z) = \sum_{l\in W} \mathrm{Res}_{s=-p_l}\left\{ e^{sz} \prod_{k\in W} \frac{-1}{A_k(s-q_k)(s+p_k)} \right\}$$

The residue can be easily evaluated for the 2 cases — (i) when each $|\rho_k|$ is different from the other and (ii) when $|\rho_k| = \rho \ \ \forall \ \ k \in W$.

Case (i) Each $|\rho_k| < 1$ is different from the other

In this case the density of z for $z>0$ is

$$f(z) = \sum_{l\in W} \frac{e^{-p_l z}}{A_l(p_l+q_l)} \prod_{k\in W, k\neq l} \frac{1}{A_k(q_k+p_l)(p_k-p_l)}$$

The probability of error is evaluated as

$$\begin{aligned}
\Pr(\mathbf{X}^1 \to \mathbf{X}^2) = \int_0^{+\infty} f(x)dx &= \sum_{l\in W} \frac{1/p_l}{A_l(p_l+q_l)} \prod_{k\in W,k\neq l} \frac{1}{A_k(q_k+p_l)(p_k-p_l)} \\
&= \left(\prod_{j\in W} \frac{1}{A_j}\right) \sum_{l\in W} \left(\frac{1/p_l}{(p_l+q_l)} \prod_{k\in W,k\neq l} \frac{1}{(q_k+p_l)(p_k-p_l)} \right) \\
&= \frac{(T^2\gamma_s^2(T\gamma_s+1))^{-d_h}}{\prod_{j\in W}(1-|\rho_j|^2)} \sum_{l\in W} \left(\frac{1}{2\mu_l^2 + \frac{\mu_l}{T\gamma_s+1}} \prod_{k\in W,k\neq l} \frac{1}{\mu_k^2-\mu_l^2} \right) \qquad (5.15) \\
&= \frac{1}{T^2\gamma_s^2} \sum_{l\in W} \frac{(1-|\rho_l|^2)^{d_h-2}}{2(T\gamma_s+1)\mu_l^2+\mu_l} \prod_{k\in W,k\neq l} (|\rho_k|^2-|\rho_l|^2)^{-1} \qquad (5.16)
\end{aligned}$$

Case (ii) $|\rho_k| = \rho < 1 \ \ \forall \ \ k = 1, 2, ..., L$

Since all $|\rho_k| = \rho$ for $k \in \{1, \ldots, L\}$, $A_k = A$, $\mu_k = \mu$, $p_k = p$ and $q_k = q$ for $k \in \{1, \ldots, L\}$. The probability of error in this case is

$$\begin{aligned}\Pr(\mathbf{X}^1 \to \mathbf{X}^2) &= \left(\frac{1}{4A\mu^2}\right)^{d_h} \sum_{j=1}^{d_h} \binom{2d_h - 1 - j}{d_h - 1} \left(\frac{p+q}{p}\right)^j \\ &= \left[\frac{T\gamma_s + 1}{T^2\gamma_s^2(1-\rho^2) + 4(T\gamma_s + 1)}\right]^{d_h} \\ &\quad \sum_{j=1}^{d_h} \binom{2d_h - 1 - j}{d_h - 1} \left(\frac{2\sqrt{1 + \frac{4(T\gamma_s+1)}{T^2\gamma_s^2(1-\rho^2)}}}{1 + \sqrt{1 + \frac{4(T\gamma_s+1)}{T^2\gamma_s^2(1-\rho^2)}}}\right)^j \end{aligned} \tag{5.17}$$

5.3.2 Pairwise error probability for Multilevel signal constellations ($M = N = 1$)

An interesting problem is to generalize the above probability of error expressions for the case when the energy per coherence interval is not restricted to be equal in all blocks. In this case the decoder's decision rule will change and the derivation above has to be redone.

Consider the case when the signal energy in a block can be one of two levels, one of which is 0 and other non-zero. Assuming that the proportion of the number of zero energy blocks to the number of non-zero energy blocks is fixed, say p_0, we can set the non-zero energy level to be $\frac{T\gamma_s}{1-p_0}$, so that the average energy over time is $T\gamma_s$. With this assumption, we can simplify the maximum likelihood decision rule by canceling the multiplicative factors outside the exponential term in (3.1). The pairwise probability of error for such a receiver in decoding sequence $\mathbf{X}^2$ when

actually sequence $\mathbf{X}^1$ was transmitted is given by the expression

$$\begin{aligned}\Pr(\mathbf{X}^1 \to \mathbf{X}^2) &= \Pr\left(\sum_{k=1}^{L}\left(\frac{\mathbf{y}_k^*\mathbf{x}_k^2\mathbf{x}_k^{2*}\mathbf{y}_k}{1+\|\mathbf{x}_k^2\|^2} - \frac{\mathbf{y}_k^*\mathbf{x}_k^1\mathbf{x}_k^{1*}\mathbf{y}_k}{1+\|\mathbf{x}_k^1\|^2}\right) \geq 0\right) \\ &= \Pr\left(\sum_{k=1}^{L}|x_k^2|^2 - |x_k^1|^2 \geq 0\right) \text{ where,} \\ x_k^2 &= \frac{\mathbf{x}_k^{2*}\mathbf{y}_k}{\sqrt{1+\|\mathbf{x}_k^2\|^2}} \\ \text{and } x_k^1 &= \frac{\mathbf{x}_k^{1*}\mathbf{y}_k}{\sqrt{1+\|\mathbf{x}_k^1\|^2}}\end{aligned}$$

As seen int he previous section, x_k^1 and x_k^2 are correlated jointly complex gaussian random variables (because they are linear combinations of the same jointly complex gaussian random variables). Given that $\mathbf{X}^1$ was transmitted, however $\mathbf{y}_k$ are independent over k with the effect that x_k^1 and x_k^2 with $k = 1, 2, ..., L$ are L independent pairs of correlated random variables with mean 0, and the following covariance matrix.

$$E\left[\begin{pmatrix} x_k^2 \\ x_k^1 \end{pmatrix}\begin{pmatrix} x_k^{2^*} & x_k^{1^*} \end{pmatrix}\right] = \begin{pmatrix} \frac{T^2\gamma_s^2|\rho_k|^2+\|\mathbf{x}_k^2\|^2}{1+\|\mathbf{x}_k^2\|^2} & T\gamma_s\rho_k\sqrt{\frac{1+\|\mathbf{x}_k^1\|^2}{1+\|\mathbf{x}_k^2\|^2}} \\ T\gamma_s\rho_k^*\sqrt{\frac{1+\|\mathbf{x}_k^1\|^2}{1+\|\mathbf{x}_k^2\|^2}} & \|\mathbf{x}_k^1\|^2 \end{pmatrix} = \begin{pmatrix} a' & c' \\ c'^* & b' \end{pmatrix}$$

where $\rho_k = \frac{\mathbf{x}_k^{2^*}\mathbf{x}_k^1}{T\gamma_s}$. Letting $z_k = |x_k^2|^2 - |x_k^1|^2$, the characteristic function of z_k can be calculated as

$$\begin{aligned}\Phi_{z_k}(s) &= \frac{1}{\left|\mathbf{I}_2 + s\begin{pmatrix} a' & c' \\ c'^* & b' \end{pmatrix}\begin{pmatrix} 1 & 0 \\ 0 & -1 \end{pmatrix}\right|} \\ &= \frac{1}{(1+sa')(1-sb') + s^2|c'|^2}\end{aligned}$$

Now a',b', and c' take different values under the following 4 cases and hence the respective characteristic functions for z_k are

1. When $\|\mathbf{x}_k^1\|^2 = \|\mathbf{x}_k^2\|^2 = \frac{T\gamma_s}{1-p_0}$,

$$\Phi_{z_k}^1(s) = \frac{1}{(|c|^2 - ab)\left(s - \frac{(a-b)+\sqrt{(a+b)^2-4|c|^2}}{2(|c|^2-ab)}\right)\left(s + \frac{-(a-b)+\sqrt{(a+b)^2-4|c|^2}}{2(|c|^2-ab)}\right)}$$

where

$$a = \frac{T^2\gamma_s^2|\rho_k|^2 + \frac{T\gamma_s}{1-p_0}}{1 + \frac{T\gamma_s}{1-p_0}}, \quad b = \frac{T\gamma_s}{1-p_0}, \quad c = T\gamma_s\rho_k$$

2. When $\|\mathbf{x}_k^1\|^2 = 0 = \rho_k$ and $\|\mathbf{x}_k^2\|^2 = \frac{T\gamma_s}{1-p_0}$, $\Phi_{z_k}^2(s) = \frac{1}{1+s\frac{T\gamma_s}{1-p_0+T\gamma_s}}$

3. When $\|\mathbf{x}_k^2\|^2 = 0 = \rho_k$ and $\|\mathbf{x}_k^1\|^2 = \frac{T\gamma_s}{1-p_0}$, $\Phi_{z_k}^3(s) = \frac{1}{1-s\frac{T\gamma_s}{1-p_0}}$

4. When $\|\mathbf{x}_k^2\|^2 = \rho_k = \|\mathbf{x}_k^1\|^2 = 0$, $\Phi_{z_k}^4(s) = 1$

Let $M_i \subset \{1, 2, ..., L\}$ denote the indices of the blocks in which case i happens, with the obvious restriction that $|M_1| + |M_2| + |M_3| + |M_4| = L$ and M_i are disjoint sets. The overall characteristic function for $z \triangleq \sum_{k=1}^{L} z_k$ is

$$\begin{aligned}
\Phi_z(s) &= \prod_{j=1}^{4} \prod_{i \in M_j} \Phi_{z_i}^j(s) \\
&= \left(\frac{1}{1 + s\frac{T\gamma_s}{1-p_0+T\gamma_s}}\right)^{|M_2|} \left(\frac{1}{1 - s\frac{T\gamma_s}{1-p_0}}\right)^{|M_3|} \prod_{k \in M_1} \Phi_{z_k}^1(s) \\
f_Z(z) &= \frac{1}{2\pi} \int \exp(sz)\Phi_z(s)ds \\
&= \sum_{\text{-ve poles}} \text{Res}\{\exp(sz)\Phi_z(s)\} \\
\Pr(\mathbf{X}^1 \to \mathbf{X}^2) &= \int_0^\infty f_Z(z)dz \\
&= \sum_{\text{-ve poles}} \text{Res}\{\frac{\Phi_z(s)}{s}\}
\end{aligned}$$

It is emphasized that the main difference (between the fading channel and the AWGN channel) is that the aim of the Viterbi Algorithm is to maximize a sum of quadratics in the received signals (5.9) and not to minimize the Euclidean distance

between the received sequence and valid sequences. Thus in the following section related to the design of asymmetric unitary constellations, it should be emphasized that correlations (between subspaces spanned by the columns of the transmitted signal) and not Euclidean distances are considered as the distance notion.

5.3.3 Pairwise error probability ($M > 1$, $N = 1$)

We now consider a systems operating with $M > 1$, $N = 1$, so that the transmission is now a matrix $\mathbf{X}_k$, where $k \in \{1, 2, \ldots, L\}$. An assumption made to simplify analysis is that $\mathbf{X}_k$ is signal from an unitary space-time signal constellation. Proceeding in a fashion similar to the last section, the pairwise error probability in deciding on a sequence $\mathbf{X}^2 = (\mathbf{X}_1^2, \ldots, \mathbf{X}_k^2, \ldots, \mathbf{X}_L^2)$ instead of the transmitted sequence $\mathbf{X}^1 = (\mathbf{X}_1^1, \ldots, \mathbf{X}_k^1, \ldots, \mathbf{X}_L^1)$ is found to be

$$\begin{aligned}
\Pr(\mathbf{X}^1 \to \mathbf{X}^2) &= \Pr\left(\sum_{k\in W} \mathbf{y}_k^*(\mathbf{X}_k^2\mathbf{X}_k^{2*} - \mathbf{X}_k^1\mathbf{X}_k^{1*})\mathbf{y}_k > 0 | \mathbf{X}^1\right) \\
&= \Pr\left(\sum_{k\in W} (\|\mathbf{x}_k^2\|^2 - \|\mathbf{x}_k^1\|^2) > 0 | \mathbf{X}^1\right) \\
&= \Pr\left(\sum_{k\in W} \mathbf{z}_k^* \ \mathbf{J} \ \mathbf{z}_k > 0\right)
\end{aligned}$$

where $\mathbf{x}_k^1 = \mathbf{X}_k^{1*}\mathbf{y}_k$ and $\mathbf{x}_k^2 = \mathbf{X}_k^{2*}\mathbf{y}_k$ are column vectors of length M, and

$$\mathbf{z}_k = \begin{pmatrix} \mathbf{x}_k^2 \\ \\ \mathbf{x}_k^1 \end{pmatrix}, \mathbf{J} = \begin{pmatrix} \mathbf{I}_M & \mathbf{0} \\ \\ \mathbf{0} & -\mathbf{I}_M \end{pmatrix}$$

The covariance of $\mathbf{z}_k$ is given by the $2M \times 2M$ matrix

$$\mathbf{K}_{z_k} = \begin{pmatrix} \frac{T\gamma_s}{M}(\mathbf{I}_M + \frac{T\gamma_s}{M}\mathbf{C}_k\mathbf{C}_k^*) & (1 + \frac{T\gamma_s}{M})\frac{T\gamma_s}{M}\mathbf{C}_k \\ (1 + \frac{T\gamma_s}{M})\frac{T\gamma_s}{M}\mathbf{C}_k^* & T\gamma_s(1 + \frac{T\gamma_s}{M})\mathbf{I}_M \end{pmatrix}$$

where $\mathbf{C}_k = \frac{\mathbf{X}_k^{2*}\mathbf{X}_k^1}{T\gamma_s/M}$.The characteristic function of such a Gaussian quadratic $(\mathbf{z}_k^* \mathbf{J} \mathbf{z}_k)$is given by

$$\begin{aligned}
\Phi_k(s) &= \frac{1}{|\mathbf{I}_{2M} + s\mathbf{K}_{z_k}\mathbf{J}|} \\
&= \frac{1}{\left|\begin{pmatrix} \mathbf{I}_M + s\frac{T\gamma_s}{M}(\mathbf{I}_M + \frac{T\gamma_s}{M}\mathbf{C}_k\mathbf{C}_k^*) & -s(1+\frac{T\gamma_s}{M})\frac{T\gamma_s}{M}\mathbf{C}_k \\ s(1+\frac{T\gamma_s}{M})\frac{T\gamma_s}{M}\mathbf{C}_k^* & \mathbf{I}_M(1 - sT\gamma_s(1+\frac{T\gamma_s}{M})) \end{pmatrix}\right|} \\
&= \frac{1}{\prod_{j=1}^M \left(s^2\frac{T^2\gamma_s^2}{M^2}\left(1+\frac{T\gamma_s}{M}\right)(\lambda_j^{(k)} - 1) + s\frac{T^2\gamma_s^2}{M^2}(\lambda_j^{(k)} - 1) + 1\right)} \\
&= \frac{1}{\prod_{j=1}^M A_j^{(k)}(s - q_j^{(k)})(s + p_j^{(k)})} \qquad (5.18)
\end{aligned}$$

The simplification of the determinant was obtained by using the determinant identity,

$$\left|\begin{pmatrix} \mathbf{A} & \mathbf{B} \\ \mathbf{C} & \mathbf{D} \end{pmatrix}\right| = |\mathbf{D}||\mathbf{A} - \mathbf{B}\mathbf{D}^{-1}\mathbf{C}|$$

and subsequently performing the eigenvalue decomposition of $\mathbf{C}_k\mathbf{C}_k^*$ as $\mathbf{U}^{(k)}\mathbf{\Lambda}^{(k)}\mathbf{U}^{(k)*}$ where $\mathbf{\Lambda}^{(k)} = \mathrm{diag}(\lambda_1^{(k)}, \lambda_2^{(k)}, \ldots, \lambda_M^{(k)})$. $A_j^{(k)}$, $p_j^{(k)}$ and $q_j^{(k)}$ have forms similar to the expressions in the previous sections. The probability of error is thus

$$\Pr(\mathbf{X}^1 \to \mathbf{X}^2) = \sum_{p_{j'}^{(k')} > 0} \mathrm{Res}_{s=-p_{j'}^{(k')}} \left\{ \frac{1}{s\prod_{k\in W}\prod_{j=1}^M A_j^{(k)}(s - q_j^{(k)})(s + p_j^{(k)})} \right\} \qquad (5.19)$$

5.3.4 Pairwise probability of error - MIMO case

Adding another spanner into the works, we try to do a performance analysis similar to the first case of block independent Rayleigh fading with constellations of the unitary space-time codes for the MIMO case. Specifically we consider $M > 1$ transmit and $N > 1$ receive antennas. A space-time signal is said to be transmitted in the k^{th} block when a complex matrix $\mathbf{X}_k$ is transmitted from the M antennas. Letting the suffix j and the superfix (k) denote the j^{th} receive antenna and the k^{th}

block, $k = 1, \ldots, L$, respectively, we rearrange the observed matrix in each block as follows, for convenience in performing the subsequent analysis.

$$\mathcal{Y}^{(k)} = [\mathbf{y}_1^{(k)^T}, \mathbf{y}_2^{(k)^T}, \ldots, \mathbf{y}_N^{(k)^T}]^T, \qquad \mathcal{H}^{(k)} = [\mathbf{h}_1^{(k)^T}, \mathbf{h}_2^{(k)^T}, \ldots, \mathbf{h}_N^{(k)^T}]^T \tag{5.20}$$

$$\mathcal{N}^{(k)} = [\mathbf{n}_1^{(k)^T}, \mathbf{n}_2^{(k)^T}, \ldots, \mathbf{n}_N^{(k)^T}]^T, \qquad \mathcal{X}^{(k)} = \mathbf{I}_N \otimes \mathbf{X}^{(k)} \tag{5.21}$$

Then (1.3) can be re-written in the new notation as

$$\mathcal{Y}^{(k)} = \mathcal{X}^{(k)}\mathcal{H}^{(k)} + \mathcal{N}^{(k)} \tag{5.22}$$

Given the signal transmitted in the k^{th} block, $\mathcal{Y}^{(k)}$ is $\mathcal{CN}\left(\mathcal{Y}^{(k)}; \underline{0}; \mathbf{I}_{NT} + \mathcal{X}^{(k)}\mathcal{X}^{(k)^*}\right)$ distributed. The fading process being block independent, if we observe a sequence of L blocks, the likelihood function of a sequence of space-time signals $\{\mathcal{X}^{(k)}\}_{k=1}^L$ is

$$\begin{aligned} p(\{\mathcal{Y}^{(k)}\}_{k=1}^L | \{\mathcal{X}^{(k)}\}_{k=1}^L) &= \prod_{k=1}^{L} p(\mathcal{Y}^{(k)} | \mathcal{X}^{(k)}) \\ &= \prod_{k=1}^{L} \frac{\exp\{-\mathcal{Y}^{(k)^*}(\mathbf{I}_{NT} + \mathcal{X}^{(k)}\mathcal{X}^{(k)^*})^{-1}\mathcal{Y}^{(k)}\}}{\pi^{NT}|\mathbf{I}_{NT} + \mathcal{X}^{(k)}\mathcal{X}^{(k)^*}|} \\ &= \frac{\exp\{-\sum_{k=1}^{L}\left(\mathcal{Y}^{(k)^*}\mathcal{Y}^{(k)} - \frac{1}{1+T\gamma_s/M}\,\mathcal{Y}^{(k)^*}\mathcal{X}^{(k)}\mathcal{X}^{(k)^*}\mathcal{Y}^{(k)}\right)\}}{\left(1 + \frac{T\gamma_s}{M}\right)^{LNT}\pi^{LNT}} \end{aligned}$$

The last step has been derived using the properties of the Kronecker product ($\otimes$), the properties of the unitary space-time constellation and the matrix inverse identities listed previously. The Maximum Likelihood Sequence Detector detects that sequence of space-time signals that maximises $\mathcal{Y}^{(k)^*}\mathcal{X}^{(k)}\mathcal{X}^{(k)^*}\mathcal{Y}^{(k)}$. Thus the pairwise sequence error probability is given by the probability

$$\Pr(\{\mathbf{X}^{(k)}\}_{k=1}^L \to \{\widehat{\mathbf{X}}^{(k)}\}_{k=1}^L) = \Pr\left(\sum_{k=1}^{L}\left(\mathcal{Y}^{(k)^*}(\widehat{\mathcal{X}}^{(k)}\widehat{\mathcal{X}}^{(k)^*} - \mathcal{X}^{(k)}\mathcal{X}^{(k)^*})\mathcal{Y}^{(k)}\right) \geq 0\right) \tag{5.23}$$

Let us define the following vectors.

$$\mathbf{z}_k = \begin{bmatrix} \widehat{\mathcal{X}}^{(k)^*}\mathcal{Y}^{(k)} \\ \mathcal{X}^{(k)^*}\mathcal{Y}^{(k)} \end{bmatrix}, \mathbf{z} = \begin{bmatrix} \mathbf{z}_1 \\ \mathbf{z}_2 \\ \vdots \\ \mathbf{z}_L \end{bmatrix}, \mathbf{J} = \begin{bmatrix} \mathbf{I}_{MN} & \mathbf{0} \\ \mathbf{0} & -\mathbf{I}_{MN} \end{bmatrix}$$

Note that because of the block independence of the fading process the vectors $\mathbf{z}_k$ are independent over k. With these definitions the required probability of error is

$$\Pr(\{\mathbf{X}^{(k)}\}_{k=1}^{L} \to \{\widehat{\mathbf{X}}^{(k)}\}_{k=1}^{L}) = \Pr(\beta = \mathbf{z}^*(\mathbf{I}_L \otimes \mathbf{J})\mathbf{z} \geq 0)$$

$$\Phi_\beta(s) = \frac{1}{|\mathbf{I} + s\mathbf{K}_z(\mathbf{I}_L \otimes \mathbf{J})|}$$

where $\mathbf{K}_z = \text{diag}(\mathbf{K}_{z_k} : 1 \leq k \leq L)$ is the covariance (and also correlation) matrix of the random vector $\mathbf{z}$ where

$$\begin{aligned} \mathbf{K}_{z_k} &= \mathrm{E}[\mathbf{z}_k\mathbf{z}_k^*|\mathbf{X}^{(k)}] \\ &= \begin{bmatrix} \frac{T\gamma_s}{M}(\mathbf{I}_{MN} + \frac{T\gamma_s}{M}\mathbf{C}^{(k)}\mathbf{C}^{(k)^*} & \left(1 + \frac{T\gamma_s}{M}\right)\mathbf{C}^{(k)} \\ \left(1 + \frac{T\gamma_s}{M}\right)\mathbf{C}^{(k)^*} & \left(1 + \frac{T\gamma_s}{M}\right)\frac{T\gamma_s}{M}\mathbf{I}_{MN} \end{bmatrix}, \text{where} \\ \mathbf{C}^{(k)} &= \frac{M}{T\gamma_s}\widehat{\mathbf{X}}^{(k)^*}\mathbf{X}^{(k)} \end{aligned}$$

With the structure of the signals assumed, the analysis that continues is similar to that done in the previous section, with the change that for $N > 1$, each root in (5.18) has multiplicity N.

5.4 Asymmetric Unitary Constellations

In [2], trellis coded unitary space-time modulations are suggested based on trellis coded modulation systems for the AWGN channel, the difference being the use of a unitary space-time constellation as the signal constellation. The output signal

assignment to each transition is made using the Ungerboeck partitioning. In the Ungerboeck partitioning for the unitary space-time constellations, the 'distance' notion used is the average sum of squares of the singular values (δ as in (1.12)) between 2 signal points. This procedure is explained with an example with $S = 4$ signals in $T = 2$ complex dimensions with $M = N = 1$ and a 2 state, rate 0.5 convolutional code with overall rate 0.5 bits/sec/complex dimension.

The best unitary space-time constellation is first generated using the systematic procedure (as suggested by [29]) which tries to minimizes the δ over all the constellations. This constellation was found to have the correlation profile as in table 5.1. Note that $\delta_{i,j}$ depends only on $(i-j) \mod S$, so that only 4 correlations specify the

Table 5.1: Correlation profile of designed symmetric signal constellation. $S = 4$ signals in $T = 2$ dimensions with $M = N = 1$.

i	0	1	2	3
$\delta_{i,0}$	1	0.7071	0	0.7071

entire correlation profile. The worst correlation (between distinct signals) is 0.7071 for differences 1 and 3 (mod 4) and the best correlation is 0 for a difference of 2 mod 4. The Ungerboeck partitioning for this is done as follows. $S_1 = \{0,2\}$ and $S_2 = \{1,3\}$. This way the signals with the best correlations are in the same subset - *i.e.*, *intra-subset* correlations are the best possible correlations and worse correlations occur between signals in different subsets - *i.e.*, *inter-subset* correlations are bad. This is analogous to signals with large distances being in the same subset and signals with smaller distances being in different subsets in the AWGN case.

The trellis code assignment is then done as in Fig. 5.4. As in the symmetric AWGN example presented earlier, there is no difference if the signals 1 and 3 are exchanged. The shortest length error event is depicted in the Fig. 5.4 and this path has the correlations (0,0.7071). This is also the path that has the minimum output

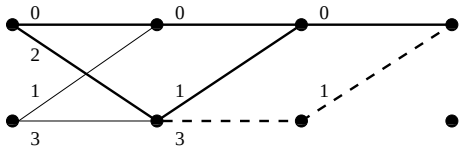

Figure 5.4: 2 state trellis with output label assignment (symmetric constellation) for the fading channel. Error events of length 2 and 3 shown.

Hamming distance which actually determines the time diversity of the code. The upper bound can be written in this case just as in (5.1) with the slight difference that now the pairwise error probability is the corresponding expression derived in Section 5.3 and not a Q(.) function. The general bound can be written as and specialized for this example as

$$\mathrm{P}_b \leq \sum_l d_h^{(l)} N_l \, \mathrm{P}_2(\mathbf{c} \to \mathbf{e}; \eta) \tag{5.24}$$

$$= \sum_l d_h^{(l)} N_l \, \mathrm{P}_2(\rho_1, \rho_2, \ldots, \rho_l; \eta) \tag{5.25}$$

where $\mathrm{P}_2(\rho_1, \rho_2, \ldots, \rho_l; \eta)$ is the pairwise error probability at the SNR η, for an error event of length l with correlation ρ_k at the k^{th} transition. The quantities $d_h^{(l)}$, N_l, and the specific combination of ρ_i's are obtained from the transfer function, which for this case is

$$T(N, I, D_1, D_2, D_3) = \frac{NI^2 D_2 D_1}{1 - NID_3} \tag{5.26}$$

$$= \sum_{l=2}^{\infty} N^{l-1} I^l D_1 D_2 D_3^{l-2} \tag{5.27}$$

$$\left.\frac{\partial T(N, I, D_1, D_2, D_3)}{\partial N}\right|_{N=1, I=1} = \sum_{l=2}^{\infty} (l-1) \mathrm{P}_2(\rho_1, \rho_2, \underbrace{\rho_3, \ldots, \rho_3}_{(l-2)\text{times}}; \eta) \tag{5.28}$$

where, the exponent of N is the Hamming weight of the input bit sequence that resulted in the error, the exponent of I is the length of the error event. D_j is the dummy variable that stands for the correlation between signals 0 and j. The exponent of D_j refers to the number of times the correlation between signals 0 and

j occur in the error sequence. This has use in the computation of the exact pairwise error probability function $\mathrm{P}_2(.)$.

For the specific example we are considering, the upper bound expression simplifies to,

$$\mathrm{P}_b \leq \sum_{l=2}^{\infty}(l-1)\mathrm{P}_2(0, 0.7071, 0.7071, \ldots, 0.7071; \eta) \tag{5.29}$$

At high SNR we can consider the performance to be characterized by the error events of length 2 and length 3. Under this assumption, the upper bound becomes

$$\mathrm{P}_b \lesssim \mathrm{P}_2(0, 0.7071; \eta) + 2\mathrm{P}_2(0, 0.7071, 0.7071; \eta) \tag{5.30}$$

In practice, since the pairwise error probability expressions derived in Section 5.3, were derived only for the cases of distinct ρ's or equal ρ's, the ρ's were slightly perturbed so as to avoid computational instabilities.

One possible procedure that can be followed to design constellations that we call in this thesis, *Asymmetric* Unitary Space-Time signal Constellations is as follows. First the Ungerboeck partitioning is done as mentioned above. Then one subset say S_2 is taken and a *rotation* is done as follows.

$$\mathbf{S}_1' = \mathbf{\Theta}^{\alpha}\mathbf{S}_1 \qquad \mathbf{S}_3' = \mathbf{\Theta}^{\alpha}\mathbf{S}_3 \quad \text{where } \alpha \in (-1, 1).$$

where the $\mathbf{\Theta}$ is the matrix obtained upon doing a minimization over $u_1, \ldots, u_T$ to find the smallest δ (see (1.14)). This rotation destroys the cyclic symmetry of the correlation profile and changes the correlation values as well.

For $\alpha = -0.5$ the correlation profile is given in table 5.2. For the same output label assignment the critical path is parameterized by the correlations (0,0.3827) which is better than (0,0.7071) for the code employing the symmetric constellation.

Table 5.2: Correlation profile of designed asymmetric signal constellation, $\alpha = -0.5$.

$\delta_{i,j}$	0	1	2	3
0	1	0.3827	0	0.9239
1	0.3827	1	0.9239	0
2	0	0.9239	1	0.3827
3	0.9239	0	0.3827	1

The error path of length 3 has the correlations (0,0.9239,0.3827) which is worse than the error path with correlations (0,0.7071,0.7071).

For $\alpha = -0.2$ the correlation profile is given in table 5.3. In this case, the critical

Table 5.3: Correlation profile of designed asymmetric signal constellation, $\alpha = -0.2$.

$\delta_{i,j}$	0	1	2	3
0	1	0.5878	0	0.8090
1	0.5878	1	0.8090	0
2	0	0.8090	1	0.5878
3	0.8090	0	0.5878	1

path is parameterized by the correlations (0,0.5878) which is better than (0,0.7071) for the code employing the symmetric constellation but slightly worse than (0,0.3827). However the length 3 error path has the correlations (0,0.8090,0.5878) which is better than the one for $\alpha = -0.5$.

At high SNR, if we consider the performance to be determined by the length 2 error event, then we can get an upper bound on the achievable gain by changing the correlation between signals 0 and 1 from 0.7071 to 0.0. Thus, the length 2 error event has the correlations (0,0) which is expected to be better than (0,0.7071). The performance of these three codes and the upper bounds to the bit error probability are presented in Fig. 5.5.

As expected the performance of the code employing the asymmetric signal constellation is better by about 0.45 dB at 2×10^{-4} bit error probability. However this performance gain is seen only at high SNR and this is what is expected to occur. As

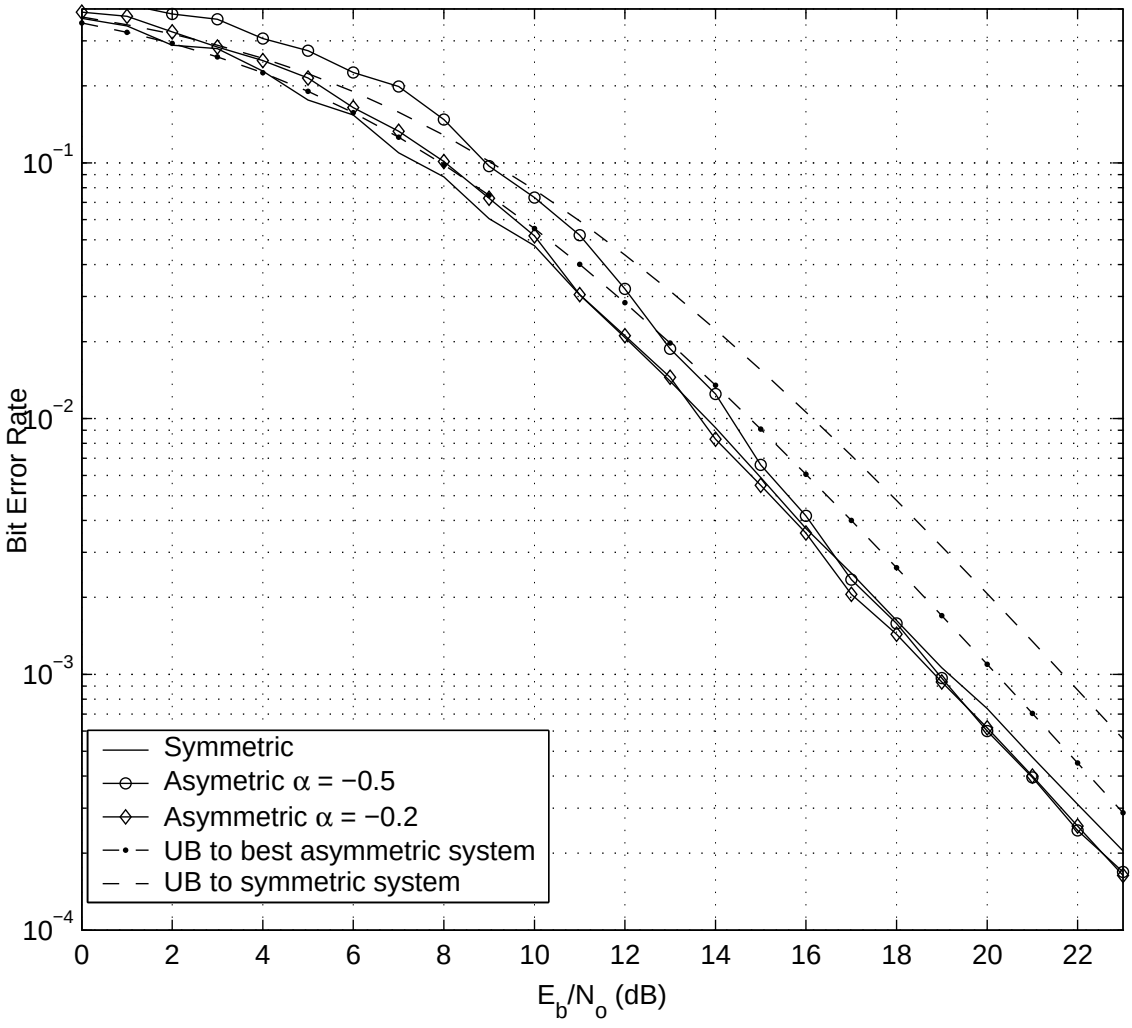

Figure 5.5: Simulation results for the $T = 2$, $M = N = 1$, $S = 4$, rate 0.5 trellis code for the fading channel.

noticed above, the length 3 error path is best for the symmetric code, a little worse for the asymmetric code with $\alpha = -0.2$ and the worst for the asymmetric code with $\alpha = -0.5$. The effect of these and higher length error events cause the symmetric code to perform better at low SNR than the asymmetric codes. It must be stated that although the values of α were chosen here randomly, the optimum value of α computed based on the upper bound expression resulted in a performance almost identical to the one produced by $\alpha = -0.2$. From the bit-error probability upper bounds plotted in Fig. 5.5, it is seen that the maximum gain achievable through the use of asymmetric constellation is 1.5 dB.

Although the gains seen in this case are minimal, it must be understood that the space over which the modulation design was done was restricted, since the energy of the signal transmitted by each antenna at any time is 1. We expect that expanding the design space to include modulations that don't have this restriction might produce some gain. To do this, one has to move away from creating constellations from the DFT matrices as done in [29]. Using multiple energy level constellations (analogous to moving from PSK to QAM modulations in the AWGN case) might give some more gain. Also, as seen from Fig. 5.5, the gains are visible only at high SNR. For many applications, however, the performance at low SNR may actually be more important, *e.g.*, Turbo Codes. With a low SNR gain in mind, another asymmetric modulation scheme involving 4 signals over a 4-state code is produced in the following section.

5.5 Effect of increasing the state space

The main theme of this procedure is to redistribute resources among the 4 signals such that there is a gain at low SNR over a symmetric system used with the code in

Fig. 5.6. The trellis with the output label assignment and length 3 and 4 simple error

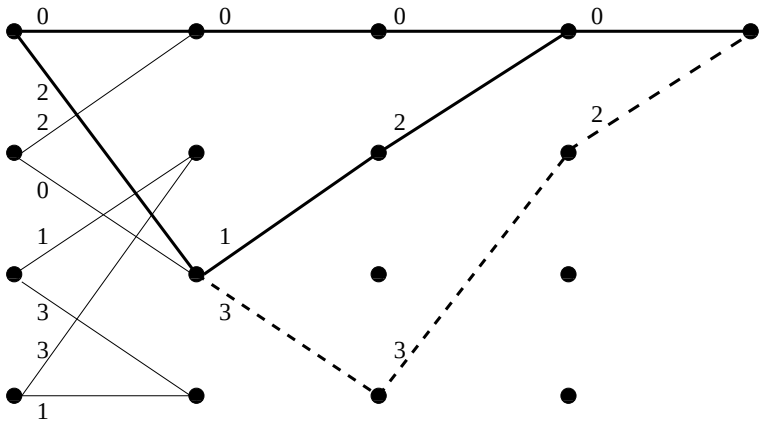

Figure 5.6: 4 state trellis for $S = 4$ signals in $T = 2$ dimensions, $M = N = 1$. Overall rate 0.5 bps/dimension.

events are shown in Fig. 5.6. For the symmetric constellation with the correlation profile as in Table 5.1, the length 3 error event has the correlations (0, 0.7071, 0) and the length 4 error event has the correlations (0, 0.7071, 0.7071, 0). The transfer function for the trellis in Fig. 5.6 is

$$T(N, I, D_1, D_2, D_3) = \frac{NI^3D_1D_2^2 + N^2I^4D_2^2D_3^2 - N^2I^4D_1^2D_2^2}{1 - (NID_1 + N^2I^3D_0D_3^2 + NI^2D_0D_1 - N^2I^3D_0D_1^2)} \quad (5.31)$$

$$= (NI^3D_1D_2^2 + N^2I^4D_2^2D_3^2 - N^2I^4D_1^2D_2^2)$$
$$(1 + \sum_{l=1}^{\infty}(NID_1 + N^2I^3D_0D_3^2 + NI^2D_0D_1 - N^2I^3D_0D_1^2)^l)$$

(5.32)

where the symbols D_i are as explained earlier. From the exact pairwise error derivations we know that for a given sum of squares of the correlation, the pairwise error probability is the least when the correlations are equal. From the length 4 error event, we see that the correlations are (0, 0.7071, 0.7071, 0), *i.e.*, very biased correlations. So, the length 4 error event with the correlations (0.5, 0.5, 0.5, 0.5) would be better than one with (0, 0.7071, 0.7071, 0). In effect, the 'distance' between signals

0 and 1 and 0 and 3 has to be decreased from 0.7071 at the cost of the 'distance' between 0 and 2 and 1 and 3 which are increased from 0. Thus a new asymmetric constellation can be generated in this form from the symmetric constellation (systematically) as follows — take signals 0 and 2 (which are initially orthogonal) and separate them in space on the plane that contains both of them, while bringing the signals 1 and 3 (again initially orthogonal) closer on the plane which contains these two signals. Since the correlation between 2 signals depends on the cosine of the angle between the two, both separating and bringing the signals together (from orthogonal positions) has the effect of increasing their correlations. This is done easily by adding/subtracting a fraction of the difference between the two signals. The particular fraction used is called α. The signals are normalized once again to have unit power. The Fig. 5.7 can be used as a visualization aid for this procedure. In the

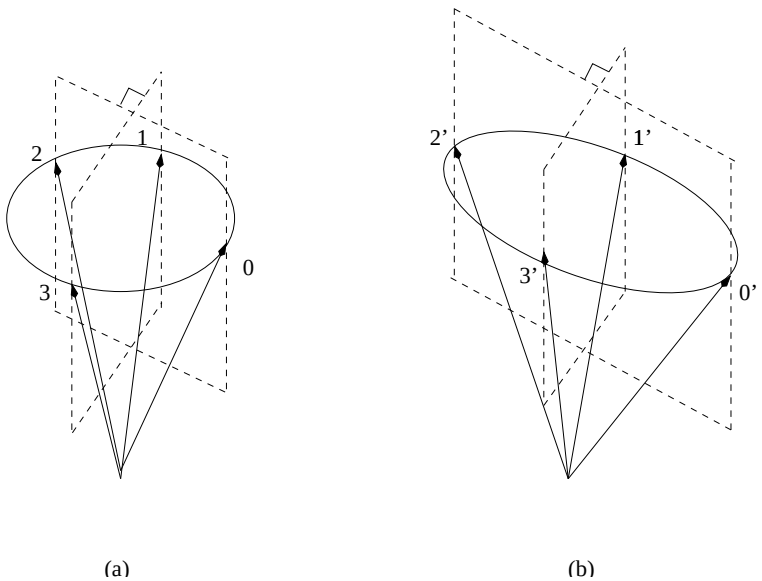

Figure 5.7: (a) Symmetric constellation. (b) Construction of Asymmetric constellation

figure, the new un-normalized signals are the primed quantities. The signals 1 and 3 have been brought closer to each other by 2α, *i.e.*, each signal was moved towards

the other by a fraction α of the length of difference between the signals (it is useful to think of the signals as vectors). It should be noted that the normalization in the construction entailed above gives signals in which all components do not have equal power. However, the total power of the signal is 1.

In bringing the two signals closer, if $\alpha = 0.5$ is used, then the two signals merge together, and the constellation becomes 3-ary instead of 4-ary. Given a starting symmetric constellation, the parameter α is sufficient to specify the asymmetric constellation. For two particular values, $\alpha = 0.2$ and $\alpha = 0.4$, the correlation tables are given in Table 5.4 and 5.5. In both these constructions, the signals 1 and 3 were brought closer to each other and the signals 0 and 2 were moved away from each other.

Table 5.4: Correlation profile of designed asymmetric signal constellation, $\alpha = 0.2$.

$\delta_{i,j}$	0	1	2	3
0	1.0000	0.6509	0.3243	0.6509
1	0.6509	1.0000	0.6509	0.4706
2	0.3243	0.6509	1.0000	0.6509
3	0.6509	0.4706	0.6509	1.0000

For $\alpha = 0.2$, the length 3 error event has the correlations (0.3243, 0.6509, 0.3243), and the length 4 error event has the correlations (0.3243, 0.6509, 0.6509, 0.3243). Thus we see that the length 4 error event has less biased correlations than (0, 0.7071, 0.7071, 0) and performs better, following the observation regarding the pairwise error probability made earlier in this section. The same holds for longer error events. However, the length 3 error event does not perform as well, but is not much worse than the one with correlations (0, 0.7071, 0). At low SNR, since the bit error probability is determined not only by the first term, but by a number of terms in the expansion in (5.32), the asymmetric system is expected to perform better at low SNR. At high

SNR, the length 3 error event dominates and hence the gain should disappear. The performance results in Fig. 5.8 confirm these expectations.

Table 5.5: Correlation profile of designed asymmetric signal constellation, $\alpha = 0.4$.

$\delta_{i,j}$	0	1	2	3
0	1.0000	0.5061	0.5283	0.5061
1	0.5061	1.0000	0.5061	0.9231
2	0.5283	0.5061	1.0000	0.5061
3	0.5061	0.9231	0.5061	1.0000

For $\alpha = 0.4$, the length 3 error event has the correlations (0.5283, 0.5061, 0.5283), and the length 4 error event has the correlations (0.5283, 0.5061, 0.5061, 0.5283). Thus we see that the length 4 error event has less biased correlations than (0, 0.7071, 0.7071, 0). In fact, these are almost the least-biased correlations possible. Therefore, the length 4 error event performs better in terms of bit-error probability than the corresponding one for the symmetric constellation. The same holds for longer error events. However, the length 3 error event performs much worse than the one with correlations (0, 0.7071, 0). At low SNR, since the bit error probability is determined by a number of terms in the expansion in (5.32), the asymmetric system is expected to perform better at low SNR. In this case however, the performance at high SNR is not only determined by the length 3 error event but also by the correlation between 1 and 3 (0.9231). The correlation of 0.9231 causes longer error events to have effectively lower output Hamming distance, *i.e.*, smaller time diversity. Hence at high SNR, this code is expected to perform much worse than the symmetric case. The performance results in Fig. 5.8 confirm these expectations.

In the following section, the signal space is increased from 4 to 8 to understand the behavior of gain from the usage of asymmetric unitary constellations with increasing signal space. In this case, we only study the signal constellations obtained from the

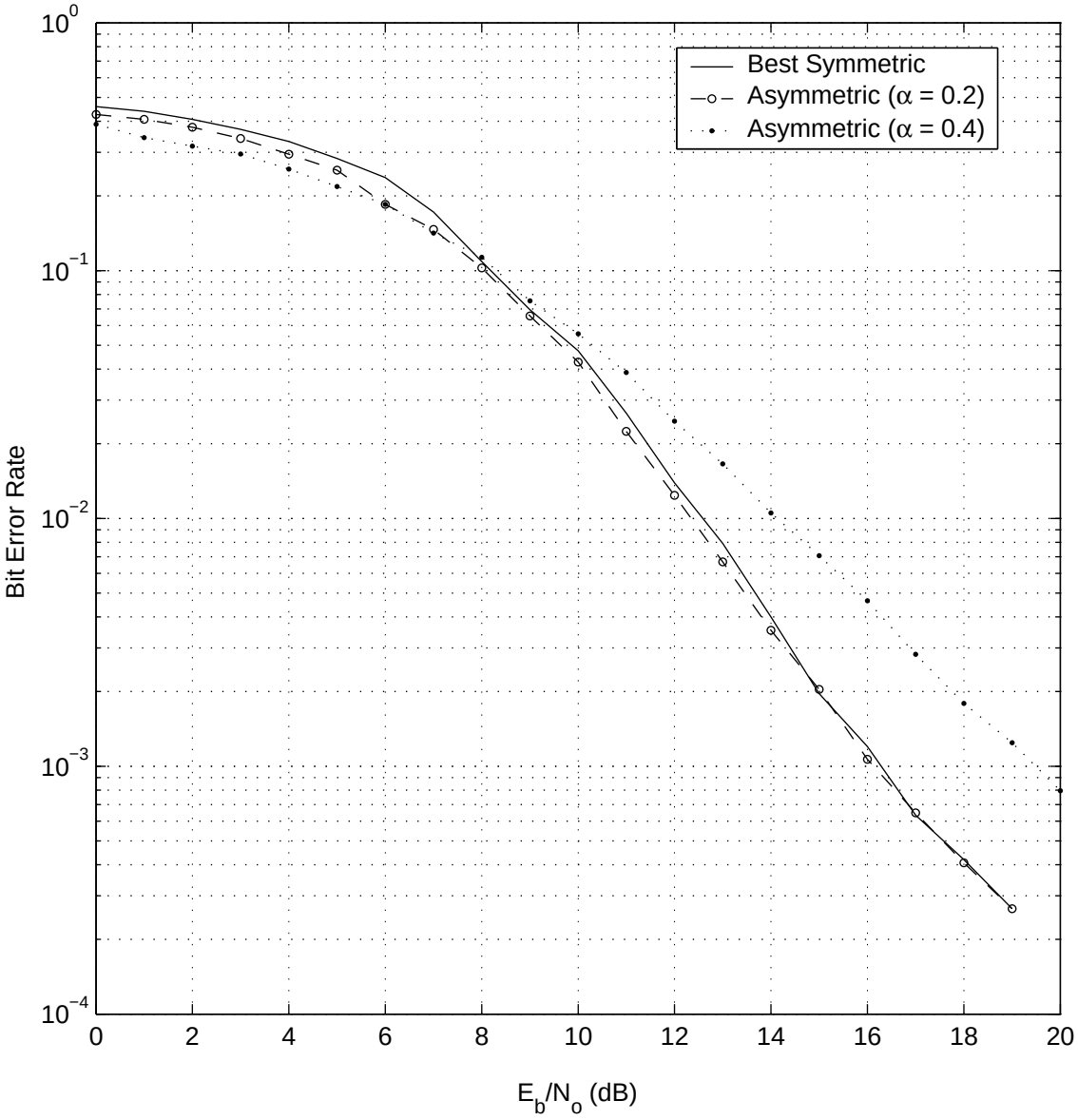

Figure 5.8: Simulation results for the $T = 2$, $M = N = 1$, $S = 4$, rate 0.5 trellis code for the fading channel.

first construction method.

5.6 Effect of increasing the signal space

By increasing the modulation size to 8, *i.e.*, 8 signals in 2 dimensions, we are crowding more number of signals in the same space. This is analogous to increasing the size M of M-PSK constellations for the AWGN channel. The best symmetric unitary signal constellation obtained by the usual systematic procedure has the correlation profile given in Table 5.6. The Ungerboeck partitioning is done as the

Table 5.6: Correlation profile of designed symmetric signal constellation. $S = 8$ signals in $T = 2$ dimensions with $M = N = 1$.

i	0	1	2	3	4	5	6	7
$\delta_{i,0}$	1	0.3827	0.7071	0.9239	0	0.9239	0.7071	0.3827

following. At the first level, $S_1 = \{0, 4, 2, 6\}$ and $S_2 = \{1, 5, 3, 7\}$. This is the best partition possible because the maximum (worst) correlation is eliminated from the intra-subset correlation. At the second level, S_1 and S_2 are partitioned into $S_{11} = \{0, 4\}$, $S_{12} = \{2, 6\}$, and $S_{21} = \{1, 5\}$, $S_{22} = \{3, 7\}$ respectively. The trellis code (hand-designed) that gives the best performance is given in Fig. 5.9, which also shows the length 3 and 4 simple error events. These two error events are characterized by the triplet and quadruplet of correlations (0, 0.7071, 0.3827) and (0, 0.7071, 0.9239, 0.3827) respectively. These correlations are the result of the errors between the pairs of sequences 0,0,0 and 4,2,1, and 0,0,0,0 and 4,6,3,1, respectively. Thus for the same trellis structure, if the correlations between 0 and 3 and 0 and 1 are reduced, then we might get a gain. Using $\alpha = -0.1$, if we rotate the signals in subset S_2, we get a constellation with the correlation profile as in Table 5.7. For this constellation, the corresponding length 3 and length 4 error events have the correlations (0, 0.7071, 0.1951) and (0, 0.7071, 0.5556, 0.1951) respectively. So we expect a gain

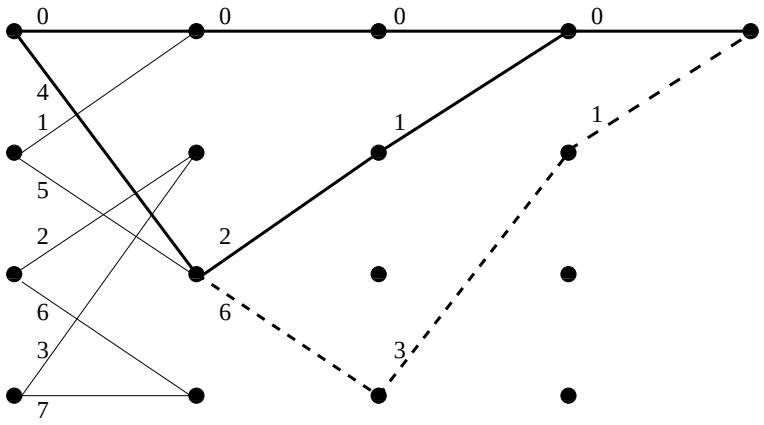

Figure 5.9: 4 state trellis for $S = 8$ signals in $T = 2$ dimensions, $M = N = 1$. Overall rate 0.5 bps/dimension.

Table 5.7: Correlation profile of designed asymmetric signal constellation, $\alpha = -0.1$. $S = 8$ signals in $T = 2$ dimensions with $M = N = 1$.

$\delta_{i,j}$	0	1	2	3	4	5	6	7
0	1	0.1951	0.7071	0.5556	0	0.9808	0.7071	0.8315
1	0.1951	1	0.8315	0.7071	0.9808	0	0.5556	0.7071
2	0.7071	0.8315	1	0.1951	0.7071	0.5556	0	0.9808
3	0.5556	0.7071	0.1951	1	0.8315	0.7071	0.9808	0
4	0	0.9808	0.7071	0.8315	1	0.1951	0.7071	0.5556
5	0.9808	0	0.5556	0.7071	0.1951	1	0.8315	0.7071
6	0.7071	0.5556	0	0.9808	0.7071	0.8315	1	0.1951
7	0.8315	0.7071	0.9808	0	0.5556	0.7071	0.1951	1

over the symmetric system. However the gain is expected to be marginal because the change in the correlation is from 0.3827 to 0.1951 in the length 3 error event, which does not produce too much improvement. The transfer function for this trellis (same notation as before) is

$$T(N, I, D_1, D_2, D_3, D_4, D_5, D_6, D_7) = \frac{NI^3D_1D_2D_4 - N^2I^4D_1D_2D_4D_7}{1 - (NID_7 + NI^2D_2D_5 - N^2I^3D_2D_5D_7)} \tag{5.33}$$

$$= (NI^3D_1D_2D_4 - N^2I^4D_1D_2D_4D_7) \\ (1 + \sum_{l=1}^{\infty}(NID_7 + NI^2D_2D_5 - N^2I^3D_2D_5D_7)^l) \tag{5.34}$$

The simulation results presented in Fig. 5.10 for these two codes indicate a 0.22 dB gain for the code using the asymmetric signal constellation over the symmetric signal constellation.

Comparing the performance of the symmetric constellation ($S = 4$) in Fig. 5.8 with that in Fig. 5.10 ($S = 8$) reveals that the $S = 8$ constellation performs better. The reason for this is that in the case of the code using $S =$ signals, each signal is repeated once (see Fig. 5.6) and therefore for sufficiently long (≥ 5) error events some of the correlations become 1. In other words, the effective hamming distance of these error events is less than the length of the error event. This does not happen in the $S = 8$ case as no signal is repeated (see Fig. 5.9). However the $S = 8$ case is only slightly better because it has a correlation 0.9239 which is almost as bad as a correlation 1.

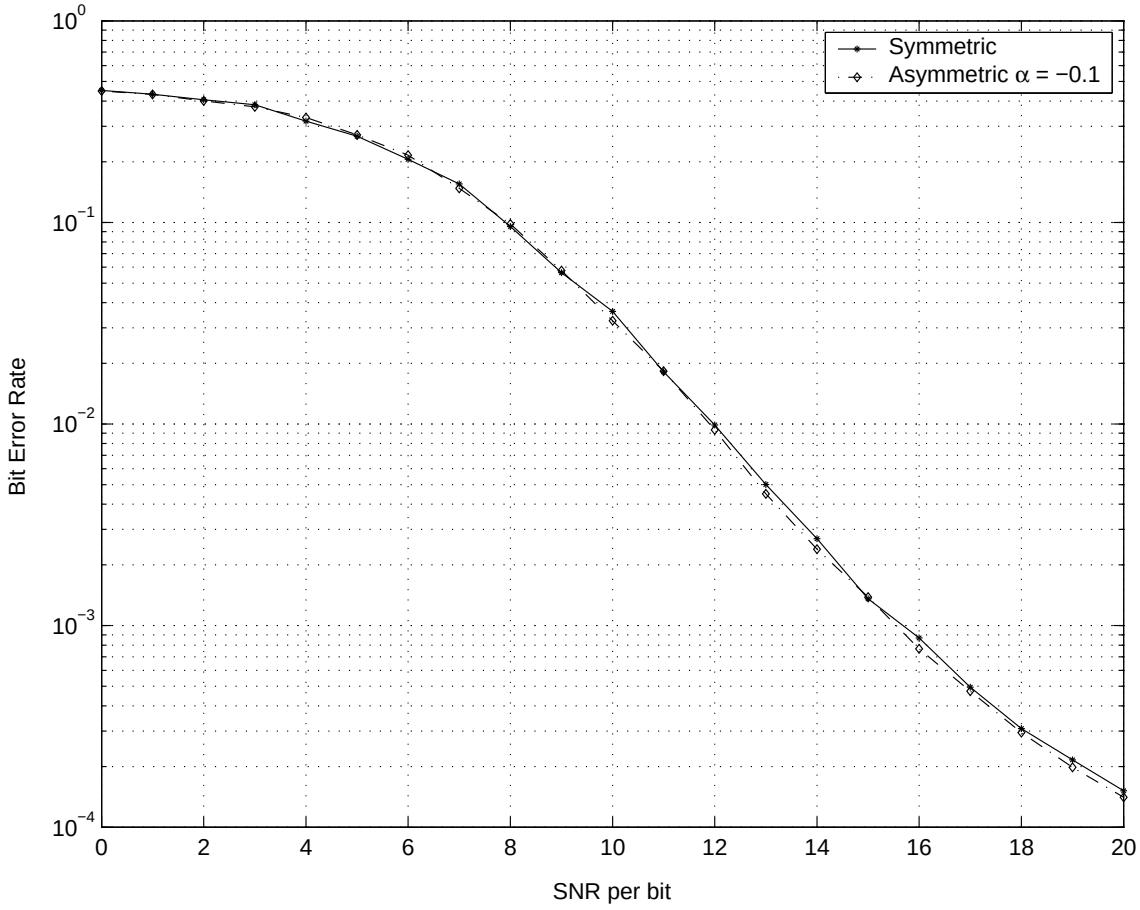

Figure 5.10: Simulation results for the $T = 2$, $M = N = 1$, $S = 8$, rate 0.5 trellis code for the fading channel.

CHAPTER 6

Conclusions

The main results presented in this thesis are briefly summarized below:

- Two transmission/reception schemes are proposed for fast fading MIMO channels with increasing degree of sophistication. The first one uses simple pilot-symbol-assisted schemes based on decomposable constellations, augmented by turbo-like outer codes. It is shown that this scheme together with a simple pilot-only demodulator is exactly equivalent to an appropriately degraded perfect CSI system. The second scheme uses pilot-assisted modulation and a near-optimal low complexity receiver algorithm that takes advantage of the signaling structure to reduce complexity. In examples of systems operating at different rates, the combination of the pilot-assisted modulation and the low-complexity demodulation scheme showed the amazing and counter-intuitive result of better performance with lower complexity. Although the examples shown above use orthogonal schemes, only the general structure in (2.43) is required for the applicability of the proposed low-complexity algorithm.

- The capacity achieving signal distribution for the block-independent Rayleigh fading channel was partially characterized. The capacity was shown to be determined by the distribution of the amplitude of the input. Further, the said

amplitude distribution was shown to have bounded support. Following indications from the literature that the amplitude distribution could be discrete, we showed that starting from a single amplitude unitary scheme, adding probability mass to the zero amplitude signal while maintaining the overall average energy, increases the mutual information. Through numerical simulations, it was found that at low SNR, this increase is significant.

- Motivated by the capacity results for the case of low SNR and very fast fading channels, a simple and novel system is proposed that incorporates in an efficient way the transmission of the zero block. Using simulations the potential of the proposed coding/modulation scheme and decoding techniques is established both in terms of performance and in terms of receiver complexity. Some analysis of the proposed scheme was presented to validate the technique and to provide projections of the expected gain.

- The concept of joint design of modulation and coding was presented. Specifically, given a particular trellis code, two design methodologies for constructing *asymmetric* unitary space-time constellations were shown. One design technique suggested here performs better than the symmetric constellation at high SNR, while the other does better at low SNR. Performance gains (albeit marginally) were seen over conventional systems without a combined modulation and code design approach. These marginal improvements are attributed to the insensitive nature of the pairwise error probability in certain ranges of the 'correlation'. To predict the performance and to design these codes, pairwise probability of error expressions were derived for the transmission of a sequence of space-time signals. For the special case of $M = N = 1$, closed form expres-

sions were obtained for a couple of special cases.

Directions for future work and extensions to the above work are listed below:

1. As mentioned above in the conclusions, one counter-intuitive fact that arose from this work is that pilot-assisted signal constellations perform better than the corresponding unitary constellations. The reason behind this is yet to be understood clearly but it relates to the possible sub-optimal nature of the specific unitary constellation used. Further work needs to be done to determine the reason for such a gain in performance and complexity and whether and how better schemes can be constructed.

2. It was shown in Chapter 3 through numerical capacity evaluations, that substantial gains are to be attained if the zero amplitude is used in conjunction with unitary signalling for the case of very fast fading. However, a formal proof of the existence of the zero amplitude in signal distributions that achieve the capacity of the SISO block fading channel is missing. In a recent work [43], a conjecture was made that for the single antenna block fading channel with average power constraint, the capacity achieving signal distribution comprises of unitary signals but with discrete amplitude levels. There is yet no knowledge of what these amplitude levels are. For that matter, the true capacity of the SISO channel with non-coherent reception at low SNR and low rates is yet an open problem. Another important extension is to see whether these results hold for multiple-antenna systems.

3. The substantial SNR gain indicated by the numerical results in Chapter 3 when using the zero symbol and the fact that some of this gain can be attained through the simple system that was proposed in Chapter 4, begs the question:

Are there any system designs that can better harness the shaping gain suggested by information theory? The reason behind asking this question is that the zero-parsing scheme suggested in Chapter 4 cannot be analyzed easily for larger values of L and L_0. This in turn raises the question, how well the zero-parsing scheme with naive soft metrics for determining the zero blocks will perform for $L > 2$. On the other hand, the optimal way of determining the bit reliabilities for Code 1, has complexity that increases swiftly with increasing L for a given p_0. Hence a different strategy must be examined in order to reach closer to the constrained 2 amplitude level capacity of the channel. The bit sequences from the turbo like codes are essentially like Bernoulli sequences of 0's and 1's appearing in an equally likely fashion. However information theory suggests that for some portion of time, the zero symbol must be transmitted while in the remaining time, the antennas must be used to transmit unitary signals of a different amplitude. This problem can be formulated as the requirement of general mapping techniques from Bernoulli sequences to non equiprobable multi-level signal constellations. Also required is a corresponding de-mapping technique so that the demodulation procedure has sufficiently low complexity so as to be implemented. There is some literature [17] on this problem which occurs for instance while attempting to capture the shaping gain in the Additive White Gaussian Noise (AWGN) channel. by mapping sequences to multi-level signalling schemes.

4. In all the examples shown in Chapter 2, when compared to the constellation constrained capacity of the channel, it is found that even optimized irregular LDPC codes are $1 - 1.5$ dB away from the respective constrained capacity calculations. Part of this gap is due to the finiteness in the codelength for

the LDPC code. However, such a gap from capacity has been reported by other researchers [8] when using codelengths in the range 64000. A conclusive explanation for this gap from theoretical limit is an interesting line of research. For the Binary Symmetric Channel (BSC), the Binary Erasure Channel (BEC), and the Binary Input AWGN (BI-AWGN) channel, a substantial body of work exists detailing the construction of turbo like codes that reach as close as tenths of a dB from capacity. For the Rayleigh fading channel with perfect CSI [30] used density evolution to get the noise thresholds of LDPC codes and further used this technique to design good irregular LDPC codes. LDPC code design for the non-coherent fading channel is still in its infancy. The most common method used for designing LDPC codes for this channel is the use of EXIT charts. The EXIT chart method essentially tracks the convergence process of iterative decoding through a single parameter. Although a number of metrics have been suggested in literature [51, 52], the most robust and hence the most commonly used metric is the mutual information between the soft information output at the end of each (SISO block) iteration and the transmitted bits. The most common turbo-like system design involves the concatenation of an outer code and an inner modulation code. At the receiver, one can either perform (repeatedly) one decoding iteration of the inner code followed by one decoding iteration of the outer code and repeat this for a specified number of iterations or repeatedly perform one decoding iteration of the inner code followed by n decoding iterations of the outer code. When using LDPC outer codes and the former reception methodology, EXIT charts can be used to design the LDPC code by combining the variable node decoder of the LDPC decoder and the inner demodulator/decoder and deriving/computing the input-output

characteristics of this combined entity. On the other hand, for the second case, EXIT charts cannot be directly used since now the LDPC decoder has memory between iterations. This cannot be modelled by an EXIT chart. One work around to this problem is to describe the EXIT chart for the LDPC code assuming the use of infinite iterations so that the internal messages have converged. Since there is no benefit to having the internal messages, the LDPC decoder can be considered to start afresh. However for the case of finite number of iterations, EXIT chart based designs must be explored. We call this the problem of describing EXIT charts for systems with memory and intend to explore this problem.

BIBLIOGRAPHY

BIBLIOGRAPHY

[1] S. M. Alamouti. A simple transmit diversity technique for wireless communications. *IEEE J. Select. Areas Commun.*, 16(8):1451–1458, Oct. 1998.

[2] I. Bahceci and T. M. Duman. Combined turbo coding and unitary space-time modulation. In *Proc. International Symposium on Information Theory*, page 106, Washington, D.C., June 2001.

[3] I. Bahceci and T. M. Duman. Combined turbo coding and unitary space-time modulation. In *Proc. International Symposium on Information Theory*, page 106, June 2001.

[4] E. Biglieri, D. Divsalar, P. J. McLane, and M. K. Simon. *Introduction to Trellis-Coded Modulation with Applications*. Macmillian, New York, 1991.

[5] M. J. Borran, A. Sabharwal, and B. Aazhang. On design criteria and construction of non-coherent space-time constellations. *IEEE Trans. Information Theory*, 49(10):2332–2351, Oct. 2003.

[6] M. J. Borran, A. Sabharwal, B. Aazhang, and D. H. Johnson. On design criteria and construction of non-coherent space-time constellations. In *Proc. International Symposium on Information Theory*, Lausanne, Switzerland, July 2002.

[7] M. Brehler and M. K. Varanasi. Training-codes for the noncoherent multi-antenna block-rayleigh-fading channel. In *Proc. Conference on Information Sciences and Systems (CISS)*, Baltimore, Maryland, Mar. 2003.

[8] R.-R. Chen, R. Koetter, U. Madhow, and D. Agrawal. Joint noncoherent demodulation and decoding for the block fading channel: A practical framework for approaching Shannon capacity. *IEEE Trans. Communications*, 51(10):1676–1689, Oct. 2003.

[9] A. P. Dempster, N. M. Laird, and D. B. Rubin. Maximum likelihood from incomplete data via the EM algorithm. *J. Roy. Stat. Soc.*, 39(1):1–38, 1977.

[10] D. Divsalar and M. K. Simon. Combined trellis coding with asymmetric modulations. In *Proc. Globecom Conf.*, New Orleans, Louisiana, Nov. 1985.

[11] D. Divsalar, M. K. Simon, and J. H. Yuen. Trellis coding with asymmetric modulations. *IEEE Trans. Communications*, 35(2), Feb. 1987.

[12] D. Divsalar and J. H. Yuen. Performance of convolutionally coded unbalanced QPSK systems. In *Proc. National Telecommunication Conf.*, pages 14.5.1–14.5.7, Houston, Texas, Nov. 1980.

[13] D. Divsalar and J. H. Yuen. Asymmetric MPSK for trellis codes. In *Proc. Globecom Conf.*, pages 20.6.1–20.6.8, Atlanta, Georgia, Nov. 1984.

[14] I. C. A. Faycal, M. D. Trott, and S. Shamai (Shitz). The capacity of discrete-time Rayleigh fading channels. In *Proc. International Symposium on Information Theory*, page 473, Ulm, Germany, June 1997.

[15] I. C. A. Faycal, M. D. Trott, and S. Shamai (Shitz). The capacity of discrete-time memoryless Rayleigh fading channels. *IEEE Trans. Information Theory*, 47(4):1290–1301, May 2001.

[16] U. Fincke and M. Pohst. Improved methods for calculating vectors of short length in a lattice, including a complexity analysis. *Mathematics of Computation*, 44:463–471, Apr. 1985.

[17] G. D. Forney, Jr. Trellis shaping. *IEEE Trans. Information Theory*, 38:281–300, Mar. 1992.

[18] G. J. Foschini. Layered space-time architecture for wireless communication in a fading environment when using multi-element antennas. *Bell System Tech. J.*, 1(2):41–59, 1996.

[19] G. J. Foschini and M. J. Gans. On limits of wireless communications in a fading environment when using multiple antennas. *Wireless Personal Communications*, 6:311–335, Mar. 1998.

[20] K. Fu and A. Anastasopoulos. Performance analysis of LDPC codes for time-selective complex fading channels. In *Proc. Globecom Conf.*, pages 1279–1283, Taipei, Taiwan, Nov. 2002.

[21] K. Fu and A. Anastasopoulos. Analysis and design of LDPC codes for time-selective complex-fading channels. *IEEE Trans. Wireless Communications*, May 2004. (Accepted for publication; can be downloaded from http://www-personal.engin.umich.edu/∼anastas/preprints.html).

[22] R. G. Gallager. *Low-Density Parity-Check Codes*. PhD thesis, MIT Press, Cambridge, MA, 1963.

[23] M. C. Gursoy, H. V. Poor, and S. Verdú. Spectral efficiency of peak power limited rician block-fading channels. In *Proc. International Symposium on Information Theory*, page 543, Chicago, Illinois, June 2004.

[24] M. C. Gursoy, H. V. Poor, and S. Verdú. The noncoherent rician fading channelpart i: Structure of the capacity-achieving input. *IEEE Trans. Wireless Communications*, 4(5):2193–2206, Sept. 2005.

[25] A. R. Hammons and H. E. Gamal. On theory of space-time codes for psk modulation. *IEEE Trans. Information Theory*, 46(2):524–542, Mar. 2000.

[26] B. Hassibi and B. Hochwald. How much training is needed in multiple-antenna wireless links? *IEEE Trans. Information Theory*, 49(4):951–963, Apr. 2003.

[27] B. Hassibi and H. Vikalo. On the expected complexity of sphere decoding. In *Proc. Asilomar Conf. Signals, Systems, Comp.*, pages 1051–1055, Nov. 2001.

[28] B. Hochwald and T. L. Marzetta. Unitary space-time modulation for multiple-antenna communications. *IEEE Trans. Information Theory*, 46(2):543–564, Mar. 2000.

[29] B. M. Hochwald, T. Marzetta, T. J. Richardson, W. Sweldens, and R. L. Urbanke. Systematic design of unitary space–time constellations. *IEEE Trans. Information Theory*, 46(6):1962–1973, Sept. 2000.

[30] J. Hou, P. H. Siegel, and L. B. Milstein. Performance analysis and code optimization of low-density parity-check codes on Raleigh fading channels. *IEEE J. Select. Areas Commun.*, 19:924–934, May 2001.

[31] C.-H. Hsu and A. Anastasopoulos. Maximum likelihood decoding of trellis codes in fading channels with no receiver CSI is a polynomial-complexity problem. In *Proc. International Symposium on Information Theory*, page 147, Chicago, IL, June 2004.

[32] M. Katz and S. Shamai. On the capacity-achieving distribution of the discrete-time non-coherent additive Gaussian noise channel. In *Proc. International Symposium on Information Theory*, page 165, Lausanne, Switzerland, June 2002.

[33] M. Katz and S. Shamai. On the capacity-achieving distribution of the discrete-time noncoherent and partially coherent AWGN channels. *IEEE Trans. Information Theory*, 50(10):2257–2270, Oct. 2004.

[34] T. L. Marzetta and B. Hochwald. Capacity of a mobile multiple-antenna communication link in Rayleigh flat fading. *IEEE Trans. Information Theory*, 45:139–157, Jan. 1999.

[35] M. L. McCloud, M. Brehler, and M. K. Varanasi. Signal design and convolutional coding for noncoherent space-time communication on the block-Rayleigh-fading channel. *IEEE Trans. Information Theory*, 48(5):1186–1194, May 2002.

[36] I. Motedayen and A. Anastasopoulos. Polynomial complexity ML sequence and symbol-by-symbol detection in fading channels. In *Proc. International Conf. Communications*, pages 2718–2722, Anchorage, Alaska, May 2003.

[37] I. Motedayen and A. Anastasopoulos. Polynomial-complexity noncoherent symbol-by-symbol detection with application to adaptive iterative decoding of turbo-like codes. *IEEE Trans. Communications*, 51(2):197–207, Feb. 2003.

[38] I. Motedayen, A. Krishnamoorthy, and A. Anastasopoulos. Optimal joint detection/estimation in fading channels with polynomial complexity. *IEEE Trans. Information Theory*, Sept. 2003. (Under Revision).

[39] R. Nuriyev. *Communication over the noncoherent channel*. PhD thesis, University of Michigan, Ann Arbor, MI, May 2003.

[40] R. Nuriyev and A. Anastasopoulos. Capacity-approaching code design for the noncoherent AWGN channel. In *Proc. Globecom Conf.*, pages 1598–1602, San Fransisco, CA, Dec. 2003.

[41] R. Nuriyev and A. Anastasopoulos. Capacity characterization for the noncoherent block-independent AWGN channel. In *Proc. International Symposium on Information Theory*, page 373, Yokohama, Japan, June 2003.

[42] R. Nuriyev and A. Anastasopoulos. Pilot-symbol-assisted coded transmission over the block-noncoherent AWGN channel. *IEEE Trans. Communications*, 51(6):953–963, June 2003.

[43] R. Palanki. On the capacity achieving distributions of some fading channels. In *Proc. Allerton Conf. Commun., Control, Comp.*, Allerton House, Illinois, 2002.

[44] T. N. Pappas and D. L. Neuhoff. Least-square model-based halftoning. *IEEE Trans. Image Processing*, 8(8):1102–1116, Aug. 1999.

[45] J. G. Proakis. *Digital Communications*. McGraw-Hill, New York, 4th edition, 2001.

[46] A. Stefanov and T. M. Duman. Turbo coded modulation for systems with transmit and receive antenna diversity over block fading channels: System model, decoding approaches on limits of wireless communications in a fading environment when using multiple antennas. *IEEE J. Select. Areas Commun.*, 19(5):958–968, May 2001.

[47] P. Stoica, H. Vikalo, and B. Hassibi. Joint maximum-likelihood channel estimation and signal detection for SIMO channels. In *Proc. ICASSP*, pages IV–13–IV–16, Hong Kong, Apr. 2003.

[48] V. Tarokh, N. Seshadri, and A. R. Calderbank. Space-time codes for high data rate wireless communication: performance criterion and code construction. *IEEE Trans. Information Theory*, 44(2):744–765, Mar. 1998.

[49] E. Telatar. Capacity of multi-antenna Gaussian channels. *Bell System Tech. J.*, June 1995.

[50] S. ten Brink. Convergence of iterative decoding. *IEE Electronics Letters*, 35(10):806–808, May 1999.

[51] S. ten Brink. Convergence behavior of iteratively decoded parallel concatenated codes. 49(10):1727–1737, Oct. 2001.

[52] S. ten Brink. Measures for tracing convergence of iterative decoding algorithms. In *Proc. IEEE/ITG Conf. on Source and Channel Coding*, pages 53–60, Berlin, Germany, Jan. 2002.

[53] S. ten Brink, G. Kramer, and A. Ashikhmin. Design of low-density parity-check codes for multi-antenna modulation and detection. *IEEE Trans. Information Theory*, June 2002. (Submitted).

[54] G. Ungerboeck. Channel coding with multilevel/phase signals. *IEEE Trans. Information Theory*, 28(1):55–67, Jan. 1982.

[55] S. Verdú. Spectral efficiency in the wideband regime. *IEEE Trans. Information Theory*, 48:1319–1343, June 2002.

[56] L. Zheng and D. N. C. Tse. Communication on the Grassmann manifold: a geometric approach to the noncoherent multiple-antenna channel. *IEEE Trans. Information Theory*, 48(2):359–383, Feb. 2002.

ABSTRACT

CODE AND RECEIVER DESIGN FOR THE NON-COHERENT FAST FADING CHANNEL

by

Arvind Krishnamoorthy

Chair: Achilleas Anastasopoulos

We consider the problem of communication over a wireless fading channel, when the channel state information (CSI) is not available at the transmitter and the receiver. To take the channel dynamics into account, we consider a block independent Rayleigh fading model. This work deals with the design of coding/modulation and demodulation/decoding schemes for single- or multiple-antenna systems with focus on fast to very fast fading channels.

We explore two possible solutions for this channel with increasing degree of sophistication. The first one utilizes pilots at the transmitter and a simple and explicit non-iterative channel estimation algorithm at the receiver. We show that this pilot-assisted system is exactly equivalent, in terms of performance analysis and design, to an appropriately "degraded" system having perfect CSI at the receiver. Noting

that this simple receiver design can be improved especially for high channel dynamics, we propose a family of well-justified and simple suboptimal iterative detection/estimation algorithms. It is shown that when turbo-like codes are considered in conjunction with the aforementioned pilot assisted transmission scheme and the proposed receiver algorithm, the unitary constellations investigated in the literature are inferior to simple pilot-assisted constellations in both complexity and performance.

Specific instances of the proposed systems (that use optimized irregular LDPC outer codes) are designed. The design examples provided show that the proposed systems can achieve a good tradeoff between complexity and performance and can be used to bridge the gap between the high complexity/high performance optimal scheme and low complexity/mediocre performance non-iterative estimation/coherent detection scheme.

In order to get a better understanding of the fundamental limitations regarding the transmission over fading non-coherent channels, we attempted to completely characterize the input distribution that achieves the capacity of the block-independent Rayleigh fading channel. The mutual information expression for this channel was reduced from a multi-dimensional integral to an integral in two real variables that represent the amplitude of the input and the output, thus determining that the capacity is completely specified by the input amplitude distribution. Particularly we show that the capacity achieving input is isotropically distributed, unitary and has an independent amplitude distribution that has bounded support. Based on a well-founded conjecture in the literature that the amplitude distribution is discrete, we show also that starting from a single amplitude scheme, adding some probability mass to the zero amplitude increases the mutual information achieved. This fact is illustrated through numerical evaluations as well.

Finally, the code design problem for very fast fading channels is considered and based on the information theoretic analysis, a novel system design that incorporates the zero mass point is proposed. Through constrained capacity analysis and Monte-Carlo simulations, this system is shown to provide some of the gain promised by the information theoretic analysis. Simulations of the proposed system report at least 0.55 dB gain over conventional systems with no additional complexity.